We are committed to providing [accessible customer service](#).
If you need accessible formats or communications supports, please [contact us](#).

Nous tenons à améliorer [l'accessibilité des services à la clientèle](#).
Si vous avez besoin de formats accessibles ou d'aide à la communication, veuillez [nous contacter](#).

Assessment Report

On

Claim 4266871 - SANDRA BRECCIA

Norberg Township

Sault Ste. Marie Mining Division
District of Algoma
N.T.S: 41N/01

VLF EM-16 Surveying

Prepared by: Shaun Parent

Claim Holder

June 20, 2017

Table of Contents

Tables, Figures & Appendicies

Executive Summary:

Claim 4266871 is located in the Sault Ste. Marie Mining Division, approximately 65 kilometers north of Sault Ste. Marie, Ontario. The Claim consists of 2 16 hectare units and is located less than 500 meters due east of the deposit known as the East Breccia. The Sandra Breccia is a new discovery in the area of the Tribag Mines.

A VLF EM-16 Survey program was carried out in January 2017, using a VLF EM-16 and a handheld Garmin GPS-60C. 1 transmitter station (NML-La Moure, North Dakota) was read at each station.

The objective of the VLF Em-16 Survey was to determine if the weak magnetic anomaly east of the East Breccia deposit represented a possible mineralized Breccia Pipe. There are three known mineralized breccia pipes located to the west of Claim 4266871. The Breton Breccia contains an estimated 40 million tons of 0.3-0.4% Copper. The West Breccia has a resource of 223,000 tons of 0.75% copper, while the East Breccia contains a historical resource of 125 million tons of 0.13% copper. The West Breccia and the East breccia deposits have associated high airborne magnetic responses.

Highlights:

➢ Ground Follow up of the VLF Em-16 survey in 2015 discovered several new sites carrying copper-malachite-pyrite mineralization. The most significant is shown in Figures 7 & 8.

➢ This new Breccia discovery has been named the "SANDRA BRECCIA"

➢ The VLF EM-16 survey outlined conductors that could be the mineralized zones near the tops of a breccia pipe

➢ The new mineralization discovered on claim 4266871 is similar to that of other breccia pipes in the area.

Introduction

The Sandra Breccia property (claim 4266871) is located in the Sault Ste. Marie Mining Division, approximately 65 kilometers north of Sault Ste. Marie, Ontario. The property consists of 3-16 hectare claim units.

In January of 2017, 11 VLF traverse lines were surveyed using a Geonics EM-16 VLF Instrument.

This Assessment report describes the findings and results of the VLF EM-16 survey utilizing the new VLF 2DMF processing software of which the author of this report has contributed to development

Location and Access

Claim 4266871 is located in the mining District of Sault Ste. Marie.

The Claim group is located near the West boundary of Norberg Township. The property is located approximately 65 km. north of the city of Sault Ste. Marie, Ontario.

The claims are located on NTS Maps 41N/1. The Mining claims are found on Norberg Plan G-3120. (See Figures 1 , 2 & 3)

Access to the property can be accomplished by a 2 wheel drive vehicle along the Carp River road. Winter access is by snow machine only, unless logging is taking place in the immediate vicinity of claims and along the East Breccia Access road.

Directions to the property is as follows:

- Drive north from Sault Ste. Marie on Highway 17 for approximately 40 minutes to the junction of the highway 538 to the Batchawana Bay.
- Continue north on Highway 17 for 200 meters to the Carp River Road.
- Follow the Carp River Road for 20 kilometers until you reach the bypass to Mile 67 Road.
- Turn right and continue on the main road. As you pass a lake on the left side, there is a steep turn to the right
- At this junction is where the #3 Post for claim 4266871 is found next to the road.

Claim Block

The claim number covered by the VLF-Em-16 survey is 4266871.   The claim consists of 3-16 Hectare claim units. (See Figure-2)

Figure 1 General Location Map

Figure-1
General Location Map of
Claim 4266871
Norberg Township

Scale 1:385,000

Figure 2 Location Map of Claim

690000E   691000E   692000E   693000E

5220000N   5220000N

N

5219000N   5219000N

5218000N   5218000N

WP2006-14

4201402

4266871

Sault Ste. Marie   NORBERG

NICOLET

4271701

4253388

4201403

East Breccia

1192202

4243482

4201404

4201405

Batchawana River

Figure-2
Location Map of Claim 4266871
within Norberg Township
Scale 1:15,000

UTM Zone 16
1000m grid

690000E   691000E   692000E   693000E

Figure 3 Claim on Airborne EM Magnetics
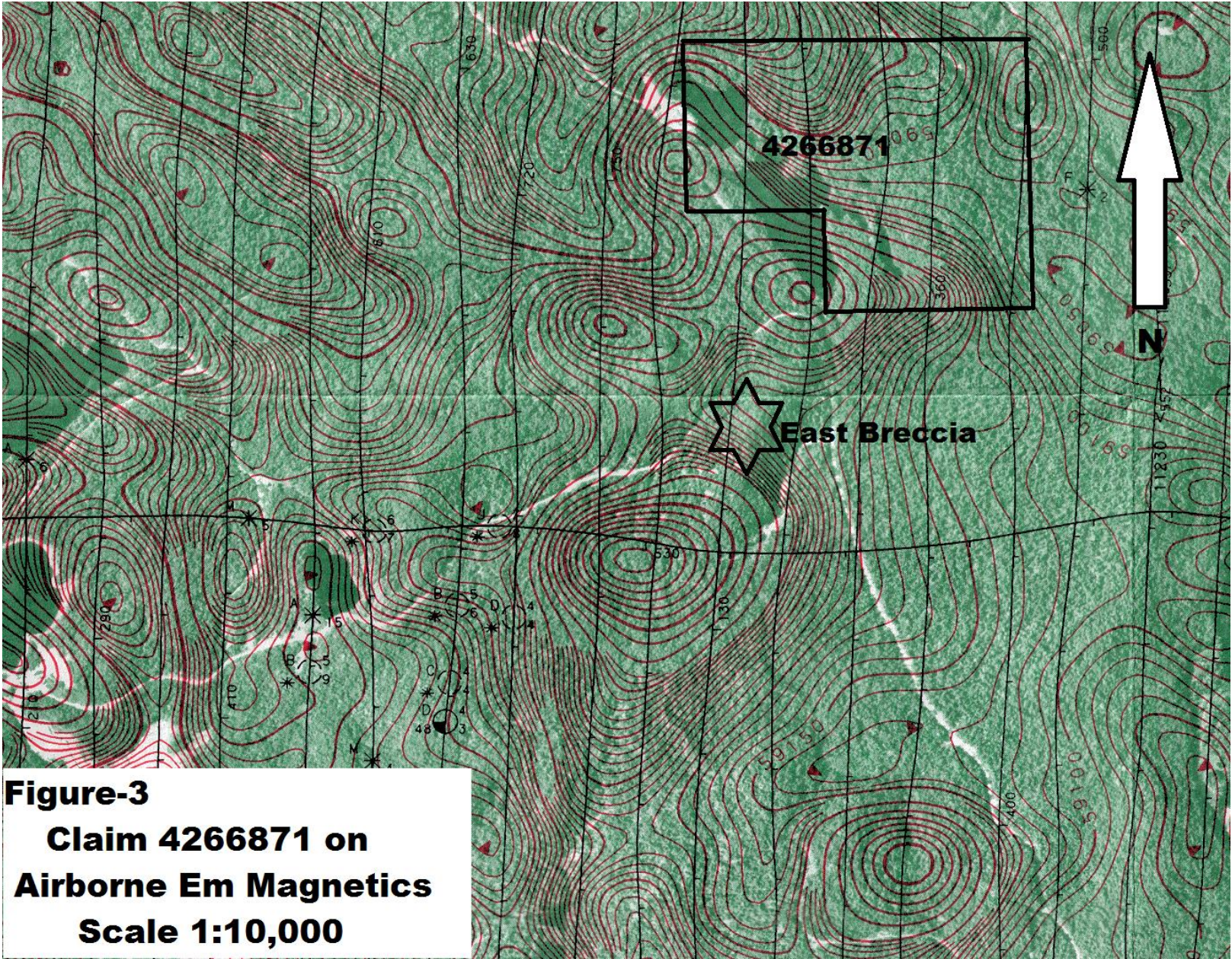
Figure-3

Claim 4266871 on

Airborne Em Magnetics

Scale 1:10,000

4266871

East Breccia

Figure 4 Google Image of VLF Lines & Claim Location

Figure-4
Google Image of VLF Lines
and Claim Location
Scale 0--------------400 meters
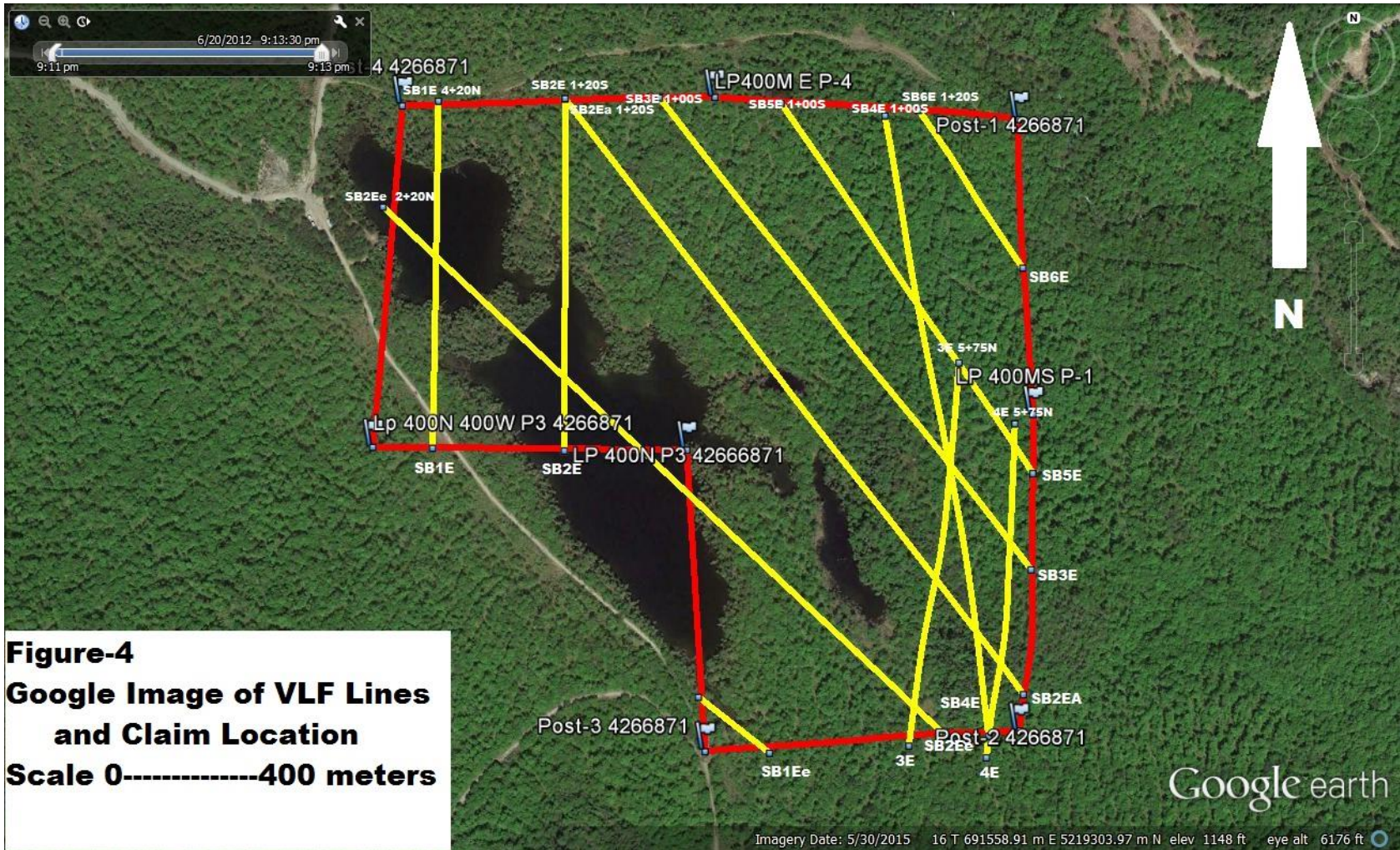
Personnel

The VLF EM-16 and GPS field navigator responsible for the collection of all raw data and the processing of raw data with the VLF2DMF Software was Shaun Parent

Work Performed

The VLF EM-16 survey consisted of running 11 VLF traverse Lines totaling 6.18 Km

The VLF survey lines were chosen to best cover the complete 4266871 Claim as in Figure-3

All VLF were aligned to cover the magnetic anomaly and are shown on a Google earth image in figure 4. A total of 6.18 Kilometers of VLF surveying was carried out on Claim 4266871.

The VLF lines were completed while using a handheld Garmin 60-CSX GPS. Each VLF station was located based on its azimuth and distance from the start of the survey line. Transmitter station NML was read using the Geonics VLF- Em-16 serial number 0236 at each line station. The following parameters were used throughout the survey.

Table 1 VLF Lines Surveyed

Line Number	Azimuth	Surveyed Stations	Line Length Meters
SB1Ee	128	2+60S to 4+00S	136
SB2Ee	133	2+20N to 7+80S	982
SB1E	180	4+40S to 0+20S	439
SB2E	180	1+20N to 2+40S	445
SB2EA	142	1+20S to 10+60S	940
SB3E	142	1+00S to 8+40S	750
SB4E	171	1+00S to 9+00S	800
SB5E	146	1+00S to 6+60S	560
SB6E	146	1+20S to 3+40S	210
3E	187	5+75N to 10+75N	500
4E	184	5+75N to 10+00N	425

VLF Data Collection:

VLF Em-16 Receiver # 236

VLF Transmitters :   NML La Moure, North Dakota 25.8 KZ
Only data collected for transmitter NML, La Moure, North Dakota has been processed for this report

VLF survey direction: See Table 1

Parameters of Measurement: In-phase and Quad-phase components of vertical magnetic field as a percentage of horizontal primary field. (Tangent of tilt angle and ellipticity). TX transmitter NML was to the west.

The VLF Field data was collected as follows on each surveyed line.

- Each station was saved using the Handheld Garmin 60CSX Handheld GPS Unit
- VLF data for Station NML was recorded in a notebook as In-Phase and Quadrature corresponding to the line and station. See example in Table 2
- The handheld Garmin Field data was downloaded onto the Garmin map source program where line information could be viewed relative to local features such as claim lines, roads.
- The Garmin filed data and the raw VLF notes were then combined and compiled onto an excel spreadsheet which was then entered into the VLF2DMF Processing software.

Table 2 Example of VLF Field Data Collection

Line 4E	NML - Inphase	NML - Quadrature
0+00	12	-7
0+20E	14	-9
0+40E	16	-10

VLF Data Processing:

The result of entering this field data into the software produced profiles of survey lines as well as plan maps of combined surveyed lines. All of which are found at the end of this report

1) Plan Map of Lines Surveyed (Figure-4)

2) Raw VLF Profiles for Transmitter NML

> The Raw data collected in the field is plotted showing the In-Phase component as a red dashed line and the quadrature component as a blue dashed line. In-Phase inflections and cross overs are usually plus to minus, while Quadrature responses are negative to positive.

3) Fraser Filter Profiles for Transmitter NML

> The data processing technique commonly referred to as the Fraser Filter was applied to the raw data. This filter transforms In-Phase cross overs and inflections into positive peaks, while Quadrature responses are negative to positive giving a negative peak anomaly when the Fraser Filter is applied.

4) Fraser Filtered Plan Maps NML In Phase and NML Quadrature (Figures 5, 6)

> The VLF2DMF software uses the Fraser filtered profiled data and produces contoured results on a plan map. Positive peaks in the In-Phase Component are shown as orange and negative peaks in the Quadrature component are shown on the plan maps as blue to dark blue. The intensity of the response is measured on the scale bar to the right of the plan maps.
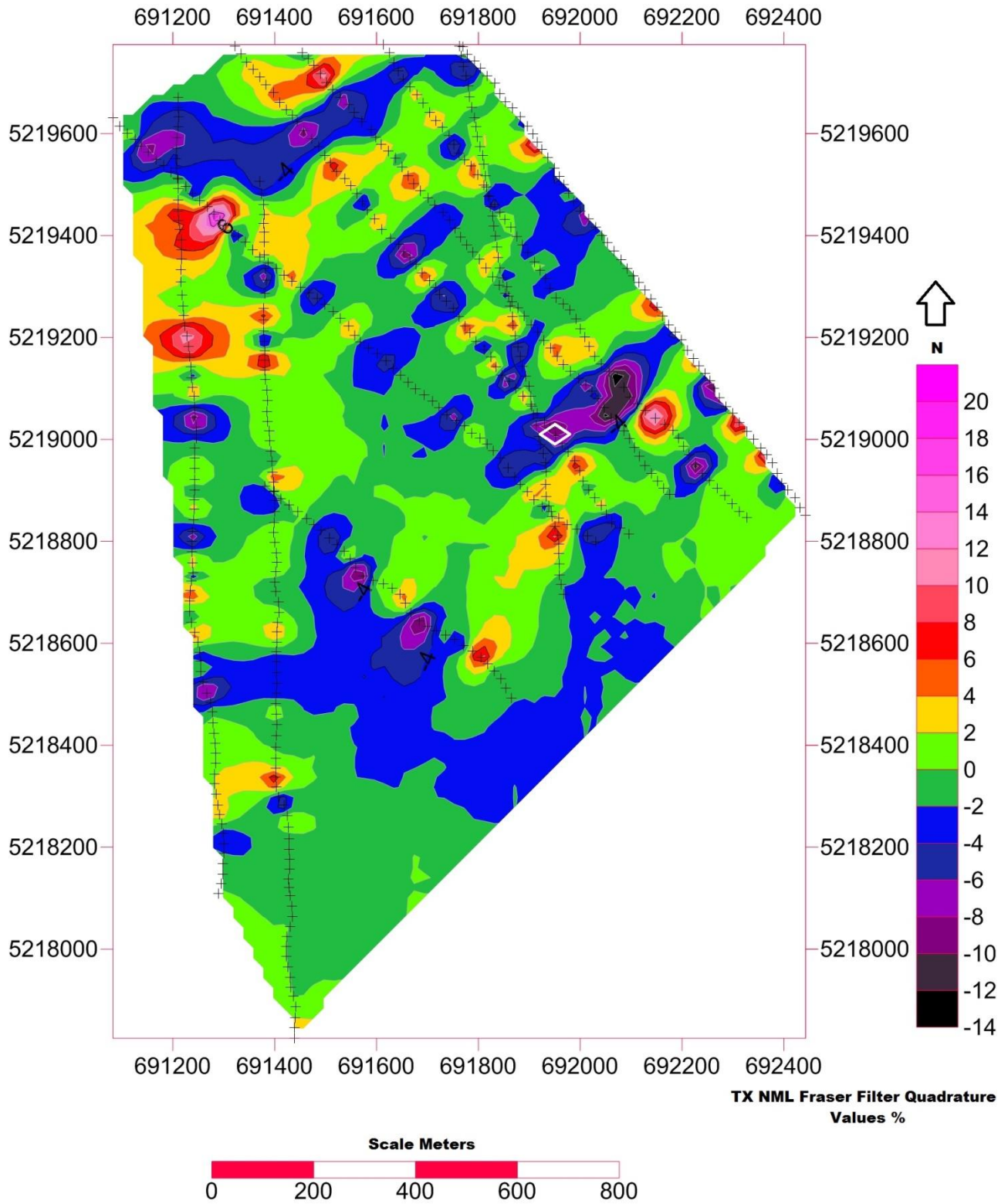
Figure 5 TX NML Fraser Filter Quadrature Values

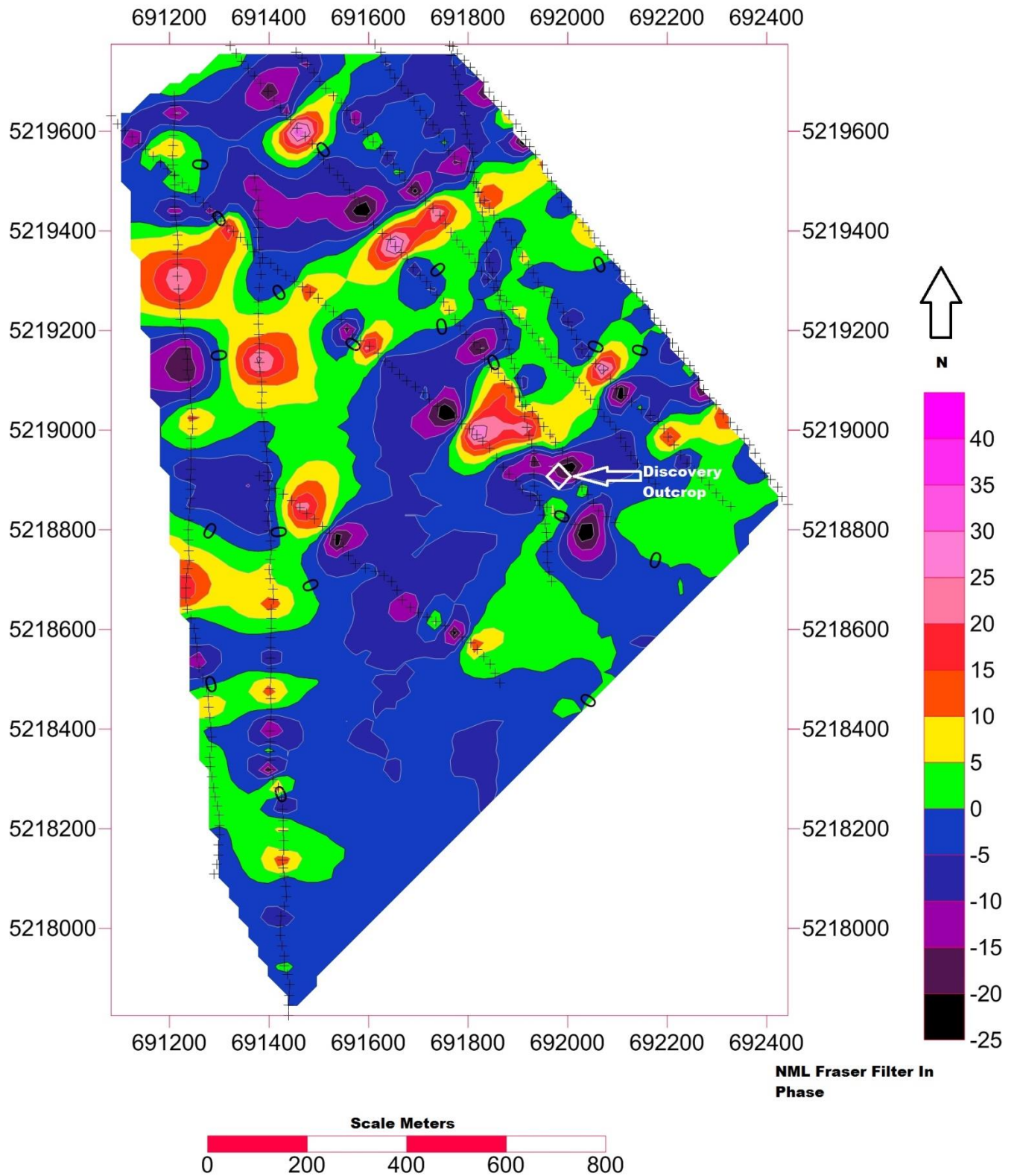**Figure 6 TX NML Fraser Filter In-Phase**

Figure 7 Line SB4E Model Cross Section
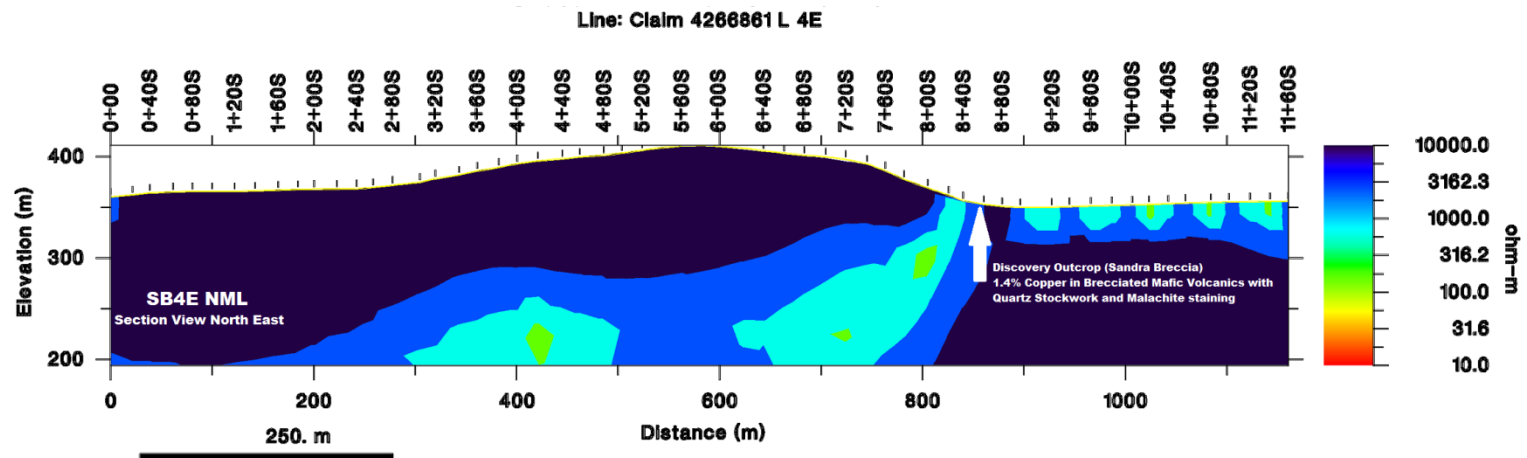
Figure-7
Line SB4E
Model Cross Section
Transmitter: NML

Vertical Exaggeration: 1.0

Figure 8 Photo of Discovery Outcrop

Discovery Sample from Outcrop. Found while doing followup of VLF MODEL ground proofing.
Contains Chalcopyrite, pyrite, molybdenum.

Surface area of the Sandra Breccia is 250 X 250 meter.
Available for Option
Contact Shaun Parent

SANDRA BRECCIA
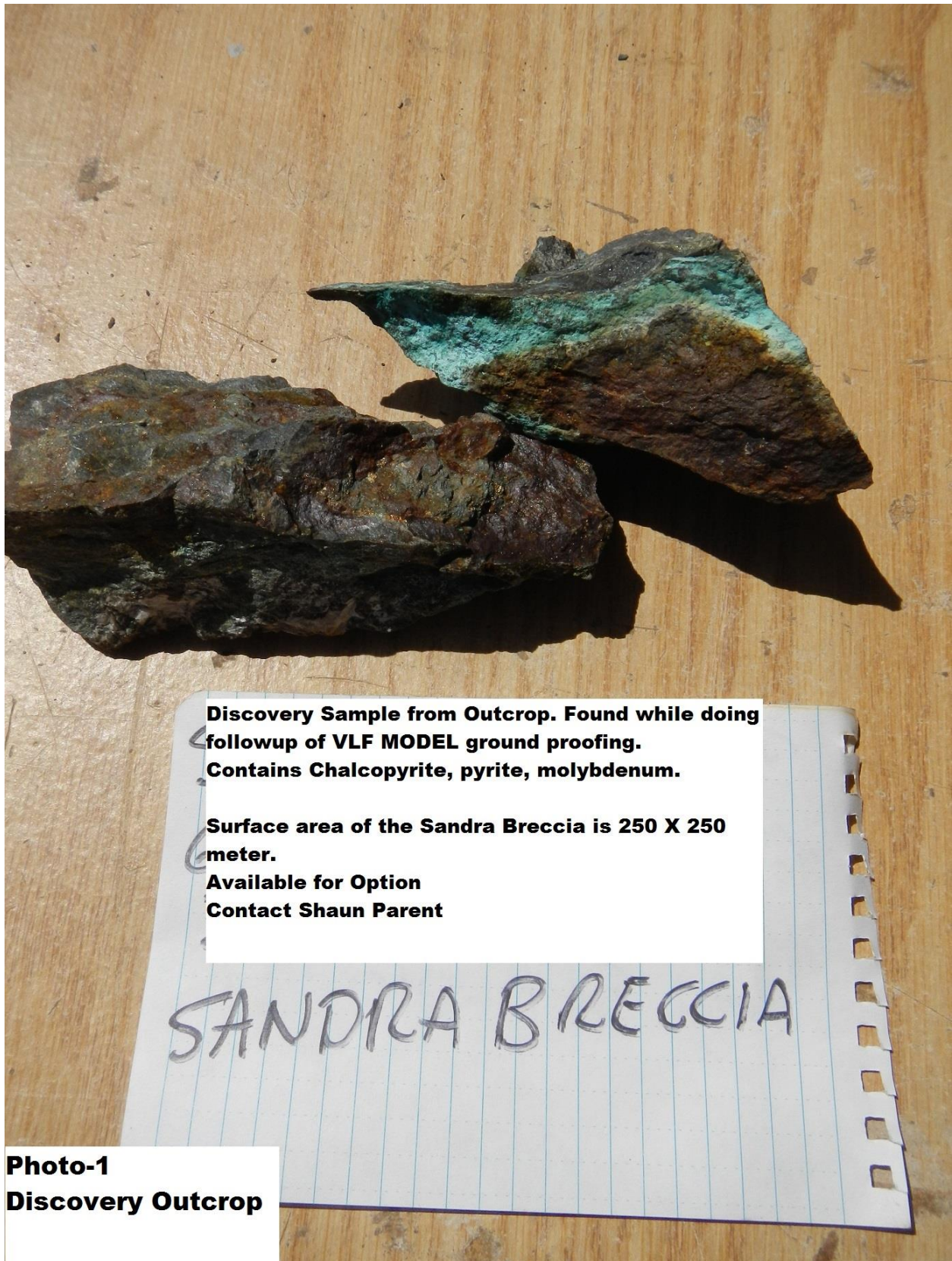
Photo-1
Discovery Outcrop

Conclusions and Recommendations

The Ground VLF Survey was successful with

1) Discovery of a new mineralized outcrop on line SB4E (Figure 7 and photo 1)
2) Finding several other VLF Tends in the area surveyed
3) Using the VLF2DMF VLF processing software
4) Further processing of VLF data to construct a cross section model similar to Figure 7.
5) The discovery of a new Breccia pipe in an area that has been explored since 1953
6) Ground Follow up of VLF trends, those under the lake are no accessible
7) Further Prospecting and sampling of outcrops near VLF trends
8) Fill in In VLF traverse lines along an azimuth of 45 degrees

List of References

Geonics Ltd. (1997): Operating Manual for VLF Em-16

McNeil, J.D. and Labson; (1991): Geological Mapping using VLF radio fields. In Nabghian, M.N Ed, Electrical Methods in Applied Geophysics 11. Soc. Expl. Geoph, p.p. 521-640

Sayden, A.S, Boniwell, J.B; (1989): VLF Electromagnetic Method, Canadian Institute of Mining and Metalurgy, Special Volume 41 p.p. 111-125 of VLF-EM Data

Monteiro Santos, F.A; (2012): VLF 2D V1.2 A program for 2D inversion

Ontario Geological Survey (1990): Airborne electromagnetic and total intensity magnetic survey, Batchawana Area, Ontario. Ontario Geological Survey Map 81447 Scale 1:20,000

Certificate of Qualifications

I, Shaun Parent, P. Geo (LTD.) residing at 282 B Whispering Pines Road, Batchawana Bay, Ontario do certify that:

1. I am a consulting Geoscientist with Superior Exploration, Adventure & Climbing Co. Ltd. which provides VLF Survey-Interpretation-Modelling using our VLF2DMF Software for the Mining Sector worldwide.

2. I am the registered owner of Claim 4266871.

3. I graduated with a Geological Technician Diploma from Sir Sandford Fleming College in 1986.

4. I graduated with a BSc. from the University of Toronto in 1986.

5. I am a member in good standing with the Association of Professional Geoscientists of Ontario #1955 and a member of the Prospectors and Developers Association of Canada.

6. I have been employed continuously as a Geoscientist for the past 26 years since my graduation from University.

7. The nature of my involvement with this assessment report was to carry out the VLF Survey
    As well as to do the interpretation of the VLF using the EMTOMO VLF2D Software of which I have been developing with the software designer Fernando Santos of the University of Lisbon, Portugal.

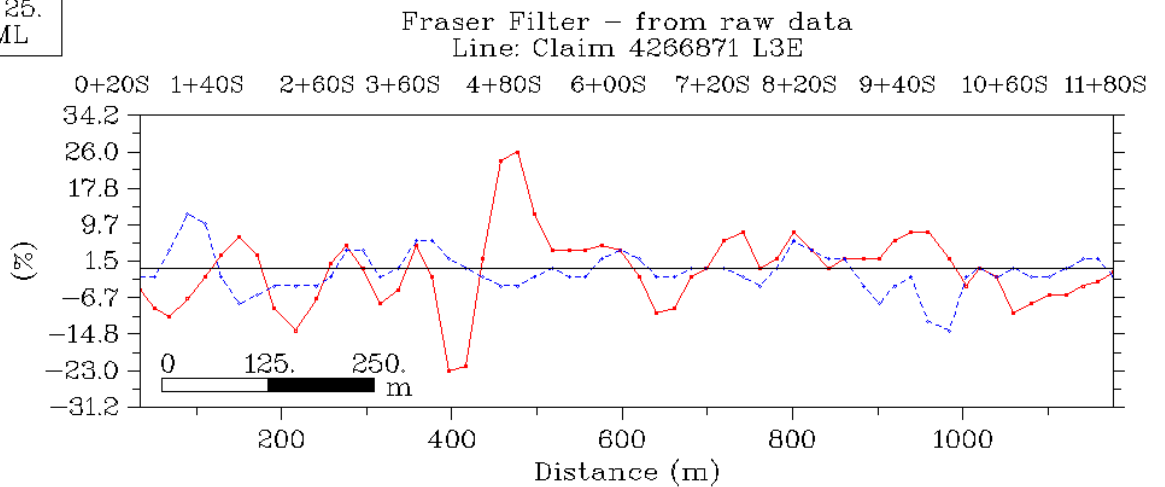Dated this 20th. day of June 2017

_____

Shaun Parent, P. Geo (Limited)

Profiles Line 3E Figure- 1 Raw Data

VLF-EM raw data
Line: Claim 4266871 L3E
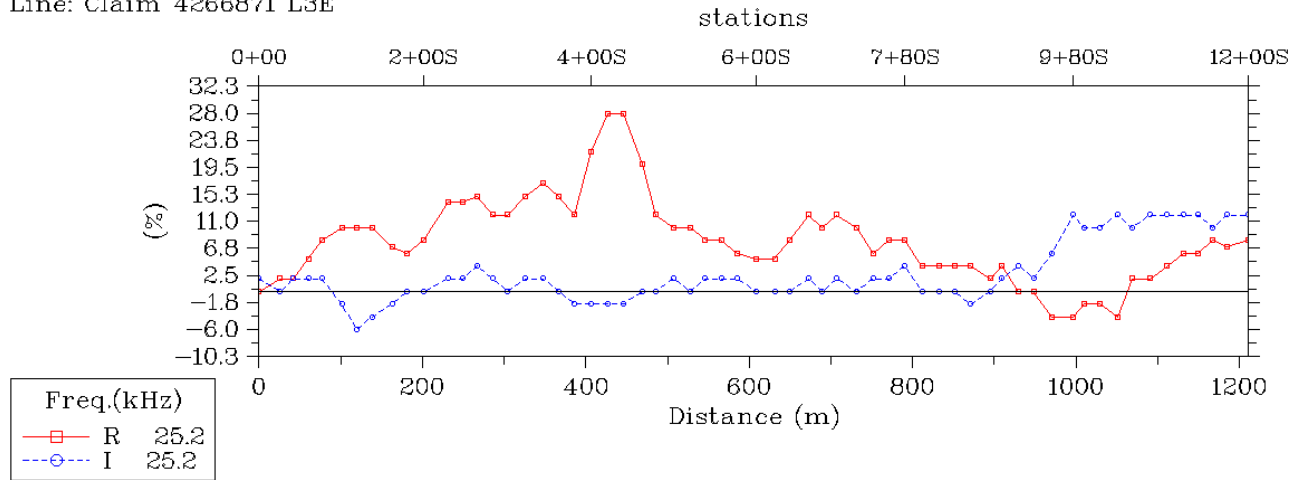
Profiles Line 3E Figure- 2 Fraser Filter

Fraser Filter - from raw data
Line: Claim 4266871 L3E

Profiles Line 4E Figure 1 Raw Data

VLF-EM raw data
Line: Claim 4266861 L 4E
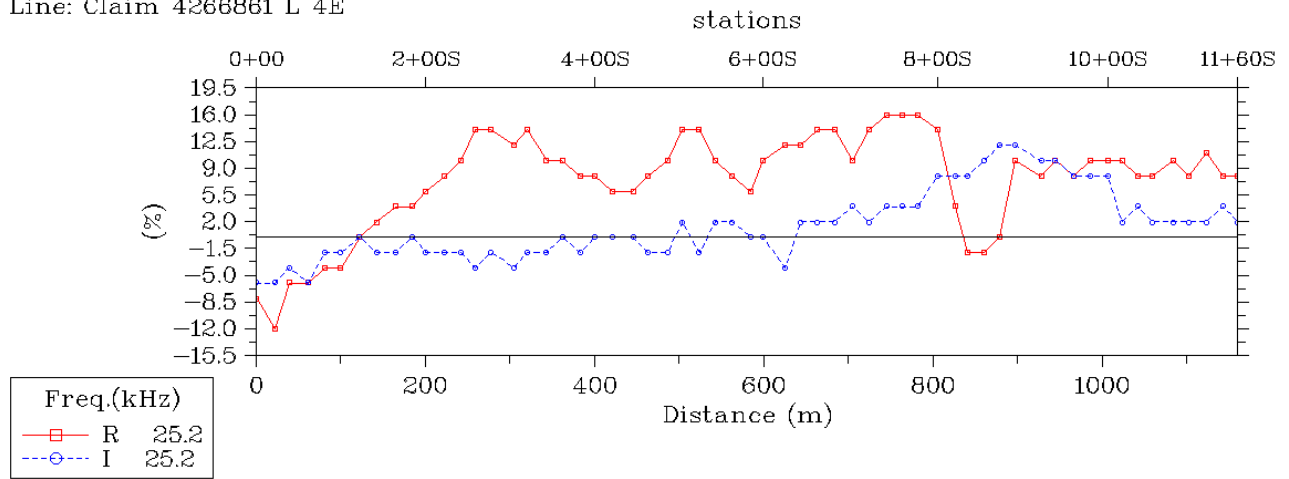
Profiles Line 4E Figure 2 Fraser Filter

Fraser Filter – from raw data
Line: Claim 4266861 L 4E

Profiles Line SB1E Figure 1 Raw Data

VLF-EM raw data
Line: Claim 4266871 SB1E
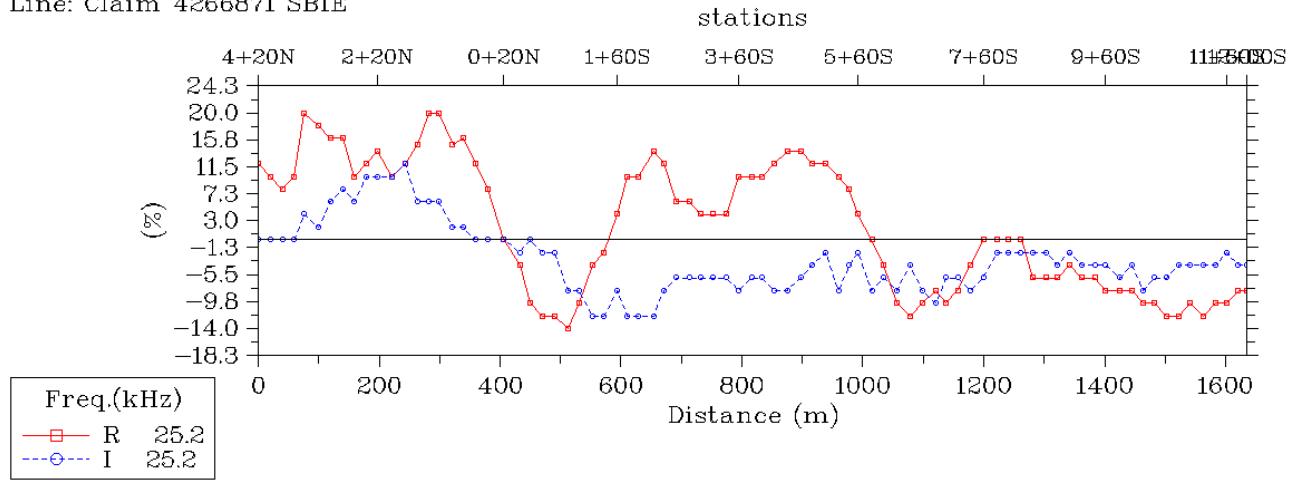
Profiles Line SB1E Figure 2 Fraser Filter
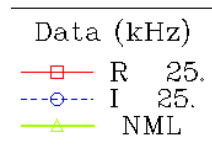
Fraser Filter – from raw data
Line: Claim 4266871 SB1E
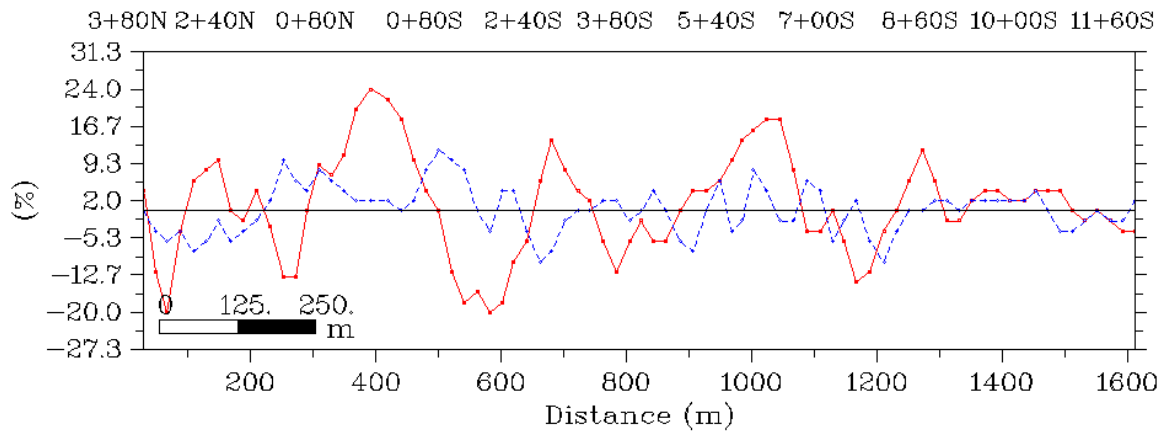
Profiles Line SB1Ee Figure 1 Raw Data

VLF-EM raw data
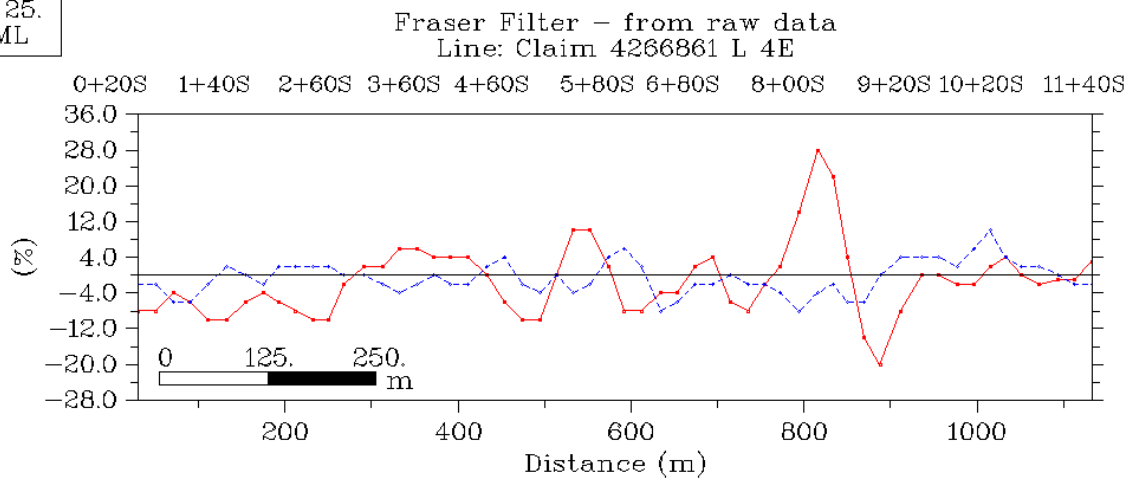Line: Claim 4266871 SB1Ee

stations

Freq.(kHz)
R   25.2
I   25.2

Profiles Line SB1Ee Figure 2 Fraser Filter

Data (kHz)
R   25.
I   25.
NAA

Fraser Filter — from raw data
Line: Claim 4266871 SB1Ee

Profiles Line SB2E Figure 1 Raw Data

VLF-EM raw data
Line: 8266871 SB2E

stations

Freq.(kHz)
R   25.2
I   25.2
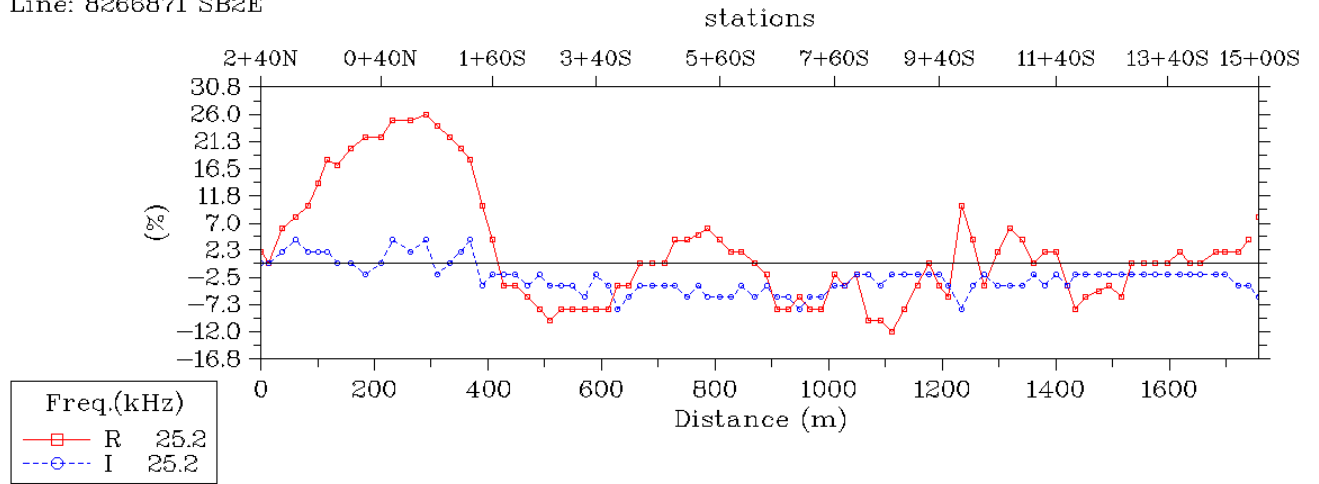
Profiles Line SB2E Figure 2 Fraser Filter

Data (kHz)
R   25.
I   25.
NML

Fraser Filter — from raw data
Line: 8266871 SB2E
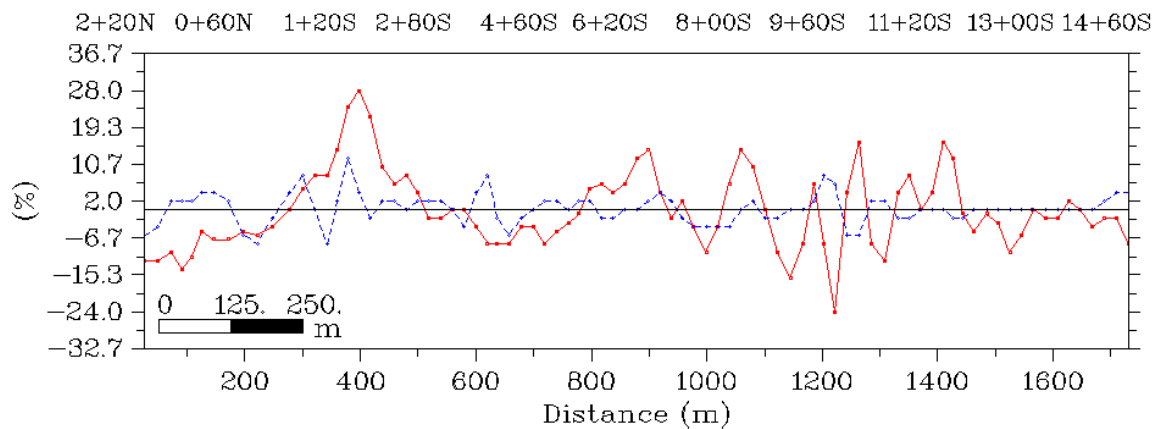
Profiles Line SB2EA Figure 1 Raw Data

VLF–EM raw data
Line: Claim 4266871 LSB2EA

Freq.(kHz)
R 25.2
I 25.2
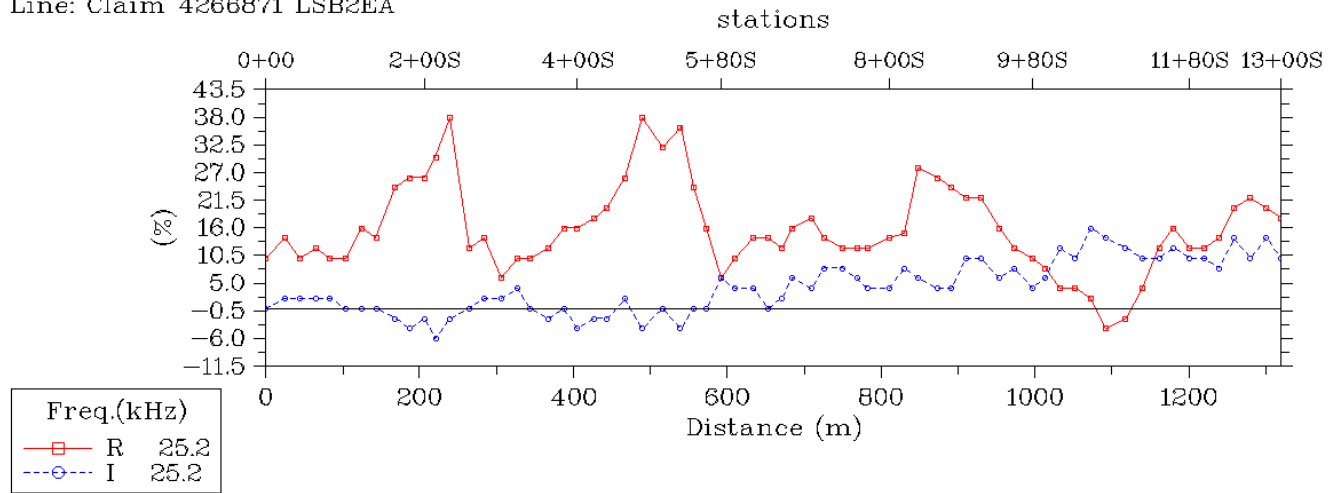
Profiles Line SB2EA Figure 2 Fraser Filter

Data (kHz)
R 25.
I 25.
NML
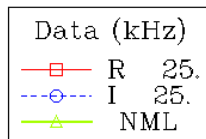
Fraser Filter – from raw data
Line: Claim 4266871 LSB2EA

Profiles Line SB2Ee Figure 1 Raw Data

VLF−EM raw data
Line: Claim 4266871 SB2Ee

stations

Freq.(kHz)
- R   25.2
- I   25.2
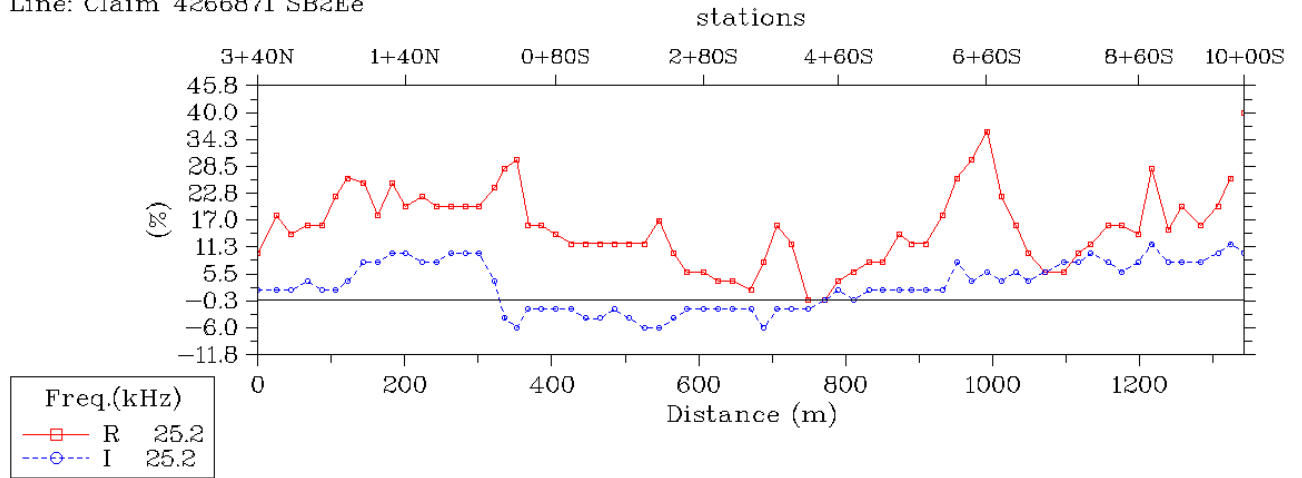
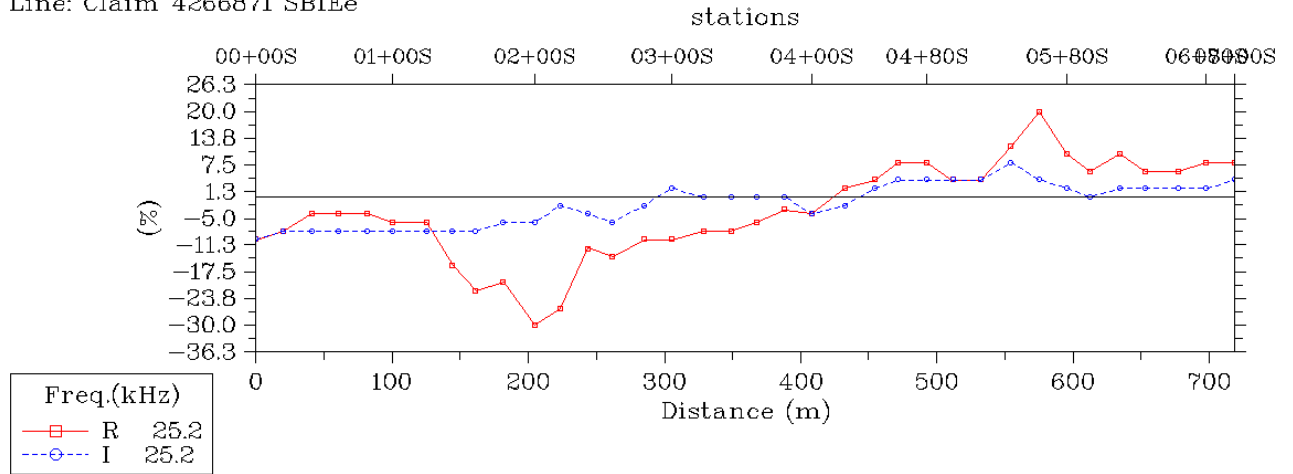## Profiles Line SB2Ee Figure 2 Fraser Filter

Data (kHz)
- R   25.
- I   25.
- NML

Fraser Filter − from raw data
Line: Claim 4266871 SB2Ee

25
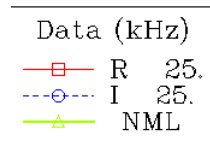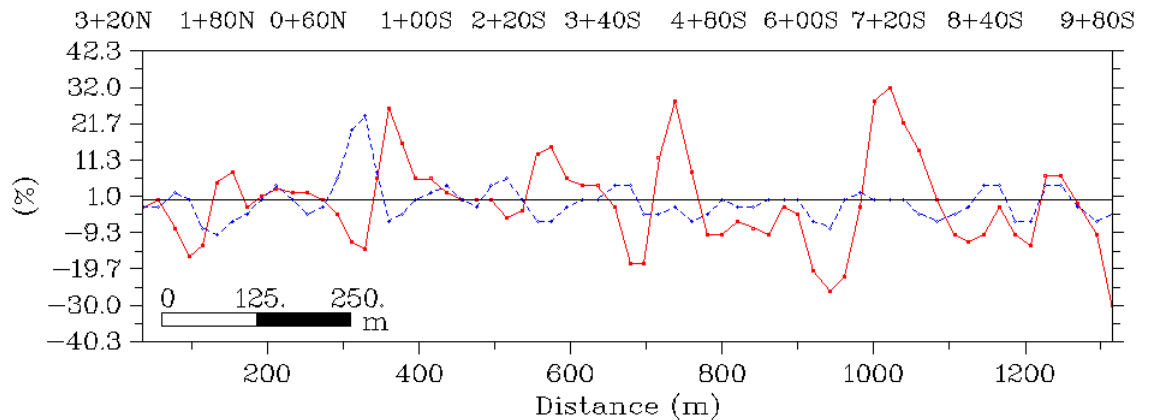
Profiles Line SB3E Figure 1 Raw Data

VLF-EM raw data
Line: Claim 4266871 L3E

stations

Freq.(kHz)	
R	25.2
I	25.2
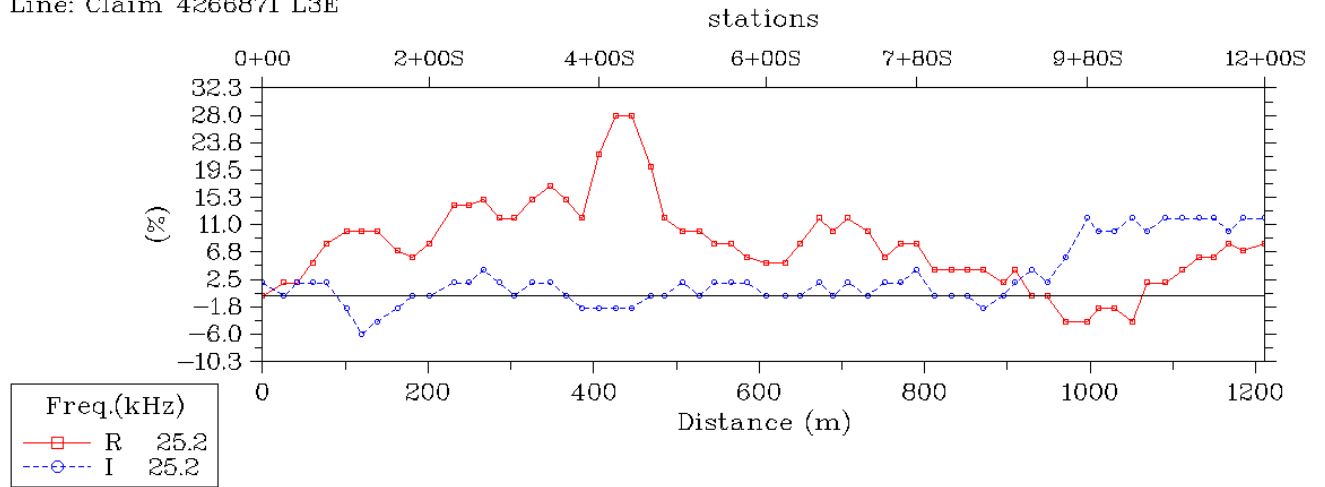
Profiles Line SB3E Figure 2 Fraser Filter

Data (kHz)	
R	25.
I	25.
NML	

Fraser Filter - from raw data
Line: Claim 4266871 L3E

26
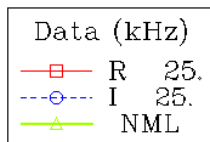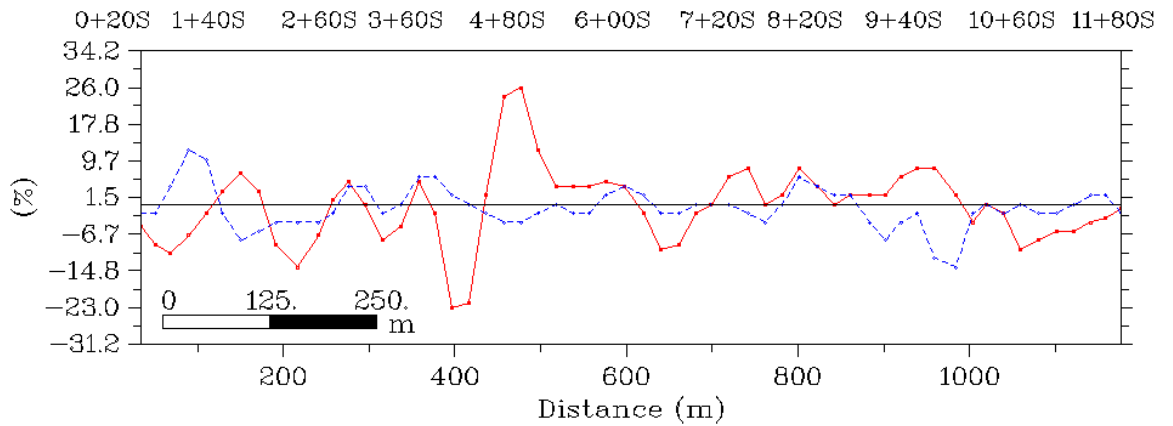
Profiles Line SB4E Figure 1 Raw Data

VLF-EM raw data
Line: Claim 4266861 L 4E
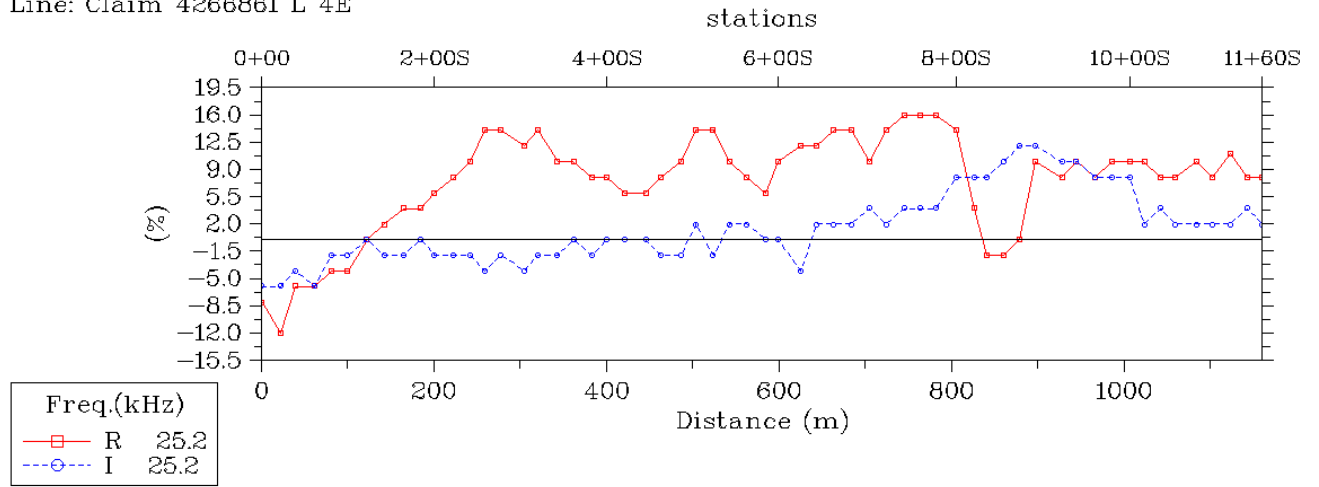
Profiles Line SB4E Figure 2 Fraser Filter

Fraser Filter — from raw data
Line: Claim 4266861 L 4E
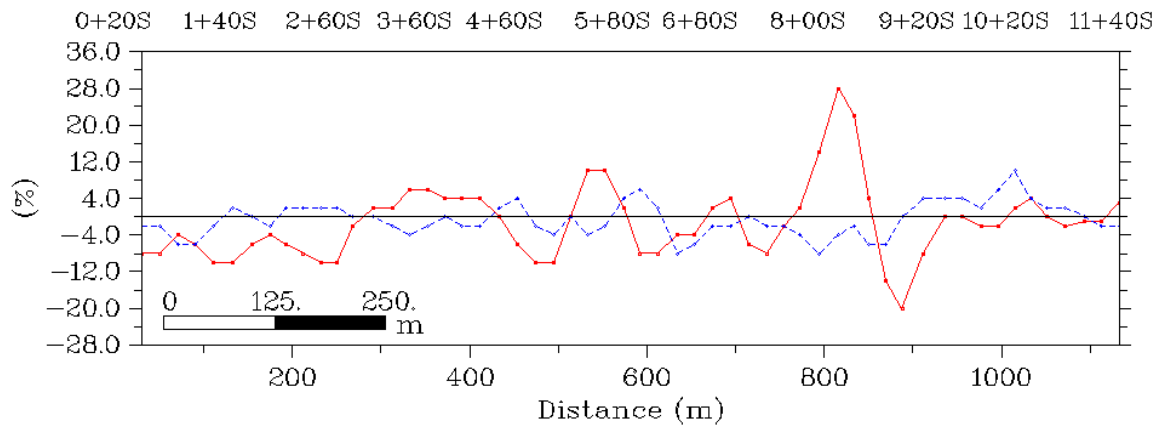
Profiles Line SB5E Figure 1 Raw Data

VLF-EM raw data
Line: Claim 4266871 L5E
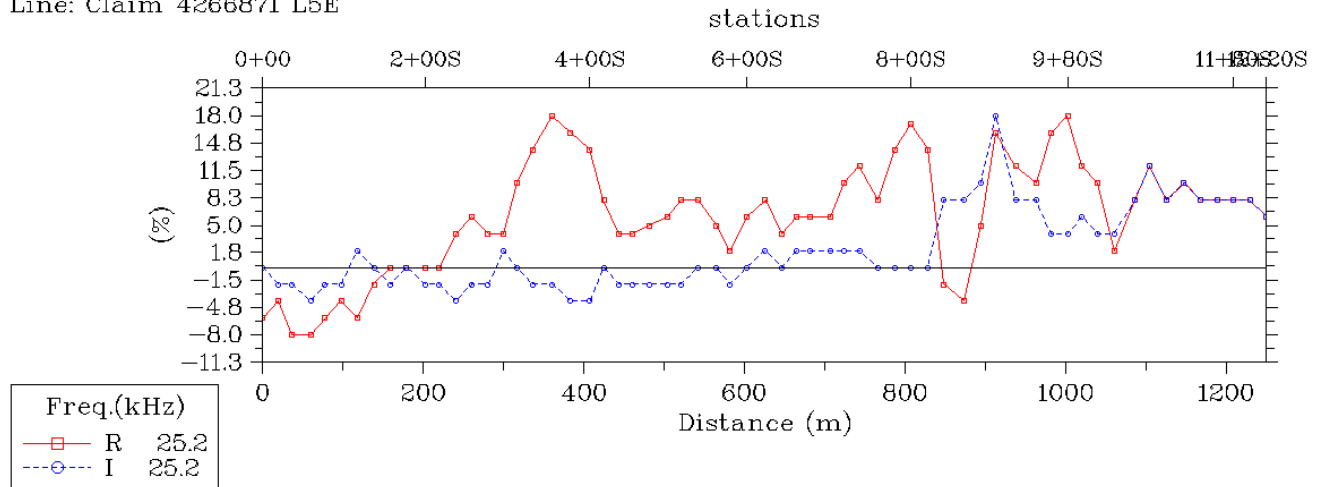
Profiles Line SB5E Figure 2 Fraser Filter

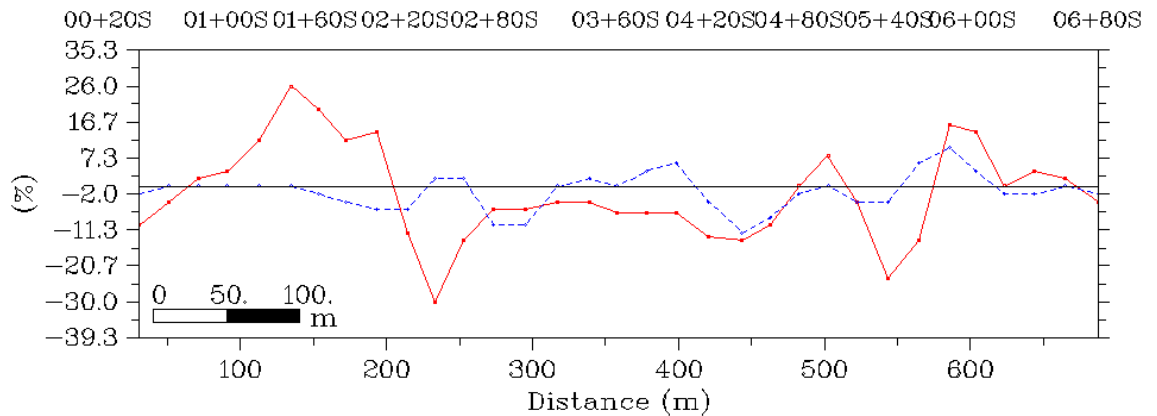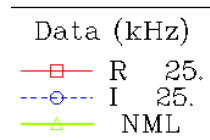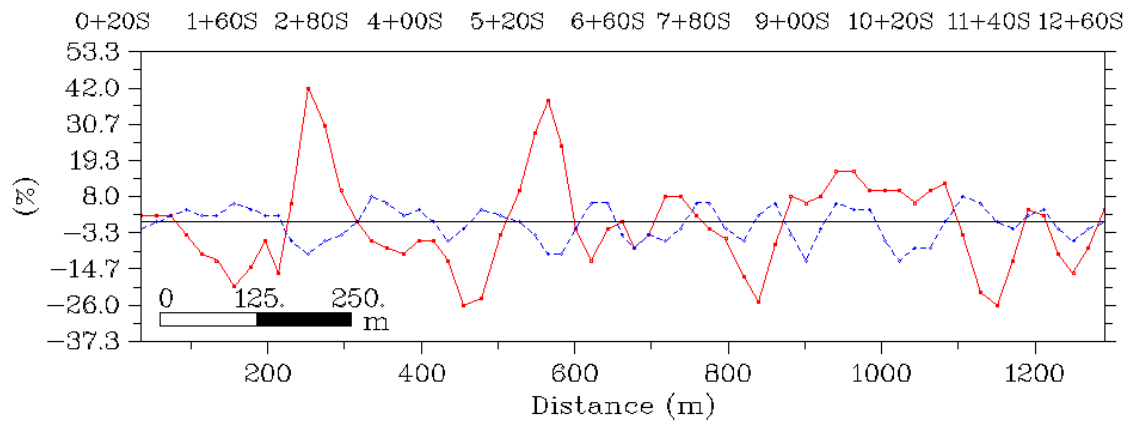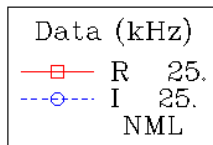Fraser Filter — from raw data
Line: Claim 4266871 L5E
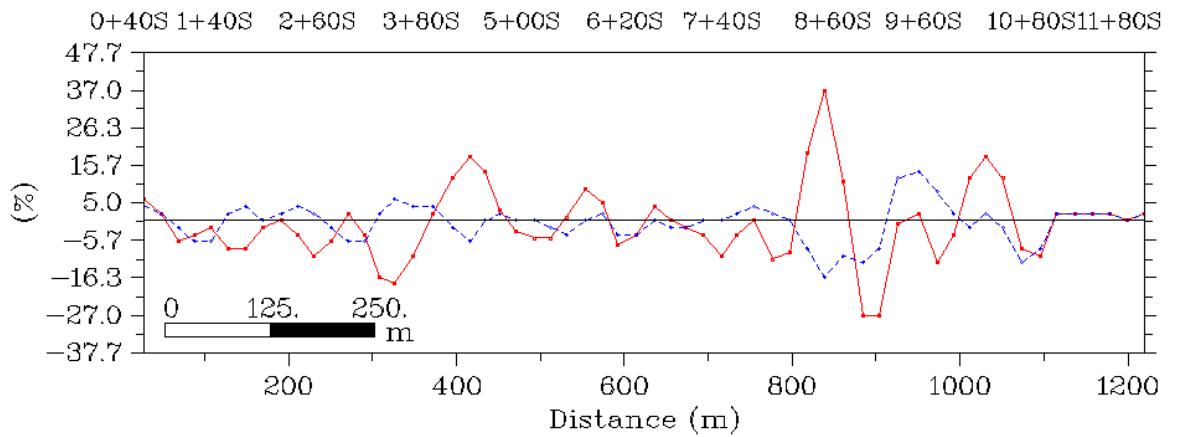
Profiles Line SB6E Figure 1 Raw Data

VLF−EM raw data
Line: Claim 4266871 SB6E

stations

Freq.(kHz)
R   25.2
I   25.2
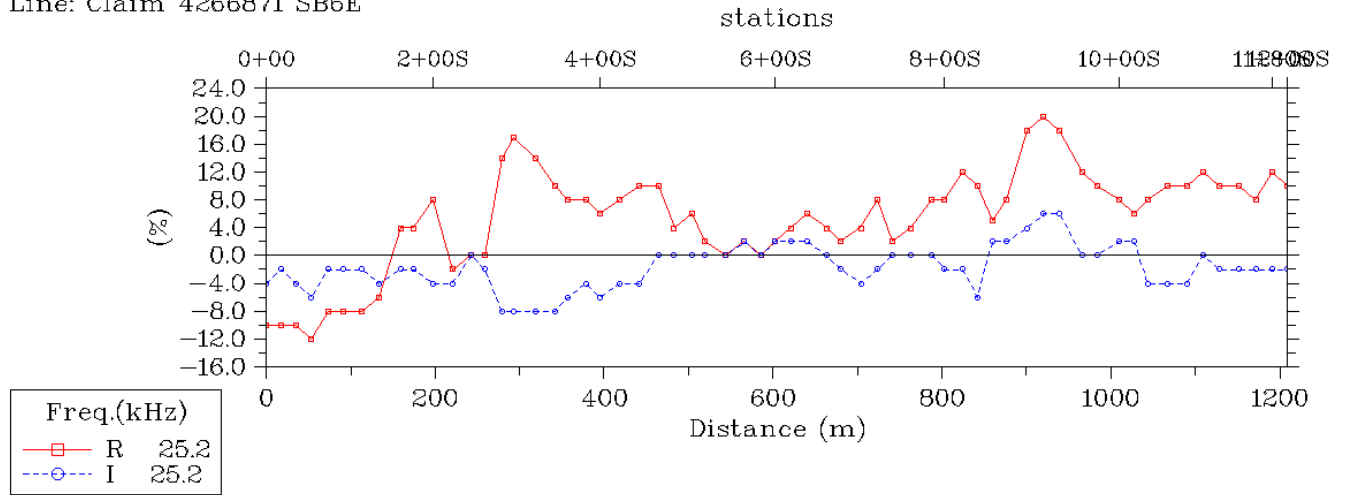
Profiles Line SB6E Figure 2 Fraser Filter

Data (kHz)
R   25.
I   25.
NML

Fraser Filter − from raw data
Line: Claim 4266871 SB6E
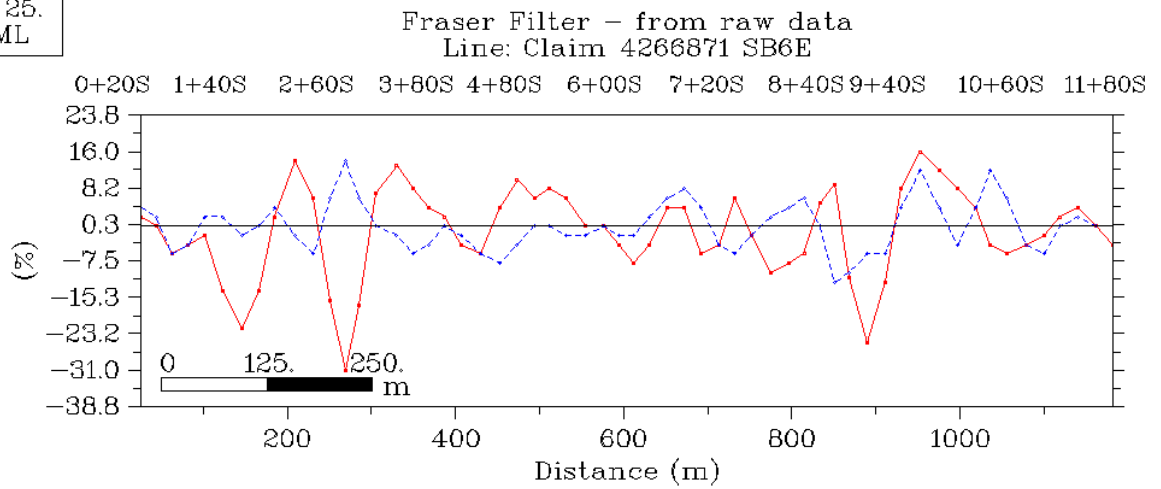
Appendix 1 EM16 Specifications

EM16 SPECIFICATIONS

MEASURED QUANTITY	Inphase and quad-phase components of vertical magnetic field as a percentage of horizontal primary field. (i.e. tangent of the tilt angle and ellipticity).
SENSITIVITY	Inphase: ±150% Quad-phase: ± 40%
RESOLUTION	±1%
OUTPUT	Nulling by audio tone. Inphase indication from mechanical inclinometer and quadphase from a graduated dial.
OPERATING FREQUENCY	15-25 kHz (15-30 kHz optional) VLF Radio Band. Station selection done by means of plug-in units.
OPERATOR CONTROLS	ON/OFF switch, battery test push button, station selector switch, audio volume control, quadrature dial, inclinometer.
POWER SUPPLY	6 disposable 'AA' cells.
DIMENSIONS	53 x 21.5 x 28 cm
WEIGHT	Instrument: 1.8 kg Shipping: 8.35 kg

CAUTION:

EM16 inclinometer may be damaged by exposure to temperatures below -30°c. Warranty does not cover inclinometers damaged by such exposure.

EM16 SPECIFICATIONS

MEASURED QUANTITY	Inphase and quad-phase components of vertical magnetic field as a percentage of horizontal primary field. (i.e. tangent of the tilt angle and ellipticity).
SENSITIVITY	Inphase: ±150% Quad-phase: ± 40%
RESOLUTION	±1%
OUTPUT	Nulling by audio tone. Inphase indication from mechanical inclinometer and quadphase from a graduated dial.
OPERATING FREQUENCY	15-25 kHz (15-30 kHz optional) VLF Radio Band. Station selection done by means of plug-in units.
OPERATOR CONTROLS	ON/OFF switch, battery test push button, station selector switch, audio volume control, quadrature dial, inclinometer.
POWER SUPPLY	6 disposable 'AA' cells.
DIMENSIONS	53 x 21.5 x 28 cm
WEIGHT	Instrument: 1.8 kg Shipping: 8.35 kg

CAUTION:

EM16 inclinometer may be damaged by exposure to temperatures below -30°c. Warranty does not cover inclinometers damaged by such exposure.

Appendix 2 Operating Manual for EM16 VLF-EM (attached)

GEONICS LIMITED

1745 Meyerside Dr. Unit 8 Mississauga, Ontario Canada L5T 1C6

Tel: (905) 670-9580
Fax: (905) 670 9204
E-mail: geonics@geonics.com
URL: http://www.geonics.com

OPERATING MANUAL

for

EM16 VLF-EM

June 1997

OPERATING MANUAL

for

EM16 VLF-EM

June 1997

<u>INDEX</u>   <u>Page</u>

EM16 SPECIFICATIONS

MEASURED QUANTITY   Inphase and quad-phase components
                            of vertical magnetic field as a
                            percentage of horizontal primary
                            field. (i.e. tangent of the tilt
                            angle and ellipticity).

SENSITIVITY   Inphase: ±150%

                            Quad-phase: ± 40%

RESOLUTION   ±1%

OUTPUT   Nulling by audio tone. Inphase in-
                            dication from mechanical inclinometer
                            and quadphase from a graduated dial.

OPERATING FREQUENCY   15-25 kHz (15-30 kHz optional) VLF
                            Radio Band. Station selection done by
                            means of plug-in units.

OPERATOR CONTROLS   ON/OFF switch, battery test push
                            button, station selector switch,
                            audio volume control, quadrature dial,
                            inclinometer.

POWER SUPPLY   6 disposable 'AA' cells.

DIMENSIONS   53 x 21.5 x 28 cm

WEIGHT   Instrument: 1.8 kg

                            Shipping: 8.35 kg

CAUTION:
_____

                            EM16 inclinometer may be damaged
                            by exposure to temperatures
                            below -30°c. Warranty does
                            not cover inclinometers damaged
                            by such exposure.

FIG. 1 EM 16

INCLINOMETER

QUADRATURE CONTROL

OPTICAL LENS

OFF-ON SWITCH

EARPHONE JACK

SPEAKER

CASE

VOLUME CONTROL

STATION SELECTOR

BATTERY TEST

HANDLE—VERTICAL & HORIZONTAL COIL
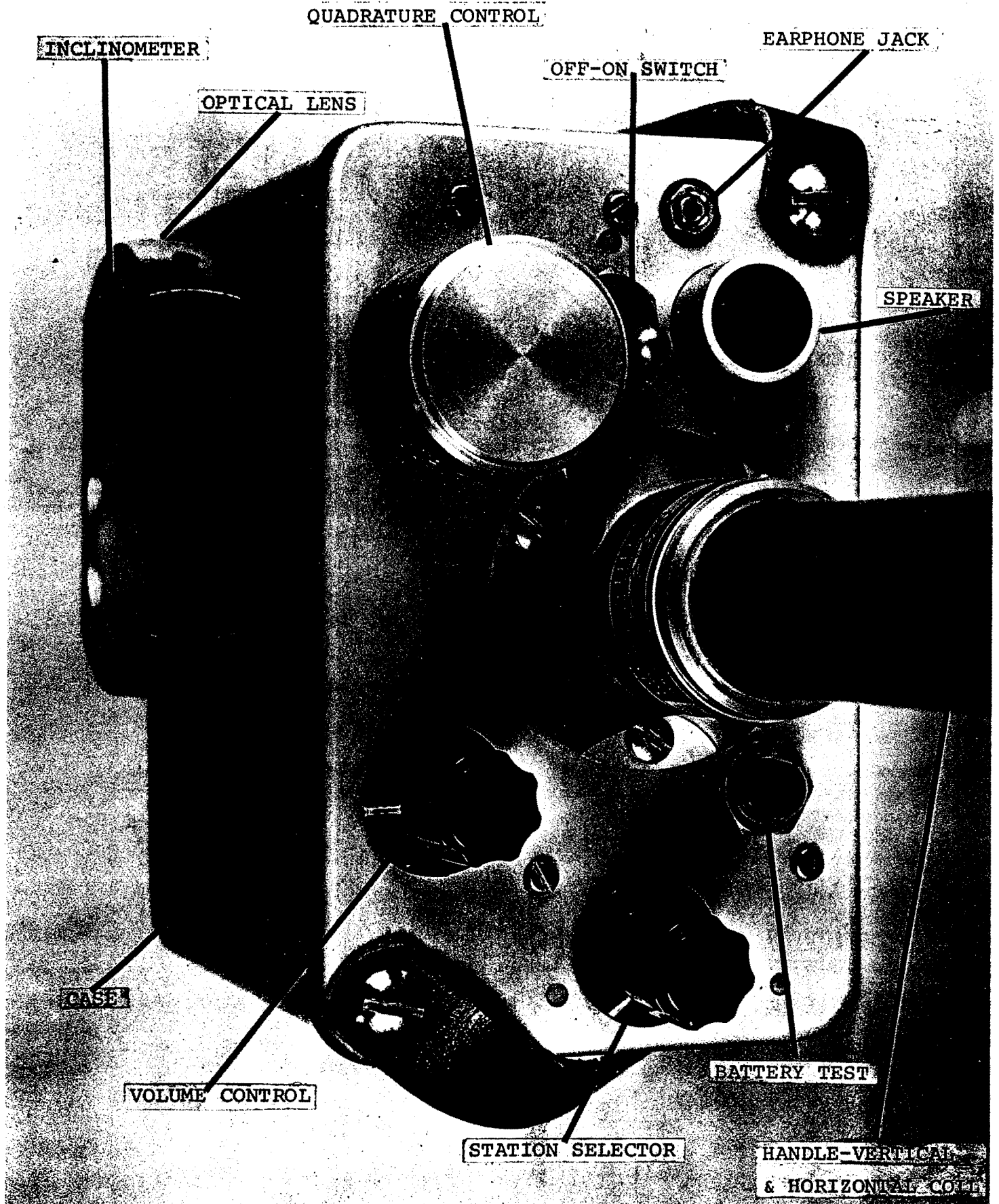
PRINCIPLES OF OPERATION

The VLF-transmitting stations operating for communications with submarines have a vertical antenna. The Antenna current is thus vertical, creating a concentric horizontal magnetic field around them. When these magnetic fields meet conductive bodies in the ground, there will be secondary fields radiating from these bodies. (See Figures 3 & 4). This equipment measures the vertical components of these secondary fields.

The EM16 is simply a sensitive receiver covering the frequency band of the VLF-transmitting stations with means of measuring the vertical field components.

The receiver has two inputs, with two receiving coils built into the instrument. One coil has normally vertical axis and the other is horizontal.

The signal from one of the coils (vertical axis) is first minimized by tilting the instrument. The tilt-angle is calibrated in percentage. The remaining signal in this coil is finally balanced out by a measured percentage of a signal from the other coil, after being shifted by 90°. This coil is normally parallel to the primary field, (See instrument Block Diagram - Figure 2).

Thus, if the secondary signals are small compared to the primary horizontal field, the mechanical tilt-angle is an accurate measure of the vertical real-component, and the compensation $\pi/2$-signal from the horizontal coil is a measure of the quadrature vertical signal.

Some of the properties of the VLF radio wave in the ground are outlined by Figures 4 thru 9.

ACCOMPANYING NOTES FOR FIGURES 2 - 9

FIGURE 2   is the block diagram of the EM16. The diagram is self-explanatory. Both the coils (reference and signal coil) are housed in the lower part of the handle. The directions of the axis of the coils are as follows: The reference coil axis is basically horizontal and is kept more or less parallel to the primary field during measurement. The signal coil is at right angles to the reference coil and its axis is, of course, vertical.

The signal amplifier has the two inputs, one connected to the signal coil and one to the reference channel. By tilting the coils, the operator minimizes the signal from the signal (vertical axis) coil. Any remaining signal is reduced to zero by the quadrature control in the reference channel. The signal amplifier has zero output

FIGURE 2   Continued...

when both input signals are equal in amplitude and phase. Thus, the setting of the quadrature control for minimum output from the receiver indicates the relative amount of the quadrature signal of the vertical coil. The measured value does not depend on the absolute value of the signal, only the relative values are measured.

FIGURE 3   shows the proper planning of survey in relation to the direction of strike and primary field, direction of survey lines etc.

FIGURE 4   explains the time delay (phase lag) ϕ of travelling electromagnetic wave above and in the conductive ground. The amplitude of the wave in the ground is also attenuated.

FIGURE 5   shows on the left the physical direction of the primary (H_x) and secondary (H_z) field vectors in relation to conductive ground and target. The location of secondary current distribution in the target is shown schematically. We see that most current concentration is in the upper edge of the good conductor. The return secondary current is more spread due to the diminishing primary field in the conductive rock. On the right, the time vectors show the retarded phase of H_x in the target and the phase advance of the secondary field H_z compared to H_x. We must remember that the H_z will have additional phase lag when it penetrates back towards the surface.

This figure shows a positive real component of the H_z while the quadrature remains negative.

FIGURE 6   This graph shows the primary field attenuation in nepers, relative amplitude and phase lag in radians of the primary field as function of depth and conductivity of the ground. This graph is for 20 kHz.

FIGURE 7   shows the maximum obtainable amplitude H_z from a sphere or horizontal cylinder as a function of the radius-to-depth ratio. The schematic on the left shows the depth determination for the spherical or cylindrical target.

FIGURE 7   Continued...

The equation for the phase shift and attenuation
of the primary field in conductive material, where
$\sigma/\epsilon\omega \gg 1$ is as follows:

$$\alpha = \beta = \sqrt{\frac{\omega\mu\sigma}{2}}$$

where α = attenuation, nepers/m
       β = phase lag, radian/m
       ω = $2\pi f$
       μ = magn. permeability = $4\pi \times 10^{-7}$

       σ = mhos/m

FIGURE 8   This graph gives the amplitude and phase shift of
the field (in conductive media) as function of
skin depth, $\delta = 1/\alpha$.

This equation gives the skin-depth in meters for
certain conductivity and frequency. Normalize
this to one, and the graph in Figure 8 gives the
amplitude and phase shift of the wave at any
relative depth.

FIGURE 9   The vertical field from a long wire source is
plotted here. A vertical semi-infinite sheet
target would be simulated this way. In practice
it hardly works accurately due to the spread of
the secondary current in the target because of
the finite conductivity and the attenuation and
phase shift of the primary field as function of
depth.
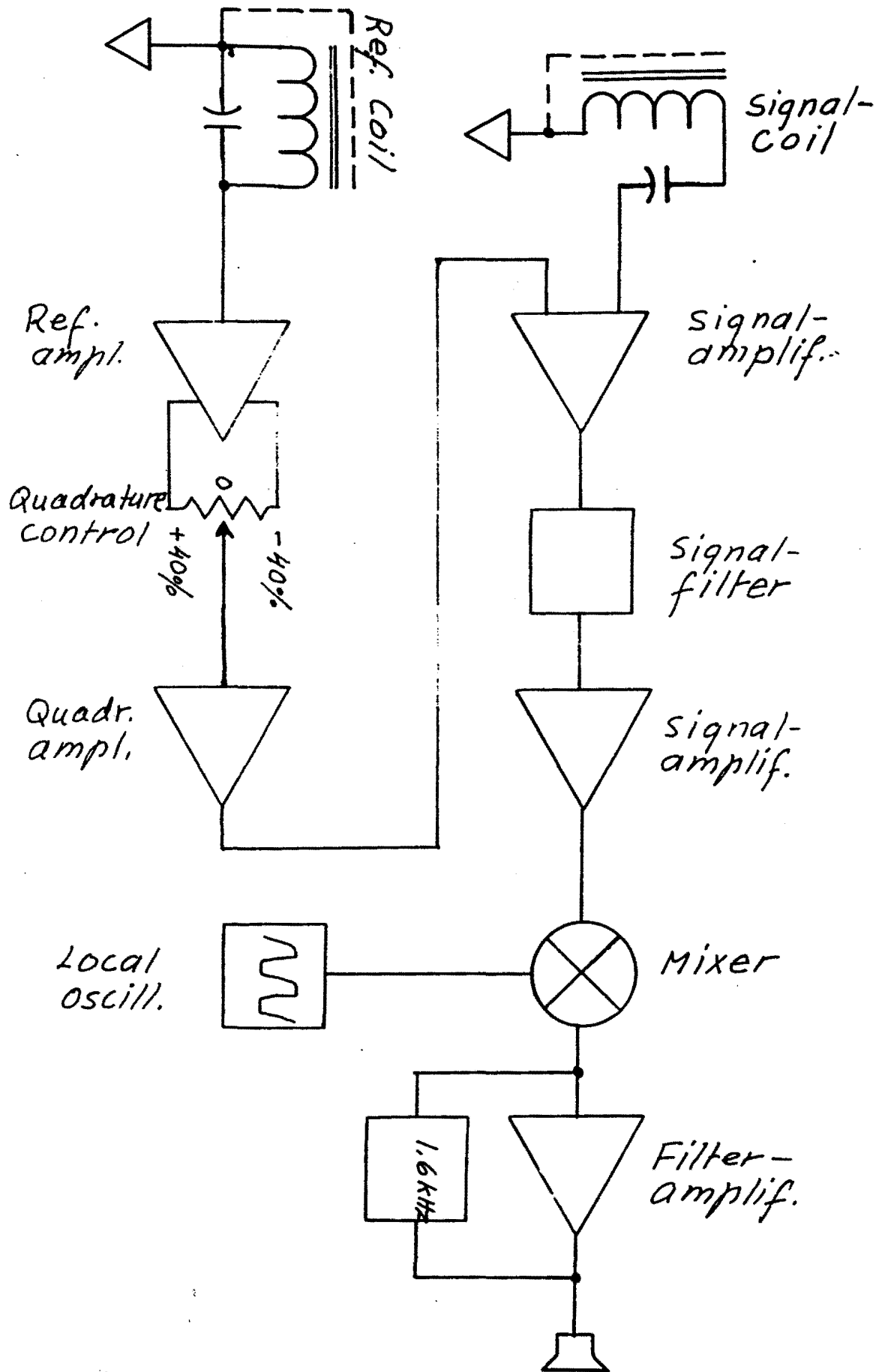
FIG. 2

EM16 VLF-EM
Block Diagram
GEONICS LTD.

Direction of readings

Finding the direction of primary field

EM16

Best survey line direction

Optimum strike direction

Transmitting station
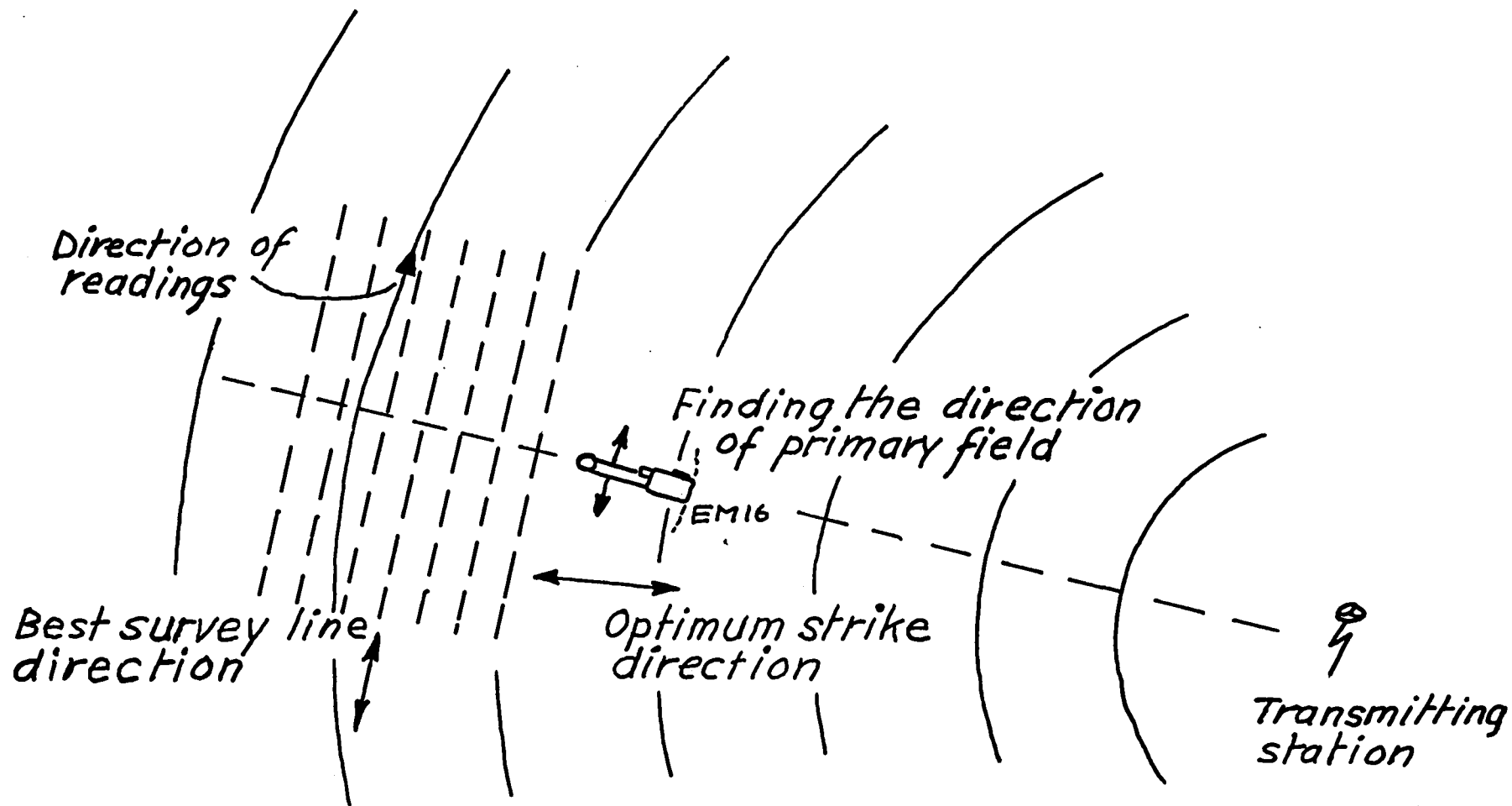
Planning of survey

FIG. 3
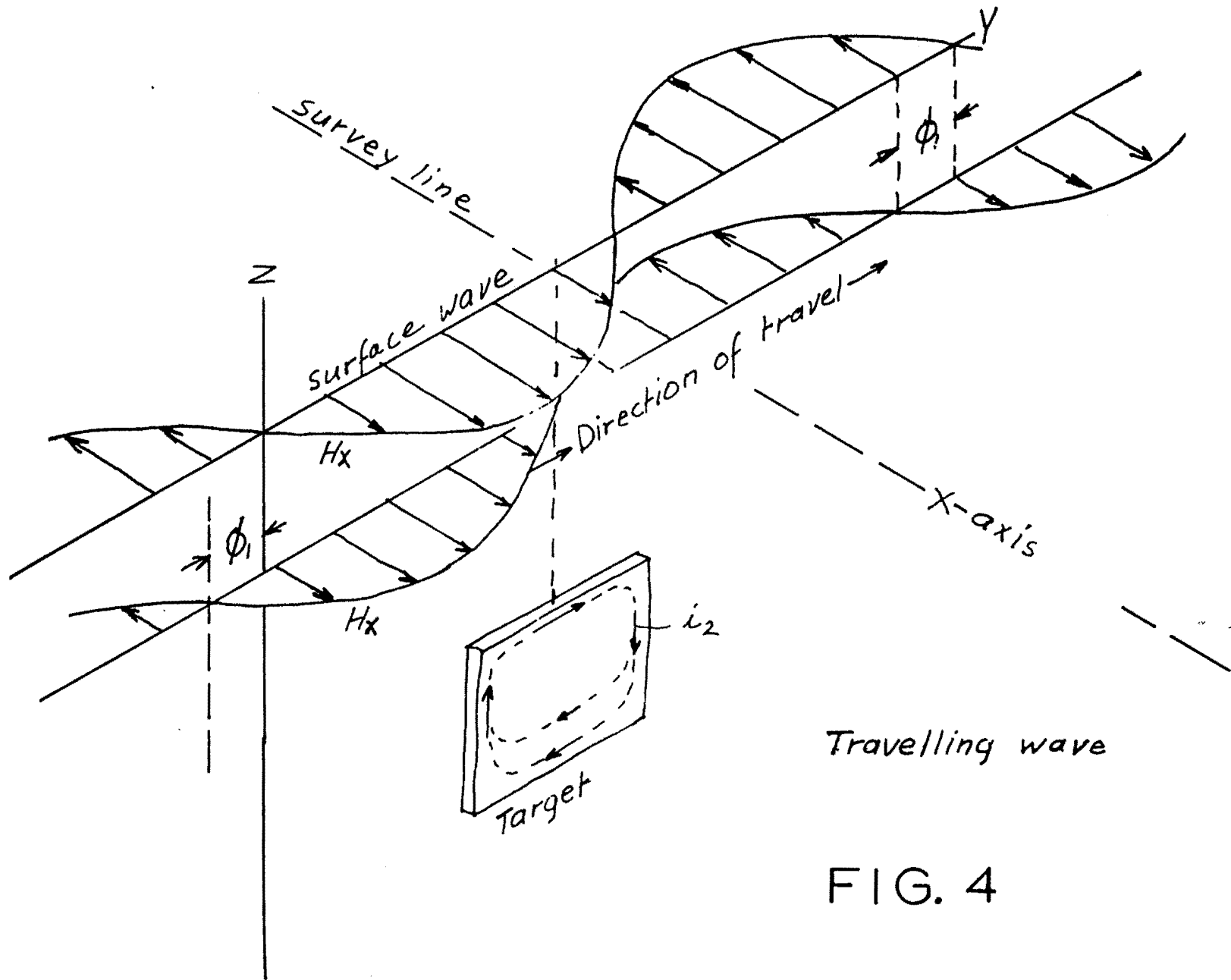
FIG. 4

Travelling wave
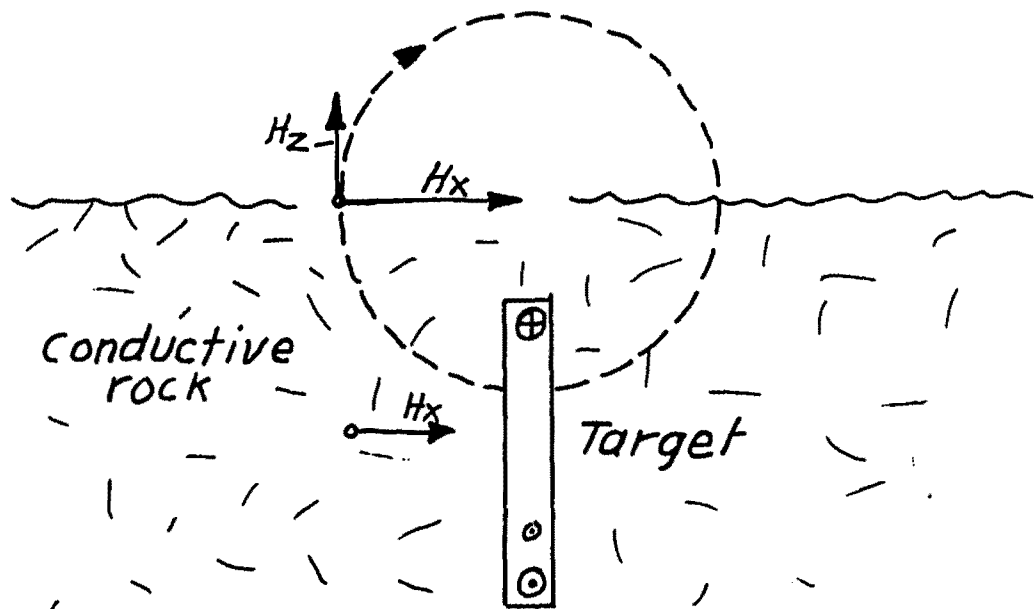
Directional vectors

H_x = primary field
H_z = sec. field, vert. component
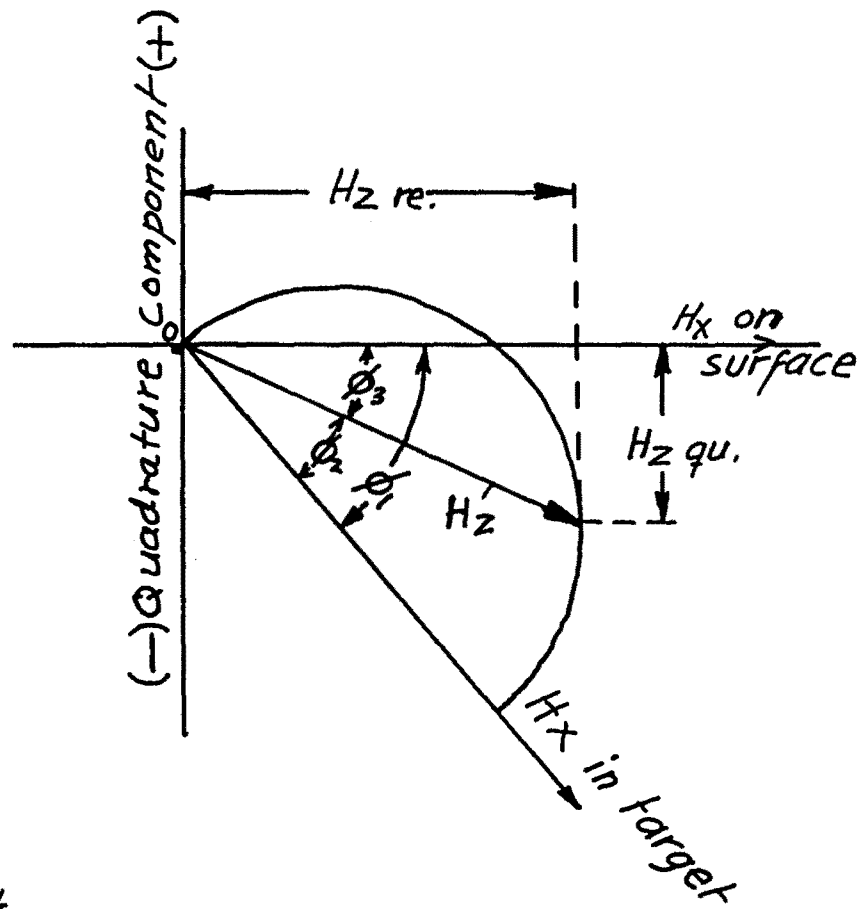
Time vectors

Conductive target in conductive medium

FIG. 5

FIG. 6

Conductivity 6 — mho/m

Amplitude

Attenuation — nepers or phase shift — radians
f = 20 kHz

Depth — meters

Example:
Effective depth = 50 m
$\sigma^{-1} = 10^{-3}$ mho-m
Primary phase lag =
= .45 radian
Primary amplitude =
= 63%
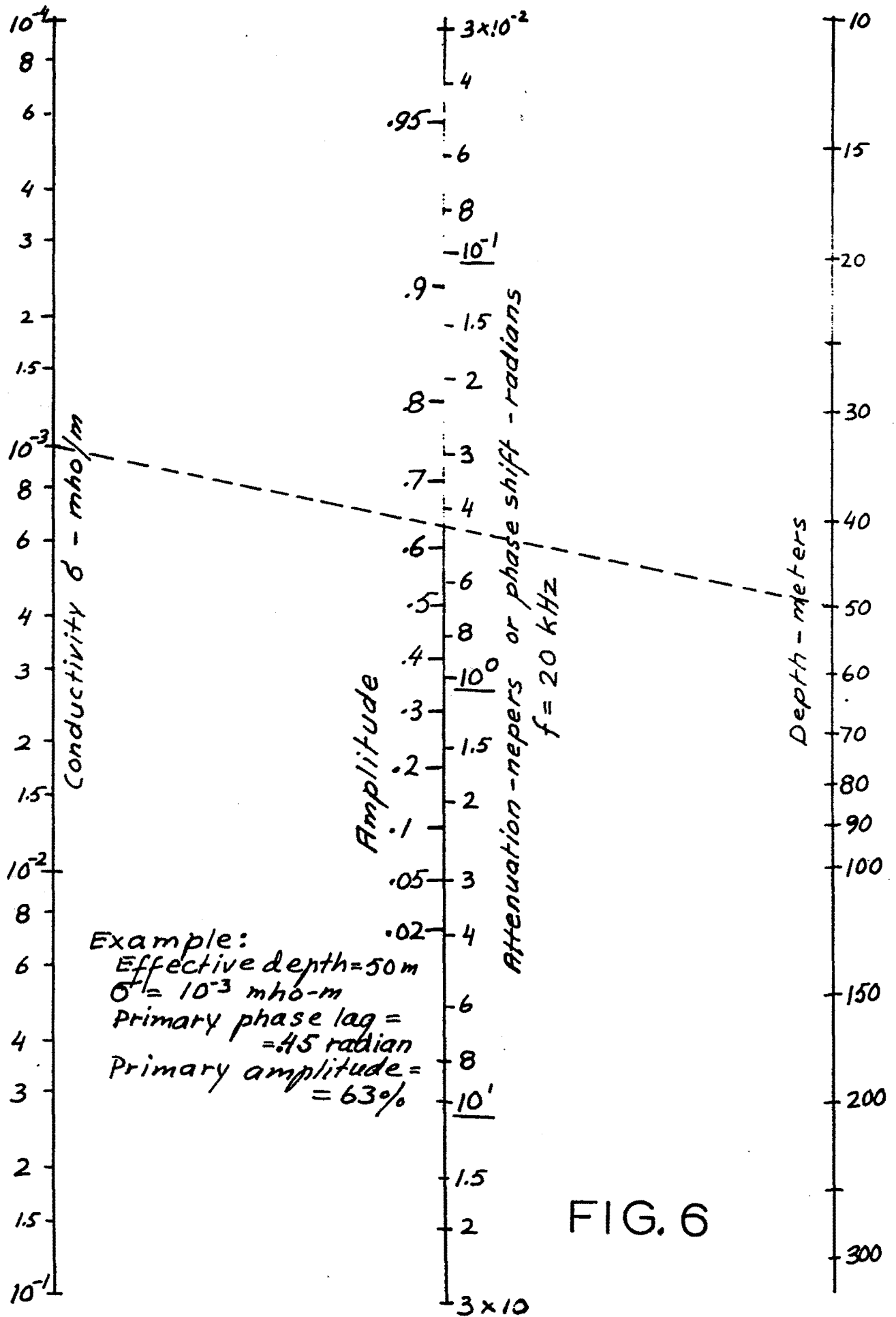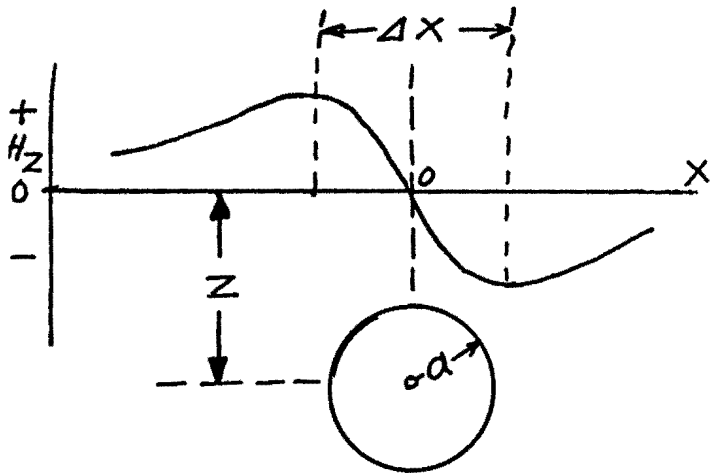
Long cylinder or sphere in horizontal field $H_x = 1$

Depth Z = 1.16 ΔX for cylinder,
Z = ΔX for sphere
$\delta = \infty$
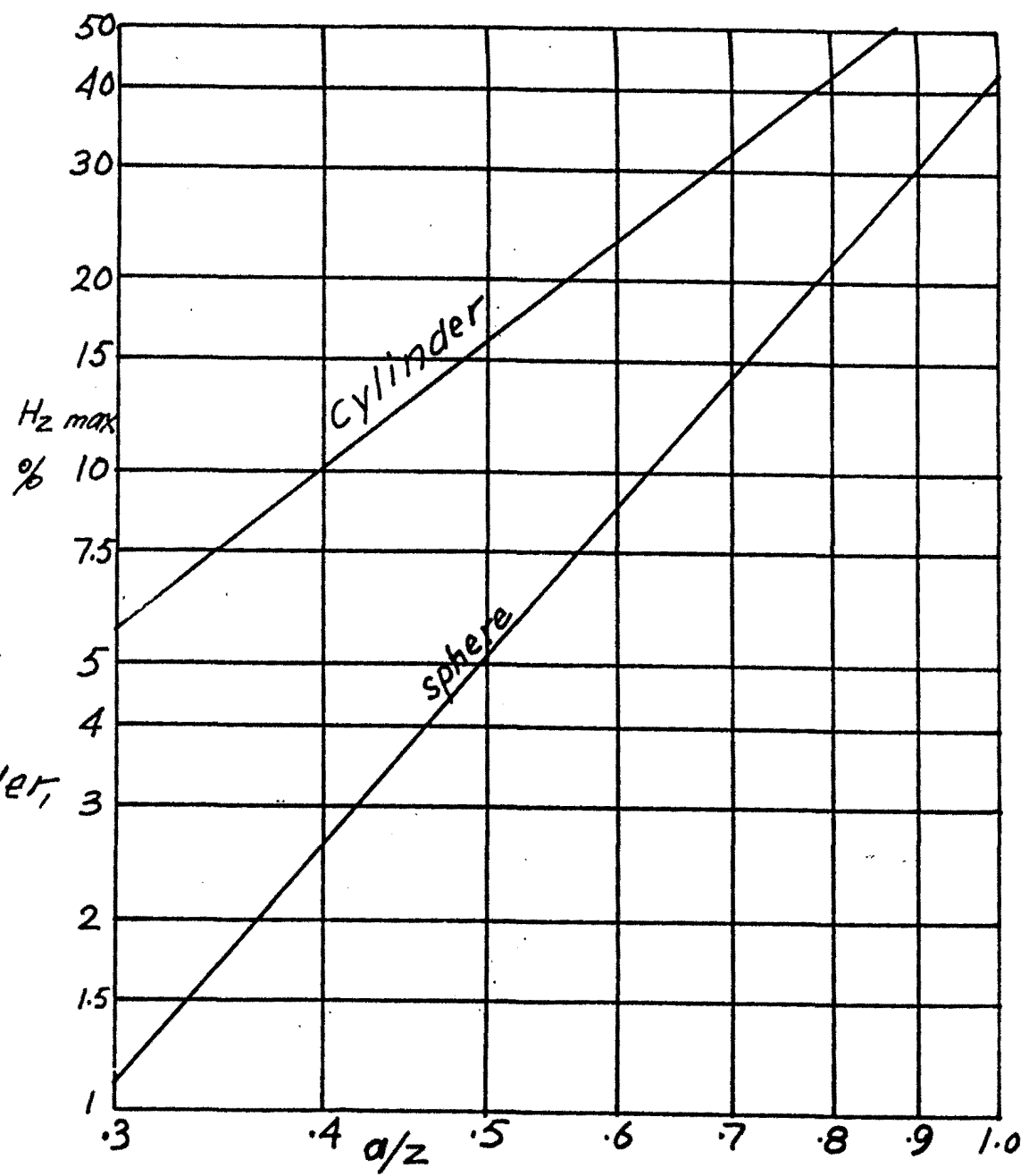
FIG. 7

Maximum available anomaly from a sphere and cylinder

Primary field in
conductive rock.

Depth, phase shift,
amplitude

FIG. 8

Hz

1.0

.9

.8

.7

.6

.5

.4

.3

.2

.1

0

X   -10   -9   -8   -7   -6   -5   -4   -3   -2   -1   0   +1

Long wire z=-1

Vertical Field
Long wire source

FIG. 9
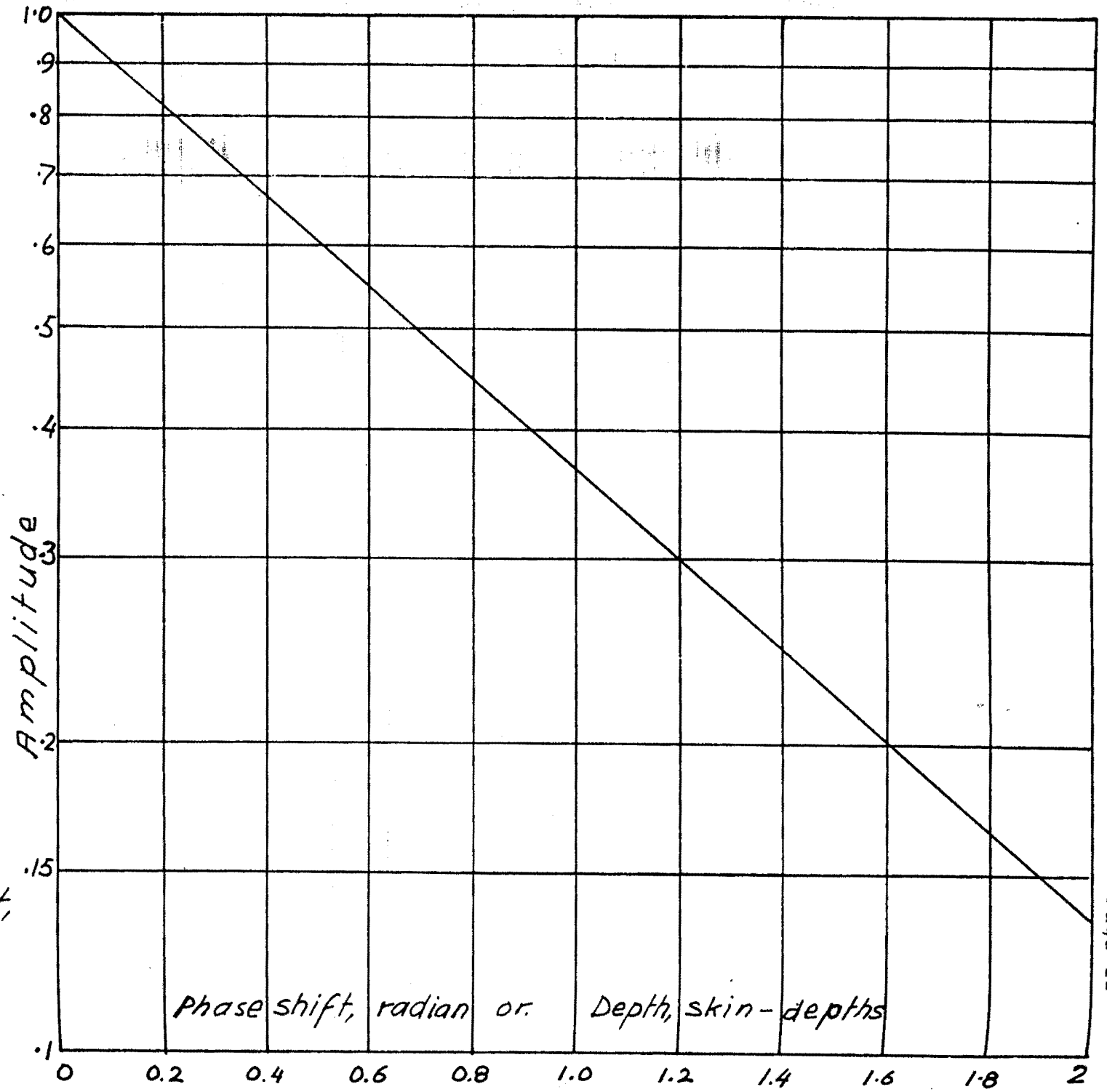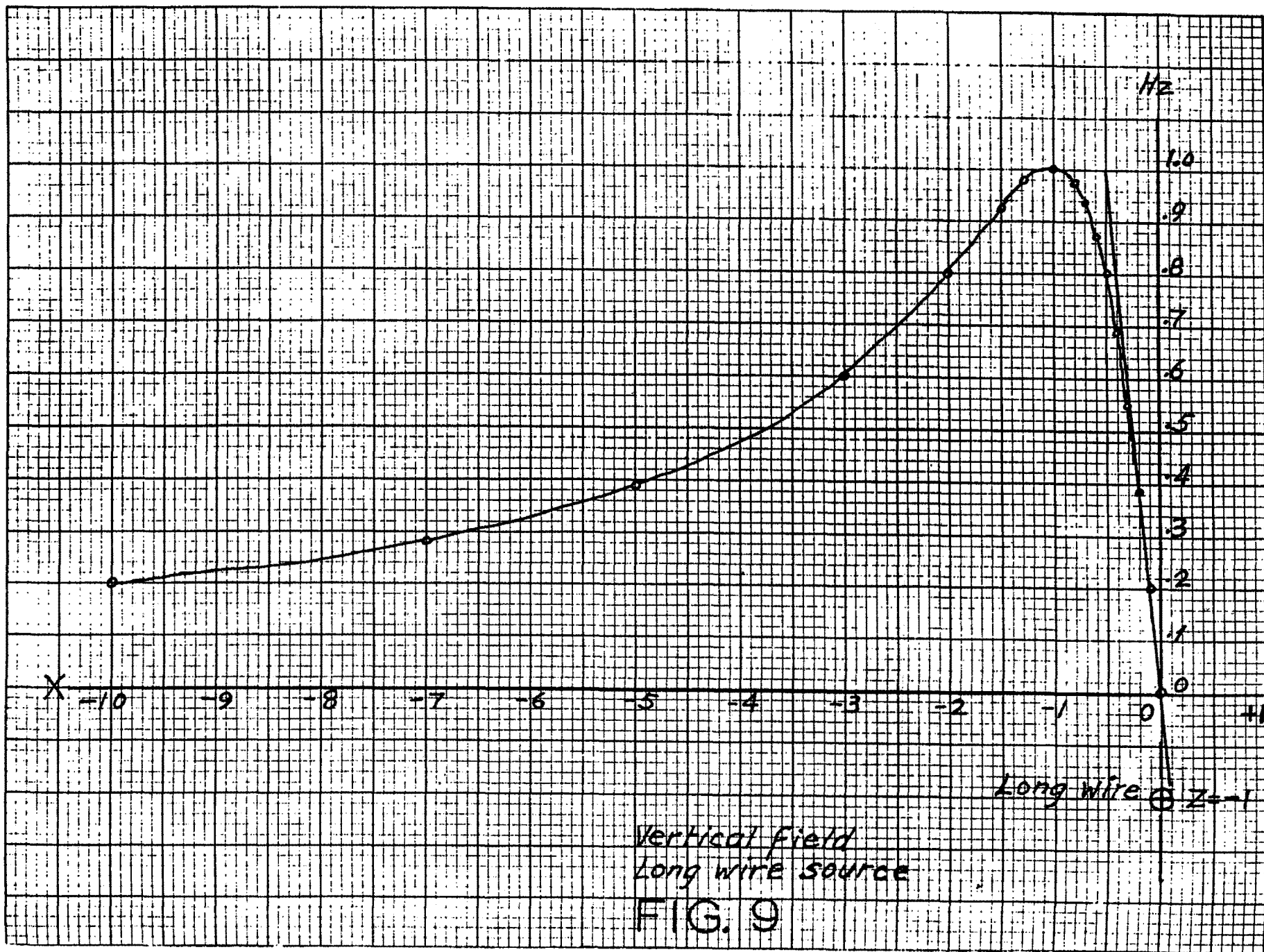
SELECTION OF THE STATION

The magnetic field lines from the station are at right
angles to the direction of the station. Always select
a station which gives the field approximately at right
angles to the main strike of the ore bodies or geological
structure of the area you are presently working on. In
other words, the strike of geology should point to the trans-
mitter. (See Figure 3). Of course, $\pm 45^{\circ}$ variations are
tolerable in practice.

Tuning of the EM16 to the proper transmitting station is
done by means of plug-in units inside the receiver. The
instrument takes two selector-units simultaneously. A
switch is provided for quick switching between these two
stations.

To change a plug-in unit, open the cover on top of the instru-
ment, and insert the proper plug. (Figure 10) Close the cover
and set the selector switch to the desired plug-in.

On the following pages is a variety of information on the
most commonly used (i.e. reliable) VLF Transmitters including
transmission frequency, geographical location and their
scheduled maintenance periods.

VLF Transmitter Information

NORMAL MAINTENANCE PERIODS:

GBR   1000 to 1400 UT each Tue.

NAA   1200 to 2000 UT, testing 2000 to 2200 UT each Mon. (if holiday falls on
      Mon., maintenance will performed preceding Fri.), may be off 1800 to
      2000 UT Thu.

NAU   1200 to 2000 UT each Wed.

NDT   2300 to 0900 UT first Thu.-Fri. of month, 2300 to 0700 UT all other Thu.-Fri.

NLK   1600 to 2400 UT each Thu. (1500 to 2300 UT during daylight saving time)

NPM   1800 to 0400 UT last Wed.-Thu. of month, 1800 to 0200 UT all other Wed.-Thu.

NSS   No longer in operation.

NWC   0000 to 0800 UT each Mon. (if holiday falls on Mon., maintenance will be
      performed Tue.), may be off 0000 to 0400 UT Tue. (Wed. if holiday falls on
      Mon.)

For further information the U.S. Naval Observatory, Time Service Division, Washington, D.C.

may be contacted at (202) 653-1525.

VLF STATION INFORMATION

Station	Frequency	Location	Co-ordinates	Kw
FUO	15.1	Bordeaux, France	00W48-44N65	500
GBR	16.0	Rugby, England	01W11-52N22	750
JXZ	16.4	Helgeland, Norway	13E01-66N25	350
NAA	24.0	Cutler, Maine	67W17-44N39	1000
NAU	28.5	Aguada, Puerto Rico	67W11-18N23	100
JJI	22.2	Ebino City, Japan	130°E46'-32°No5'	500
NLK	24.8	Seattle, Washington	121W55-48N12	234
NPM	21.4	Lualualei, Hawaii	158W09-21N25	600
NWC	22.3	N.W. Cape, Australia	114E09-21S47	1000
UMS	17.1	Moscow, Russia	37E01-55N49	1000

Notes:

1. Use of NAU (Puerto Rico) 28.5 kHz requires factory modification of VLF instrument.

2. In the event that an EM16 unit is being returned to Geonics for:

    - modification of frequency range to include NAU, 28.5 kHz, or

    - addition of the 16R resistivity attachment,

    please ensure that all station plug-ins are also returned, for proper calibration.

GEOGRAPHIC USE OF VLF STATIONS

The following list of plug-ins are the standard plug-in crystals provided with the EM16 for the various areas listed throughout the world.

Europe	:	FUO GBR JXZ NAA UMS
North America		
North	:	NAA NLK GBR
West & Alaska	:	NAA NLK NPM
Midwest	:	NAA NLK
East	:	NAA NLK GBR
South	:	NAA NLK NAU
Mexico & Central America	:	NAA NAU NLK NPM
South America		
North	:	GBR NAA NAU
West	:	GBR NAA NAU NPM
Asia		
East	:	JJI NWC UMS
Central	:	FUO UMS
Japan	:	JJI NPM NWC
Australia	:	
East	:	NWC NPM JJI
Africa		
North	:	NAA NWC FUO GBR UMS
West	:	NAA NWC FUO GBR UMS
Central	:	NAA NWC FUO GBR UMS
East	:	NAA NWC FUO GBR UMS NWC
South	:	NAA NWC (FUO GBR UMS 10% noise)

Fig 10

Direction to station

Primary Field

Survey Line

Fig.11

Primary Field And Survey Lines

Fig.12

Conductor Ahead

Fig.13

Conductor Behind →

Fig.14

IN-PHASE

RECONNAISANCE LINE 0+00

+40%
+30%
+20%
+10%

1E   3E   2E   1E   BL   1W   2W   3W   4W

-10%
-20%
-30%
-40%

OUT-OF-PHASE

felsic flow
agglomerate
MASSIVE PYRITE
sulphides
DDHL-146
POND
DUMP
OPEN PIT
DIABASE DYKE
basalt
100'
10% sulphides
25% massive sulphides
10-25% sulphides
10% sulphides
10-25% sulphides
grey chert
minor pyrite
20% sulphides
agglomerate
transition zone
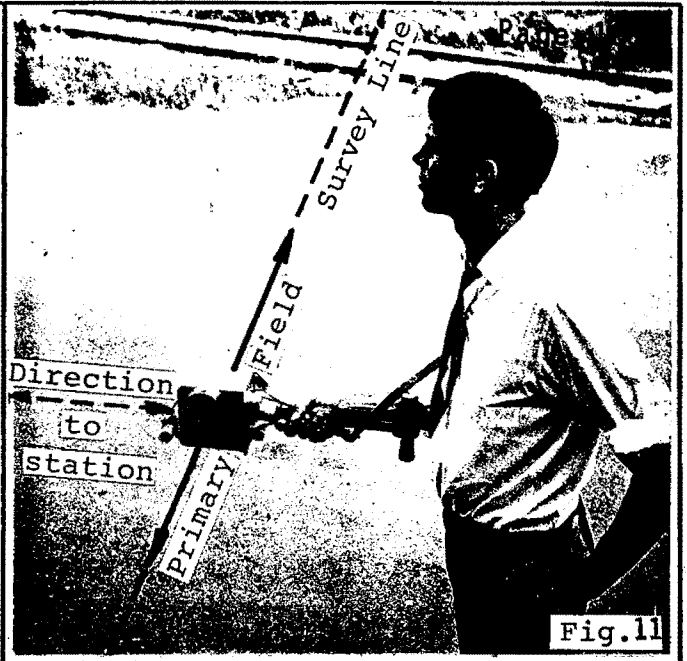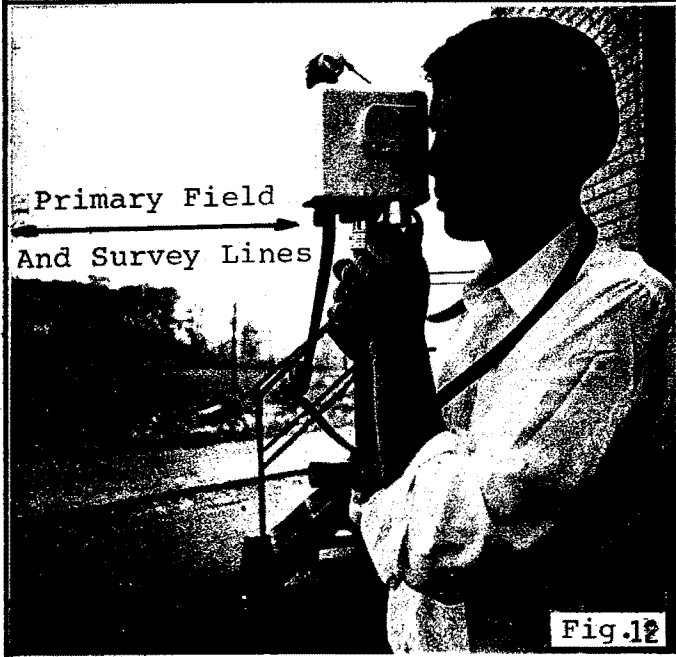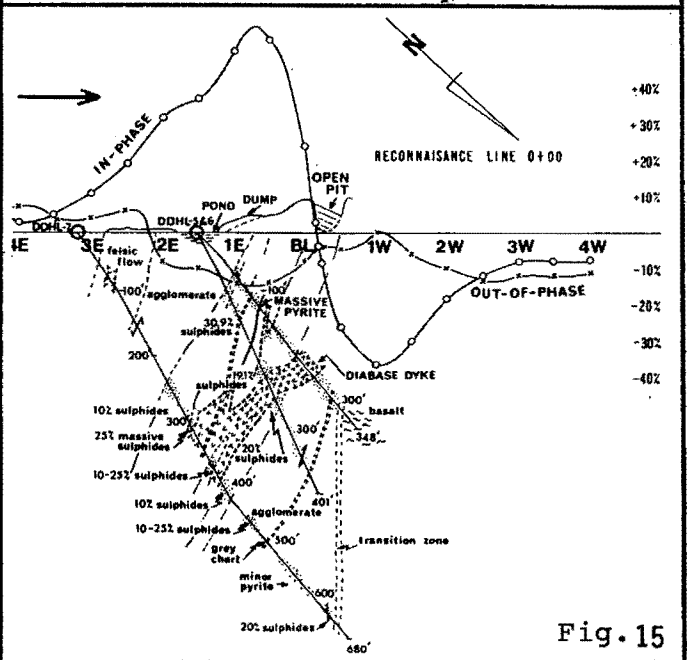
Fig.15

FIELD PROCEDURE

Orientation & Taking a Reading

The direction of the survey lines should be selected approximately along the lines of the primary magnetic field, <u>at right angles to the direction to the station being used.</u> Before starting the survey, the instrument can be used to orient oneself in that respect. By turning the instrument sideways, the signal is minimum when the instrument is pointing towards the station, thus indicating that the magnetic field is at right angles to the receiving coil inside the handle.(Fig.11).

To take a reading, first orient the reference coil (in the lower end of the handle) along the magnetic lines.(Fig.12) Swing the instrument back and forth for minimum sound intensity in the speaker. Use the volume control to set the sound level for comfortable listening. Then use your left hand to adjust the quadrature component dial on the front left corner of the instrument to further minimize the sound. After finding the minimum signal strength on both adjustments, read the inclinometer by looking into the small lens. Also, mark down the quadrature reading.

While travelling to the next location you can, if you wish, keep the instrument in operating position. If fast changes in the readings occur, you might take extra stations to pinpoint accurately the details of anomaly.

The dials inside the inclinometer are calibrated in positive and negative percentages. If the instrument is facing 180° from the original direction of travel, the polarities of the readings will be reversed. <u>Therefore, in the same area take the readings always facing in the same direction even when travelling in opposite way along the lines.</u>

The lower end of the handle, will as a rule, point towards the conductor. (Figs.13 & 14) The instrument is so calibrated that when approaching the conductor, the angles are positive in the in-phase component. Turn always in the same direction for readings and mark all this on your notes, maps, etc.

THE INCLINOMETER DIALS

The right-hand scale is the in-phase percentage(ie. Hs/Hp as a percentage). This percentage is in fact the tangent of the dip angle. To compute the dip angle simply take the arctangent of the percentage reading divided by 100. See the conversion graph on the following page.

The left-hand scale is the secant of the slope of the ground surface. You can use it to "calculate" your distance to the next station along the slope of the terrain.
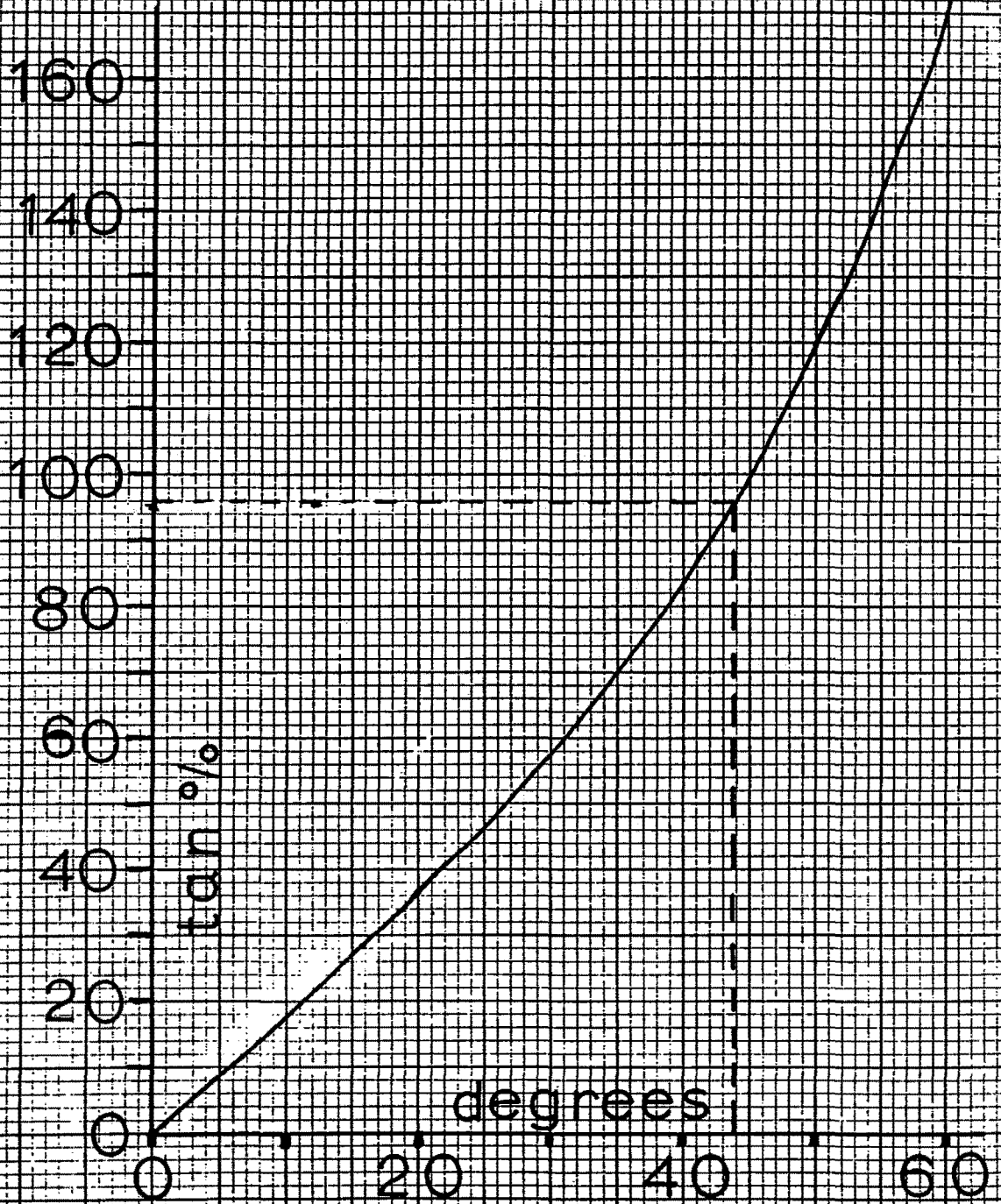
EM16 in-phase, % to degrees

example: 96% = 44°

(1)   Open both eyes.

(2)   Aim the hairline along the slope to the next station
      to about your eye level height above ground.

(3)   Read on the left scale directly the <u>distance necessary</u>
      <u>to measure along the slope to advance 100 (ft) horizon-</u>
      <u>tally.</u>

We feel that this will make your reconnaissance work easier.
The outside scale on the inclinometer is calibrated in degrees
just in case you have use for it.

PLOTTING THE RESULTS

For easy interpretation of the results, it is good practice
to plot the actual curves directly on the survey line map
using suitable scales for the percentage readings. (Fig.15)
The horizontal scale should be the same as your other maps on
the area for convenience.

A more convenient form of this data is easily achieved by
transforming the zero-crossings into peaks by means of a
simple numerical filtering technique. This technique is
described by D.C. Fraser in his paper "Contouring of VLF-EM
Data", Geophysics, Vol. 34, No. 6. (December 1969)pp958-967.
A reprint of this paper is included in this manual for the
convenience of the user.

This simple data manipulation procedure which can be imple-
mented in the field produces VLF-EM data which can be contoured
and as such provides a significant advantage in the evaluation
of this data.

INTERPRETATION

The VLF primary field's magnetic component is horizontal. Local conductivity inhomogeneities will add vertical components. The total field is then tilted locally on both sides of a local conductor. This local vertical field is not always in the same phase as the primary field on the ground surface. The EM16 measures the in-phase and quadrature components of the vertical field.

When the primary field penetrates the conductive ground and rock, the wave length of the wave becomes very short, maybe only few tens of meters, depending on conductivity and frequency. At the same time the wave travels practically directly downwards. The amplitude of the field also decreases very fast, completely disappearing within one wavelength. The magnetic field remains, however, horizontal.

Figure 16 shows graphically the length and phase angle of the primary field penetrating into a conductive material.

The phase shift in radians per meter and the attenuation in nepers per meter (1/e) is:

$$\beta = \alpha = \left[\frac{\omega \, \mu \, \sigma}{2} \right]^{\frac{1}{2}}$$

where

$\omega = 2\pi f$

$\mu = \mu_o \mu_r = 4\pi \times 10^{-7}$

$\sigma = $ conductivity mho/m

Figure 16 also reminds us of the fact that all secondary fields have a small (or large in poor conductors) positive phase shift in the target itself due to its resistive component, and that the secondary fields have another negative phase shift while penetrating back to surface from the upper edge of the target.

The targets are located somewhere in the depth scale (phase shift scale in this case). Suppose we have a semi-infinite vertical sheet target starting from the surface. Figure 17 shows that the total integrated primary field inphase and quadrature flux has a value of + 0.5 and - 0.5 respectively.

These two charts can be used to analyze the inphase and quadrature readings taken on both sides of the target. If one knows the actual conductivity of the overburden and the rock, the task is easier. Because of the many variables involved the precise analysis is usually impossible.

The most frequently encountered and easily solved problem is, however, the separation of surface conductors from the more interesting ones at depth. This is easily done by observing the negative quadrature signals compared to the usually positive or zero ones from the surface targets. See the sample profiles in Figures 18 and 19. This way we can often tell if we have a more interesting sulfide target under a swamp for example.
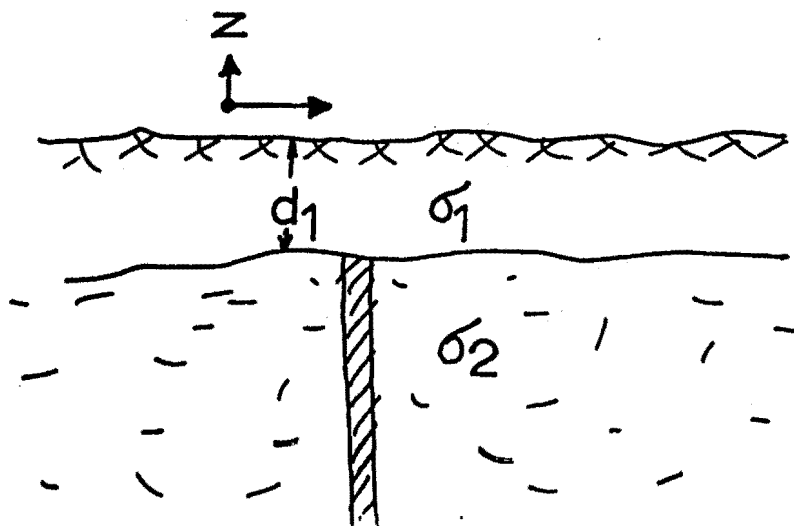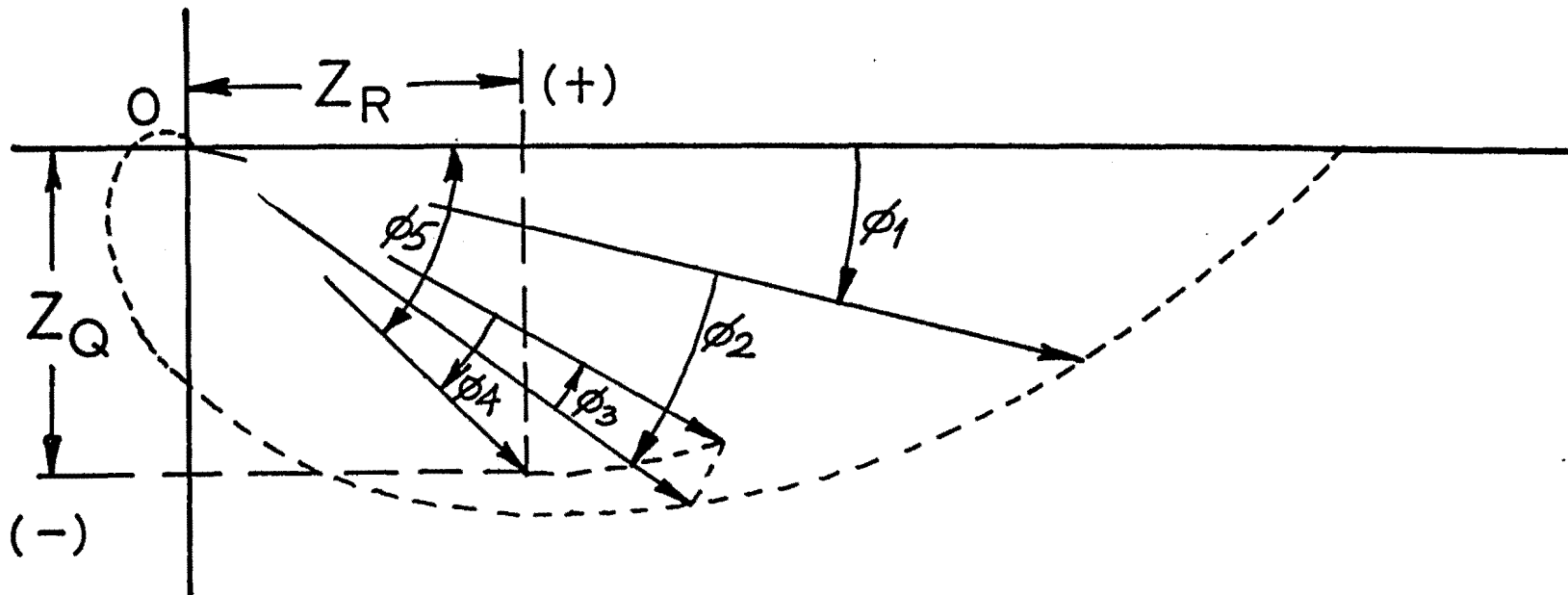
PHASE SHIFTS IN CONDUCTIVE MEDIUM

$\varnothing_1$ OVERBURDEN, DOWNWARD TRAVEL

$\varnothing_2$ ROCK FROM OVERBURDEN TO THE
        CENTER OF TARGET

$\varnothing_3$ SHIFT IN TARGET, FINITE CONDUCTIVITY

$\varnothing_4$ SECONDARY FIELD IN OVERBURDEN AND
        SOME ROCK

$\varnothing_5$ TOTAL OF ALL $\varnothing_1$ TO $\varnothing_4$

Fig. 16

R = real component
Q = quadrature component
β = phase shift, rad/meter
$\emptyset_T$ = phase shift, total from surface
d_B = depth of bottom

Fig. 17

H →

100 ft.

40—

20—

(+)—

0

Dacite, aggl.

(—)—

20—

Porphyry

Banded
Pyrite

Pillow
lava
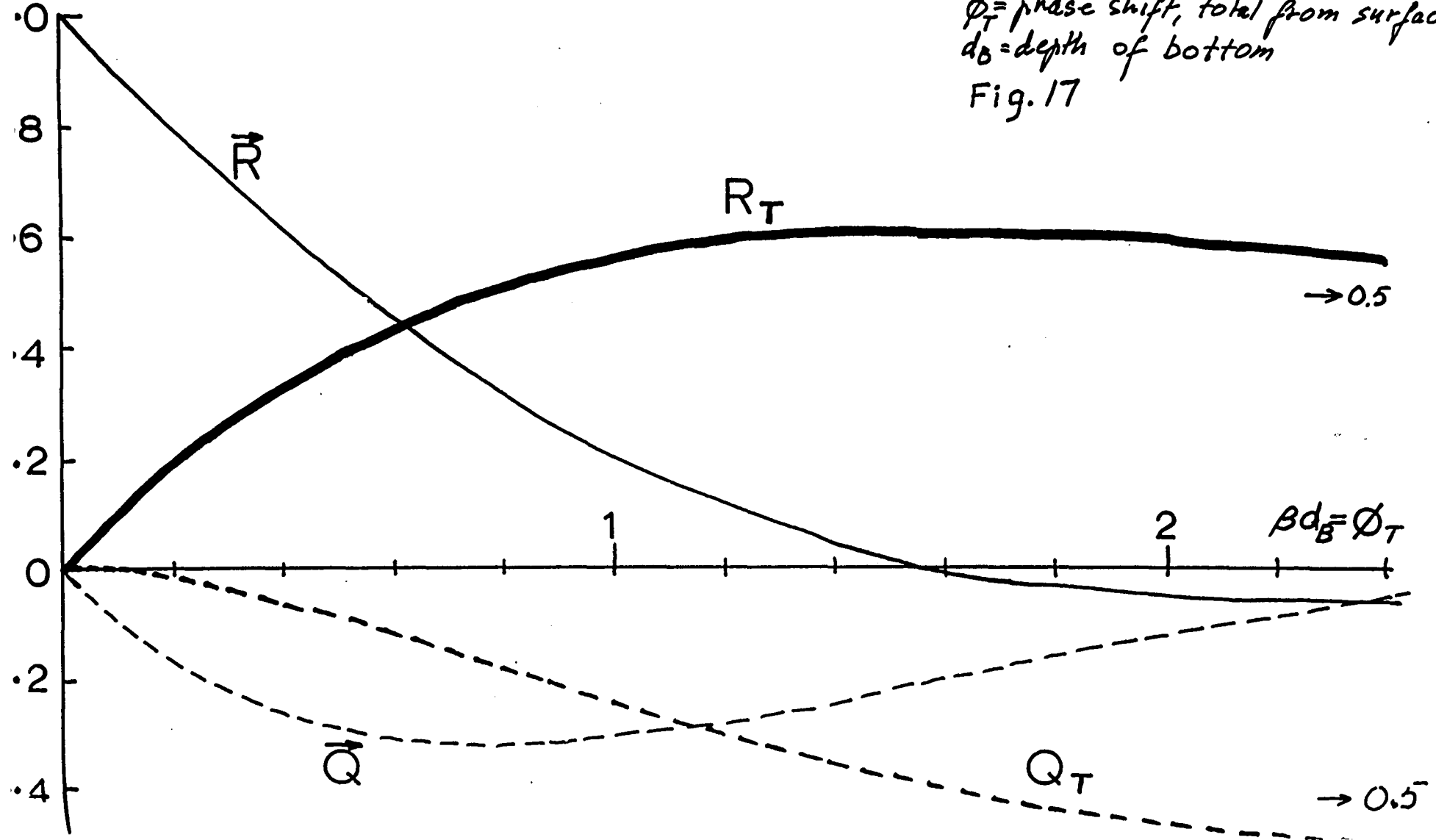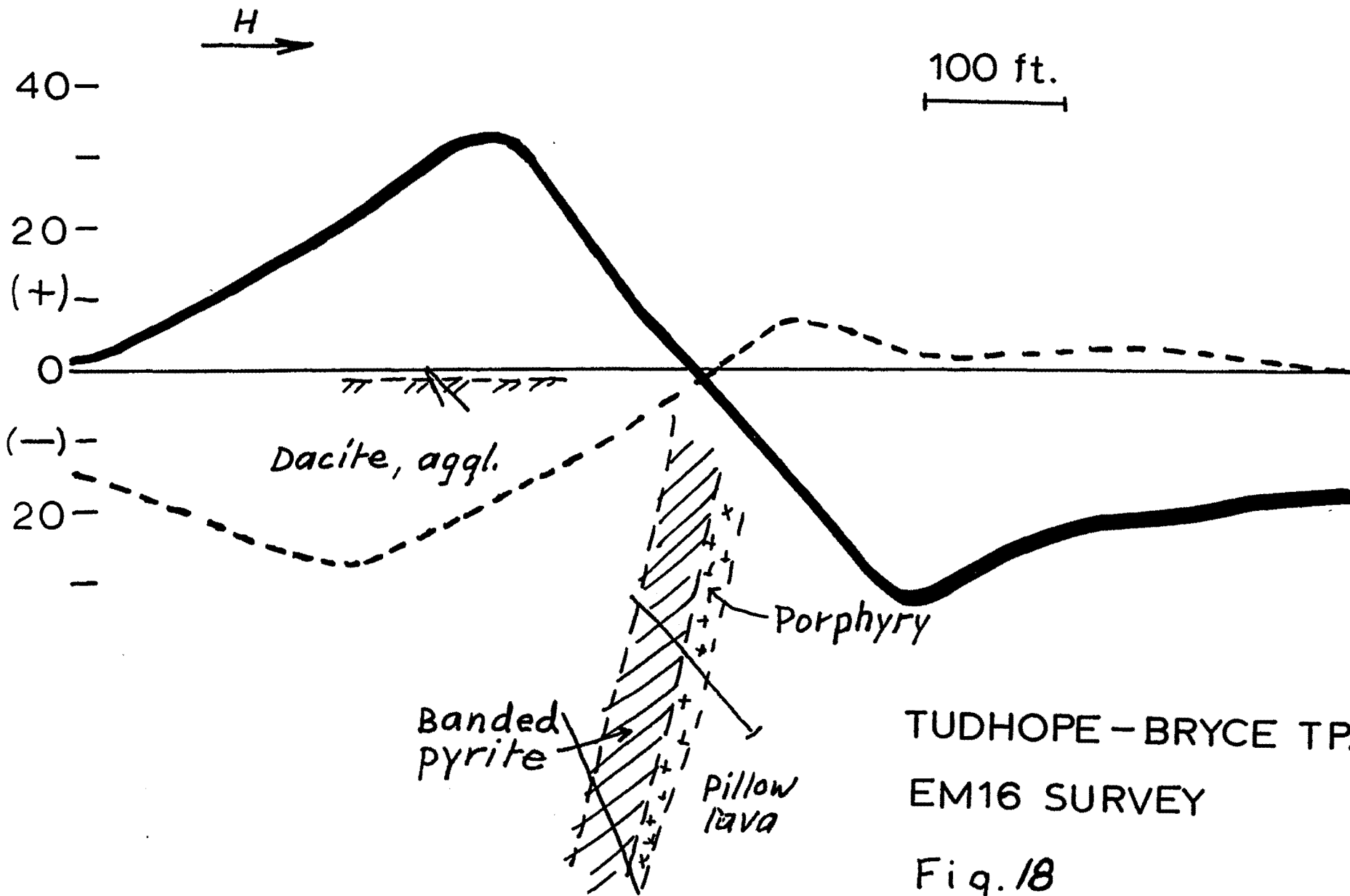
TUDHOPE—BRYCE TP.

EM16 SURVEY

Fig. 18

Page 25

200'

+20

Inphase

Qu

0

−20

swamp
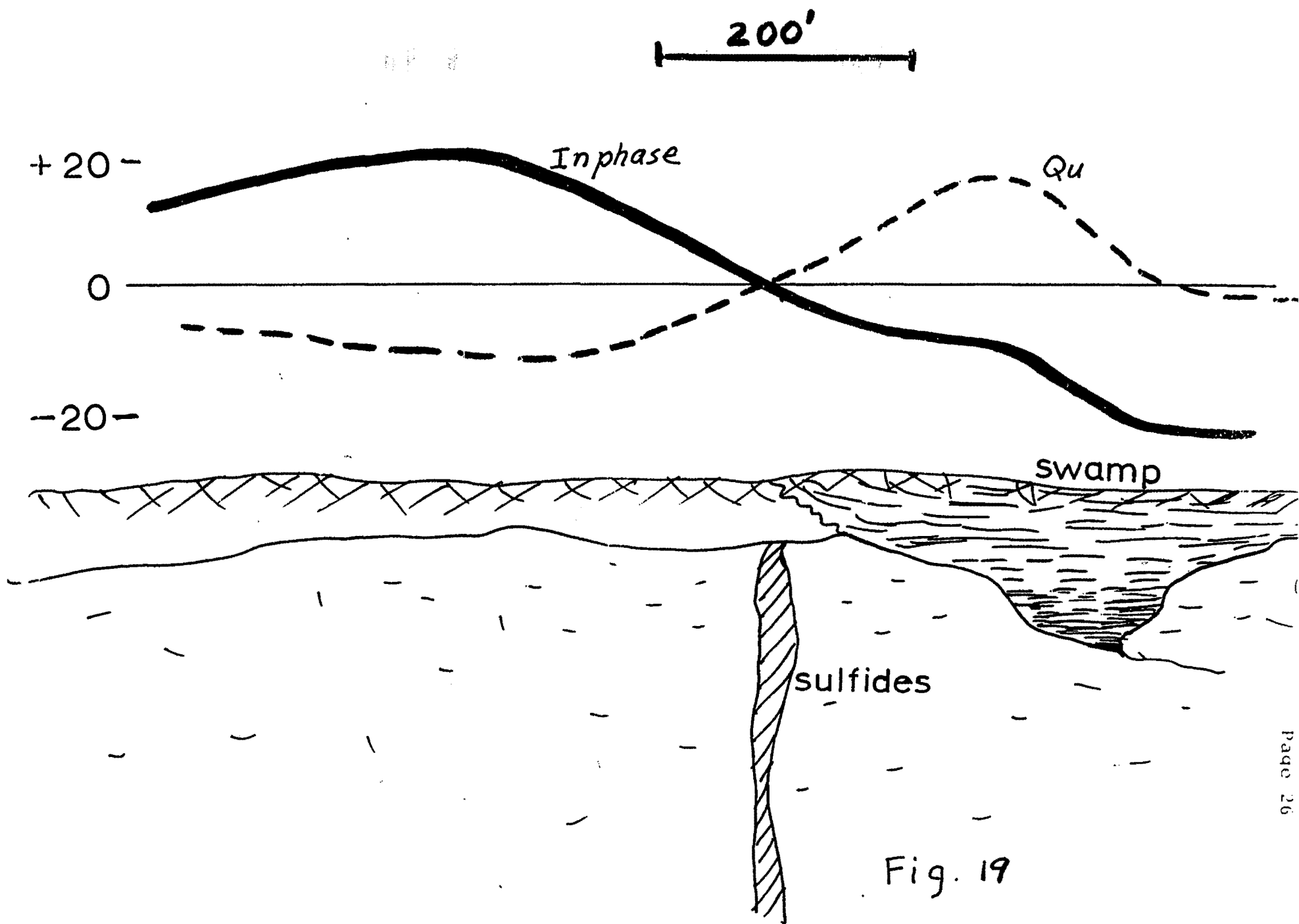
sulfides

Fig. 19

Another use for the quadrature polarity is in the tracing of
a fault or a shear zone. Normally these weak conductors
give a fair amount of positive (the quadrature follows the
in-phase polarity) quadrature. When we have a local sulfide
concentration in these structures, we get a negative quadra-
ture response.

All the interpretation is made easier by other indications
of the depth to the target. The horizontal distance between
the maximum positive and negative readings is about the same
as the actual depth from the ground surface to the centre of
the effective area of the conductive body. This point is not
the centre of the body, but somewhat closer to the upper edge.

Theoretically, the depth 'h' of a spherical conductor with
radius 'a' equals ΔX where ΔX is the horizontal distance between
the maximum points of the vertical field H_z (Fig. 20a). The
radius of the sphere is given by

$$a = 1.3 \; h \; 3 \; H_z (max).$$

For a cylindrical conductor the depth 'h' equals $1.16 \Delta X$ and
the radius of the cylinder is given by

$$a = 1.22 \; h \quad H_z (max).$$

In these equations $H_z = 1$ means 100% on the instrument dial.

The determination of the depth is generally more reliable
than the estimation of the actual dimension a. The real
component of H_z, which we should use in these calculations,
decreases proportionally for a poorer conductor and with the
depth in conductive material.

One can also draw some conclusions about the dip and shape
of the upper area of the conductor by observing the smaller
details of the profile. See the modelling curves.

A vertical sheet type conductor, if it comes close to the
surface, gives a sharp gradient of large amplitude and slow
roll-off on both sides. (Fig. 20b & 20c).

Horizontal sheets should give a single polarity on the edge
of it, and again the opposite way on the other edge.(Fig.20f)

When looking at the plotted curves, one notices that two
adjacent conductors may modify the shape of the anomalies
for each one. In cases like this, one has to look for the
steepest gradients of the vertical (plotted) field, rather
than for the actual zero-crossings. Forget the word "cross-
over". Look for the centres of slopes on the in-phase for
location of targets. See Figures 20d and 20e.

(+)

ΔX

Quadrature

Direction →

(−)

In-phase

h

$\Delta X = h$

a

Spherical body

Good conductor

Fig. 20a

In-phase

Quadrature

Vertical sheet

Poor Conductor

Fig. 20b

Quadrature

In-phase

Conductive overburden

Ore

The effect of

conductive overburden

Fig. 20c

A + B

B

A

A

B

Two vertical bodies
Fig. 20d.

A + B

Surface

B

A

Two bodies — Large and Small

Fig. 20e

Horizontal slab

Fig. 20f

Quadrature

In-phase

Conductive clay

Poor conductor

Clay etc.

Fig. 20g

Z

Total Vector

Measured Vector

$\simeq H_z$ (Quad)

H_z (Quad)

H_z (In-phase)

X

H_p (x)

Time-Vector diagr.

of the total field

Fig. 20h

As with any EM, the largest and best conductors give the highest ratio of in-phase to quadrature components. In VLF however, the surrounding conductive material influences the results so much that it is almost an irrelevant statement except in a few cases. Also in practice most of the ore bodies are composed of different individual sections, and therefore one cannot use the in-phase/quadrature ratio as the sole indicator of the conductivity-size factor. In other words the characteristic response curves are flat, much flatter than with modelling.

MISCELLANEOUS NOTES

1) It has been shown in practice that this instrument can be used (in proper areas) also underground in mines. The rails and pipes may cause background variations. It was found in one mine even at 1400 foot level, that the signal strength was good. By taking readings at two directions at each station, one could obtain a very good indication about the location of the ore pockets in otherwise difficult geology.

2) On the other hand a thick layer of conductive clay can suppress the secondary field to a negligibly small value.

3) In mountainous areas one can expect a smooth rolling background variation. However, the actual sharper anomalies induced by conductive mineral zones can be usually easily recognized. Background variations can be effectively removed by standard numerical filtering procedures to emphasize local anomalies. +

4) Faults and shear-zones can give anomalies, * but not without a reason. There must be conductivity associated with them. Reverse quadrature may indicate sulfide deposits in these structures.

SERVICING

Changing the batteries is done by removing the cover and changing the penlight batteries one by one. Please notice the polarities marked on each individual cell. To test the condition of the batteries, turn the instrument on, press the push-button on the front panel. There should be a whistling sound in the loudspeaker if the batteries are in useable condition. If the sound is not heard, the battery voltage may be low, or the battery holders may be dirty or faulty.

* Telford, King and Becker, "VLF Mapping of Geological Structure".

+ D.C. Fraser, "Contouring of VLF-EM Data".

It may be occasionally necessary to clean the contacts of
the plug-in unit. For this, use a clean rag that is very
slightly moistened with oil. The oily rag is good also for
the battery terminals.

If any repairs are necessary, we recommend that the instru-
ment be shipped to Geonics Limited for a thorough check-up
and testing with proper measuring instruments.

GEONICS LIMITED

E M 1 6   **MODEL EXPERIMENTS**

Contributed by   T.P. Rogowsky and W. A. Bowes
                            of Martin, Sykes and Associates,
                            Steamboat Springs, Colorado.
                            We wish to thank them for their
                            permission to use the very
                            illustrative results.

Target: 28 gage zinc plated roofing
                            sheet, 6 x 48 feet, above
                            ground.

Ground: The area was covered by 2.5 ft.
                            of conductive soil on top of
                            gravel and clay. The area was
                            found to be free of anomalies.

Readings: The graphs show the view (cross
                            section) to North. Readings
                            towards right (East). Primary
                            field is East-West. The
                            instrument was moved along the
                            zero-line except where shown as
                            a separate sloping line (side
                            of a hill). The quadrature
                            component was negligibly small
                            except where shown in the
                            graphs.

Station: WWVL, 20 kHz

Scale: 1 sq.   =   2 feet
                            1 sq.   =   10 %

Fig. 1

Fig. 2

Fig. 3

Fig. 4

Fig. 5

Fig. 6

Fig. 7

Fig. 8

Fig. 9

Fig.10

Fig.11

Fig.12

Fig.13

Fig. 14

Fig. 15

Fig. 16

Fig. 17
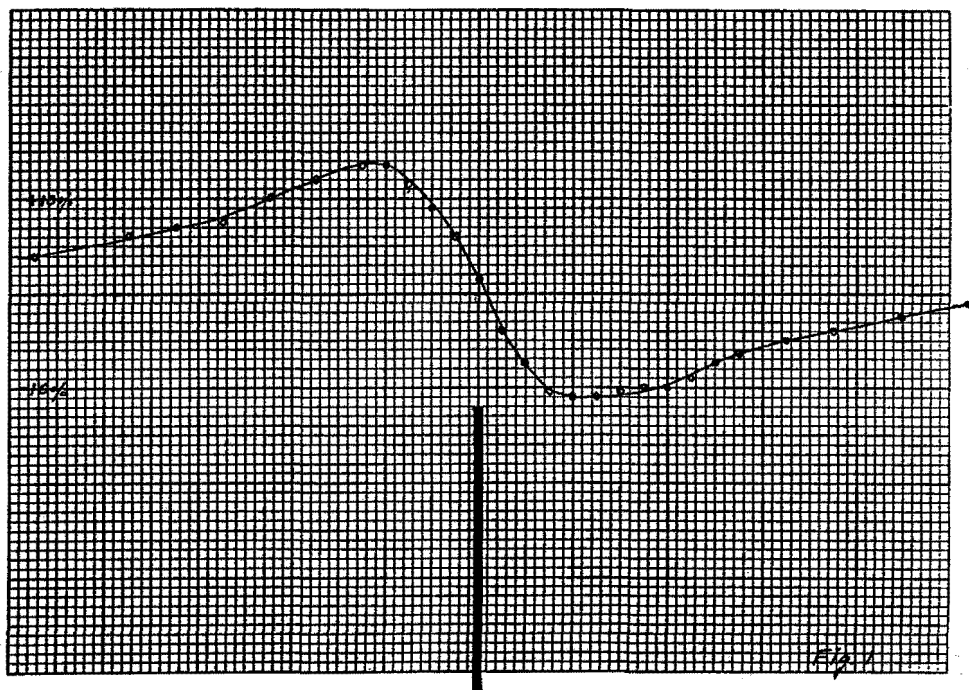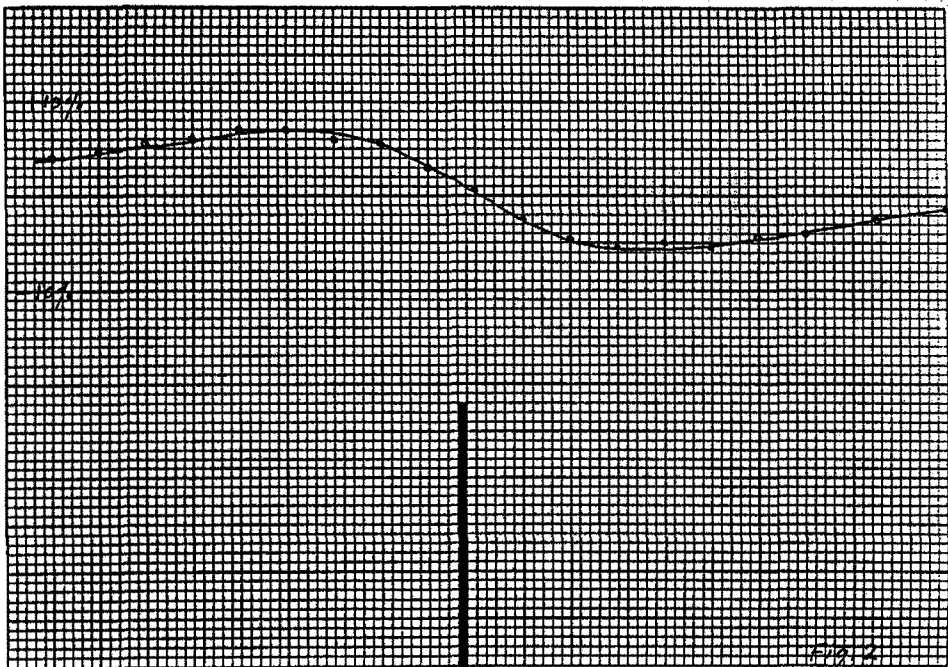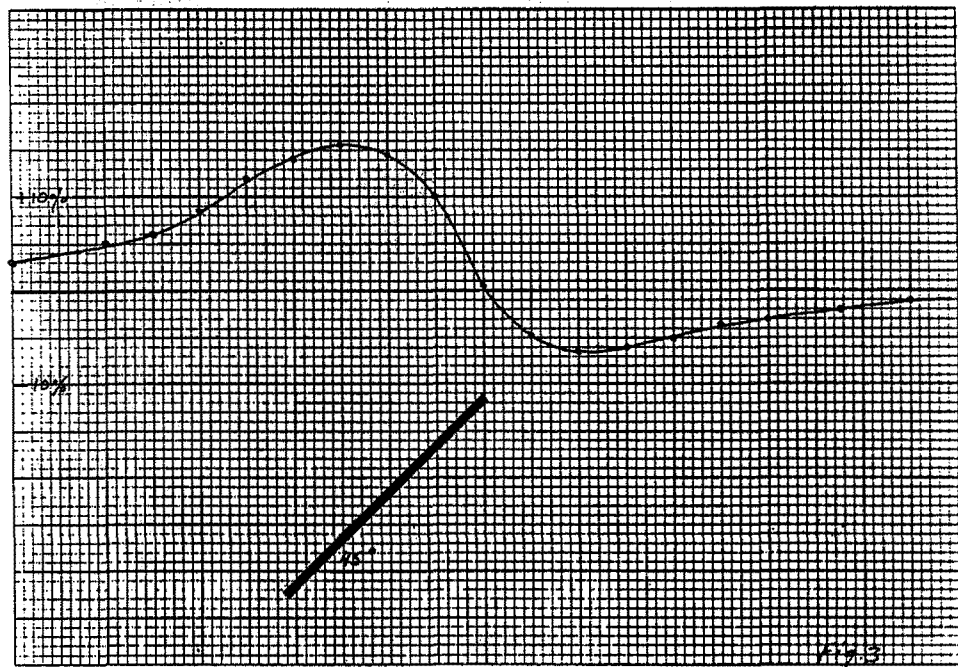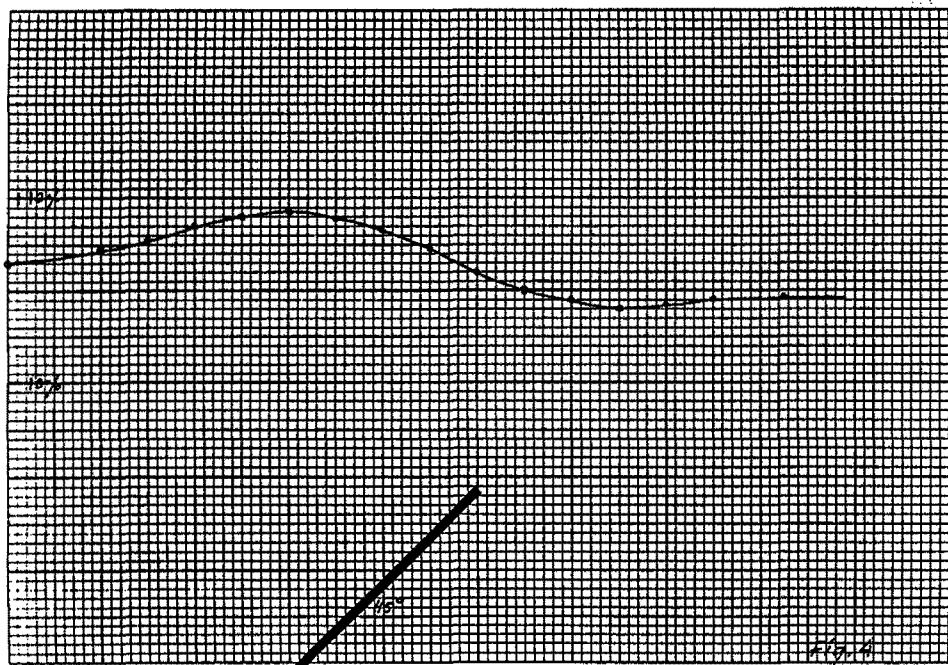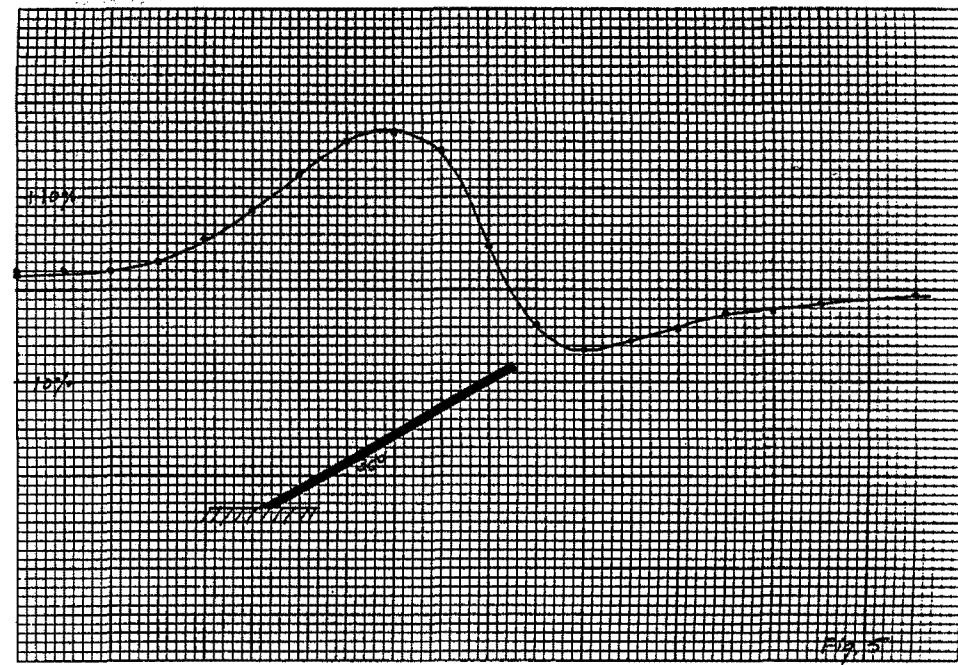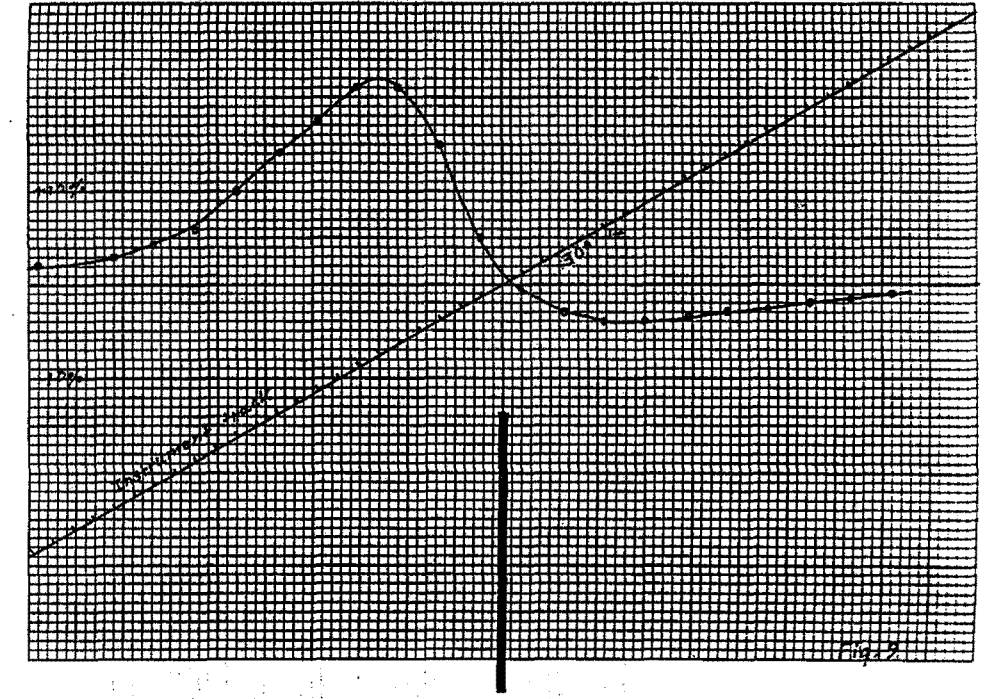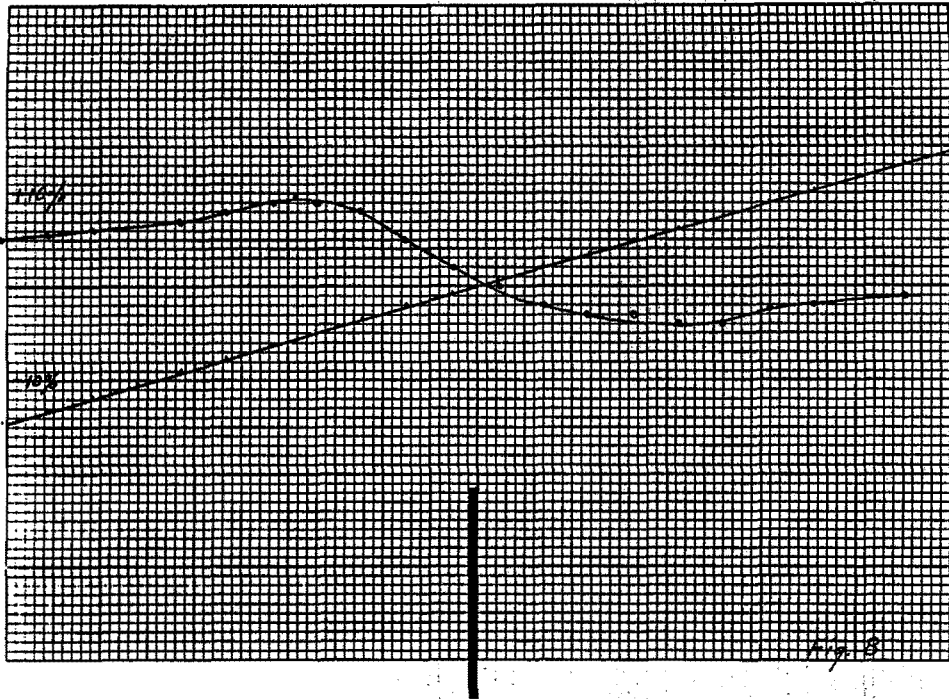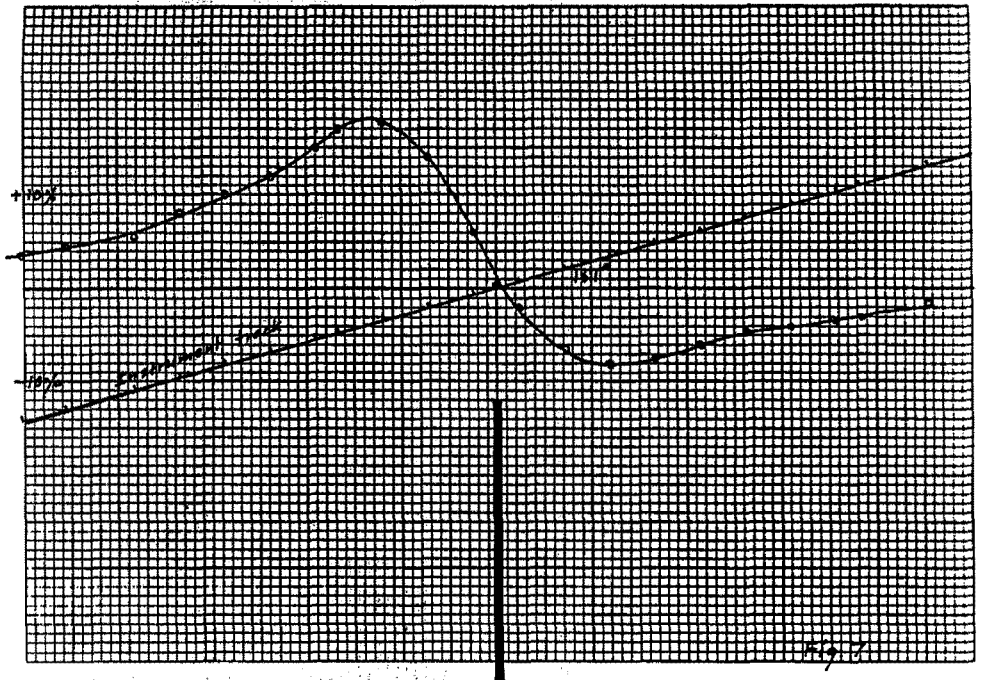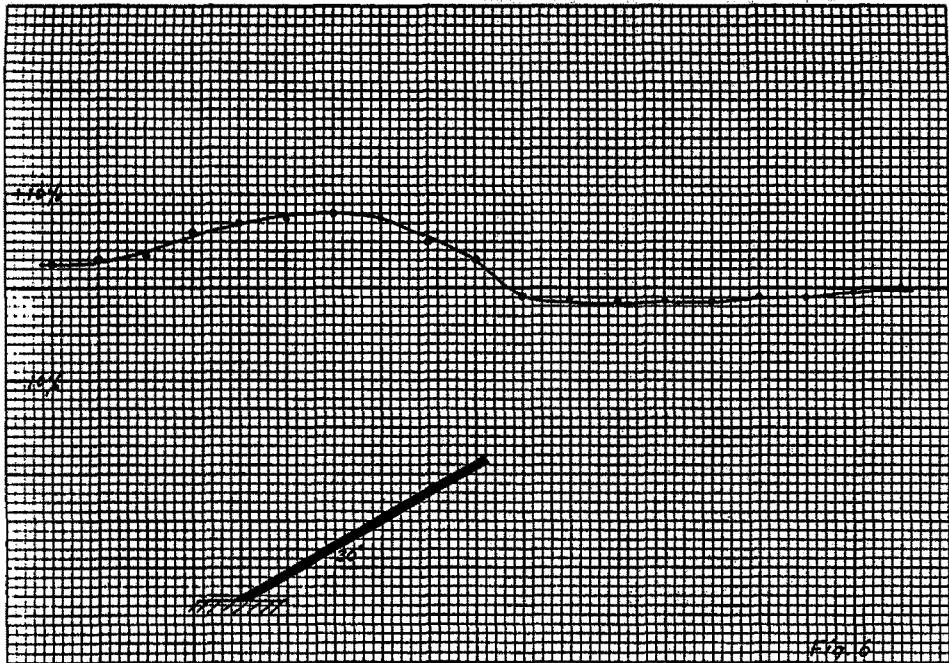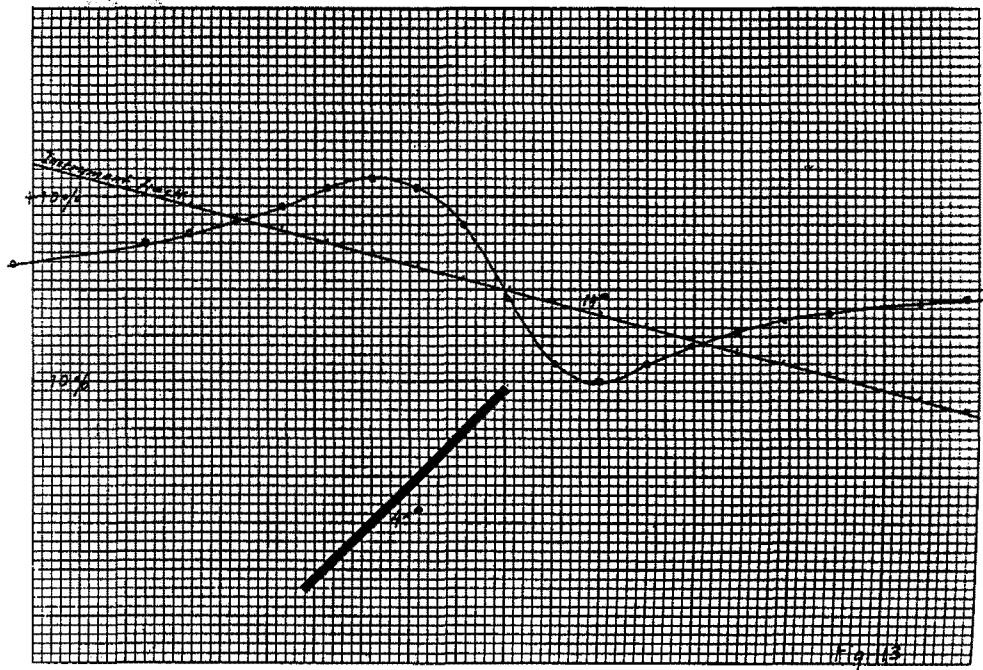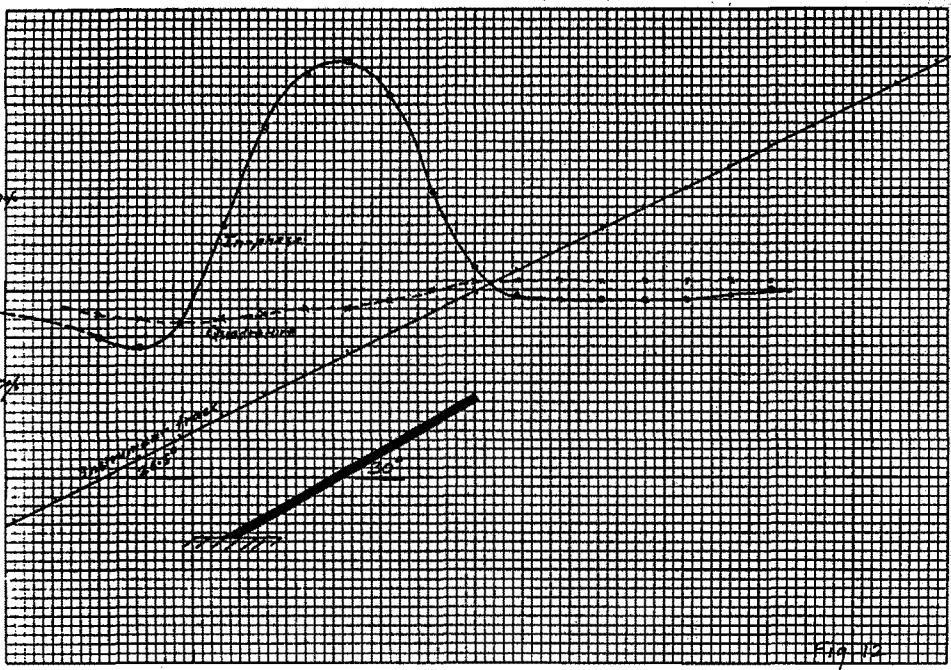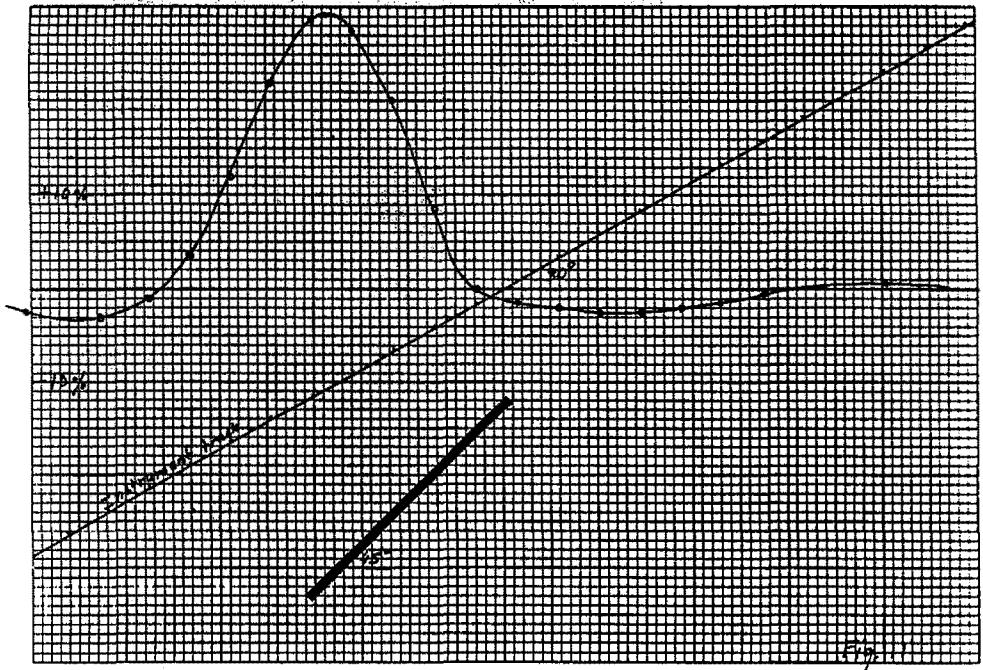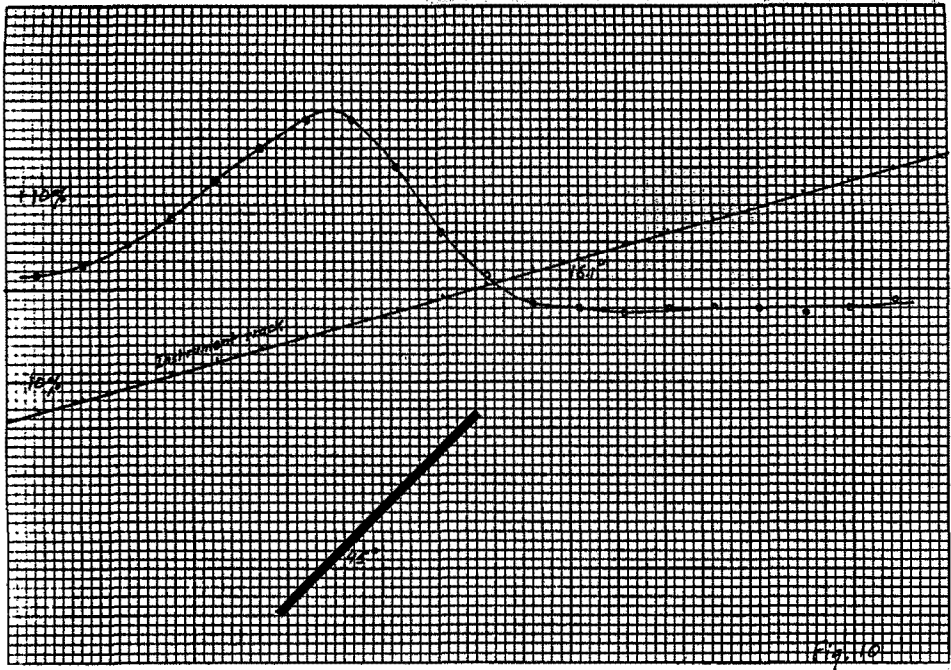
GEONICS LIMITED

2 Thorncliffe Park Drive, Toronto 17, Ontario, Canada. Telephone: 425-1821 Area Code 416

"FIVE YEARS OF SURVEYING
WITH
THE VLF - E.M. METHOD"

By

Norman R. Paterson[1]

and

Vaino Ronka[2]

**PRESENTED AT THE 1969 ANNUAL INTERNATIONAL MEETING
SOCIETY OF EXPLORATION GEOPHYSICISTS**

1. Consulting geophysicist, Toronto, Canada
2. President, Geonics Limited,Toronto, Canada

- 1 -

"FIVE YEARS OF SURVEYING WITH THE VLF - E.M. METHOD"

- by -

Norman R. Paterson and Vaino Ronka

INTRODUCTION

The idea of using radio signals for electromagnetic prospecting is not new; measurements of attenuation and polarization were made by Hack in 1908 and Feldman in 1933 (1) in various geological situations. Eve and Keyes (2) measured signal strength in the vicinity of several orebodies. Anomalous radio behaviour has often been noted near large conductive bodies.

Radio-frequency E.M. methods using ground-transportable transmitters were employed in the 1930s and, to a lesser extent, as recently as 1960, for both prospecting and geological mapping. Because of the relatively high frequencies employed, the method suffered from poor penetration and difficulty in discriminating between bodies of different conductivities. In North America the method was abandoned in favour of low-frequency E.M. for nearly all prospecting applications.

In Europe, the use of radio-frequency methods continued underground, for mapping coal-seams and for exploring in the vicinity of base-metal ore-bodies. The Russians (3) have been successful in applying radio shadow techniques in drill-holes for routine exploration and mapping of sulphide bodies to considerable depths at frequencies up to 1000 kHz. Below the overburden layer, attenuation in most rocks, even at these frequencies, is quite low.

Despite these and other activities, radio-frequency methods were not accepted for routine surface or airborne exploration until Geonics Limited introduced a "passive" instrument working in the VLF range (15 - 25 kHz) in 1964. Powerful military radio transmitters situated conveniently around the globe provided the primary E.M. signal.

Successful surveys were carried out with this instrument in 1965. By the end of 1966 the method was in widespread use, and in 1967 several similar systems were introduced or under development. At least two airborne versions were tested in 1968. By 1969 airborne and/or ground instruments were being manufactured by more than five North American firms.

In this paper we describe briefly the theory and application of the method, we outline the principle of operation of the Geonics E.M. - 16 instrument (4), and we present some field results which have been chosen to illustrate certain features of the data that are helpful in interpretation.

- 2 -

THEORY

The VLF Method

E.M. prospecting methods rely on the measurement of secondary fields generated by conducting bodies in the ground when subjected to a primary E.M. signal. "Active" methods employ transportable transmitters, generally working in the frequency range 400 to 5,000 Hz. AFMAG is a "passive" method, relying on electrical discharges generated by thunderstorms which produce measurable signals in the 50 to 500 Hz range.

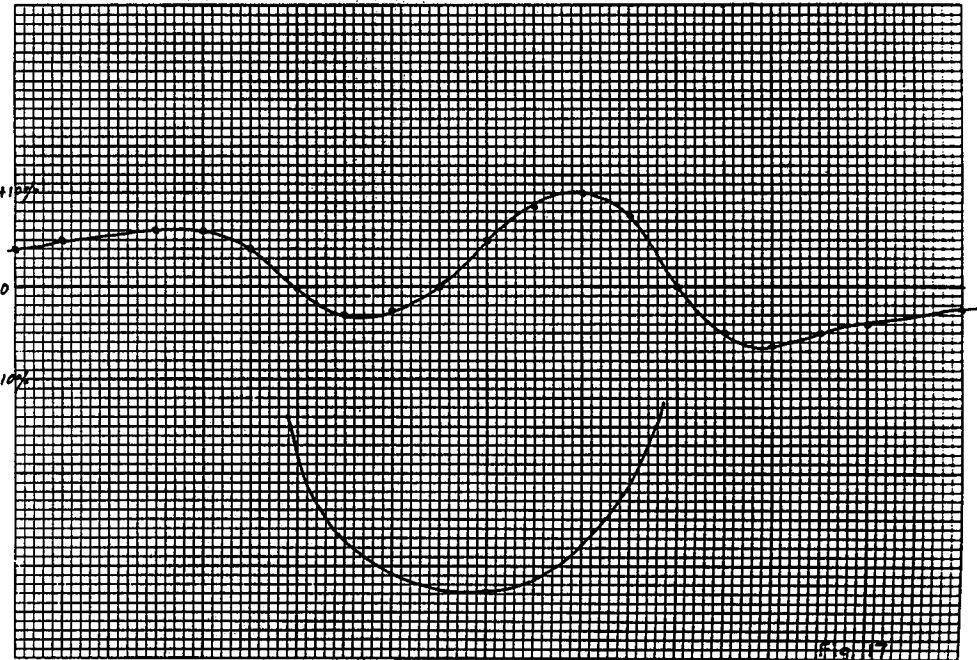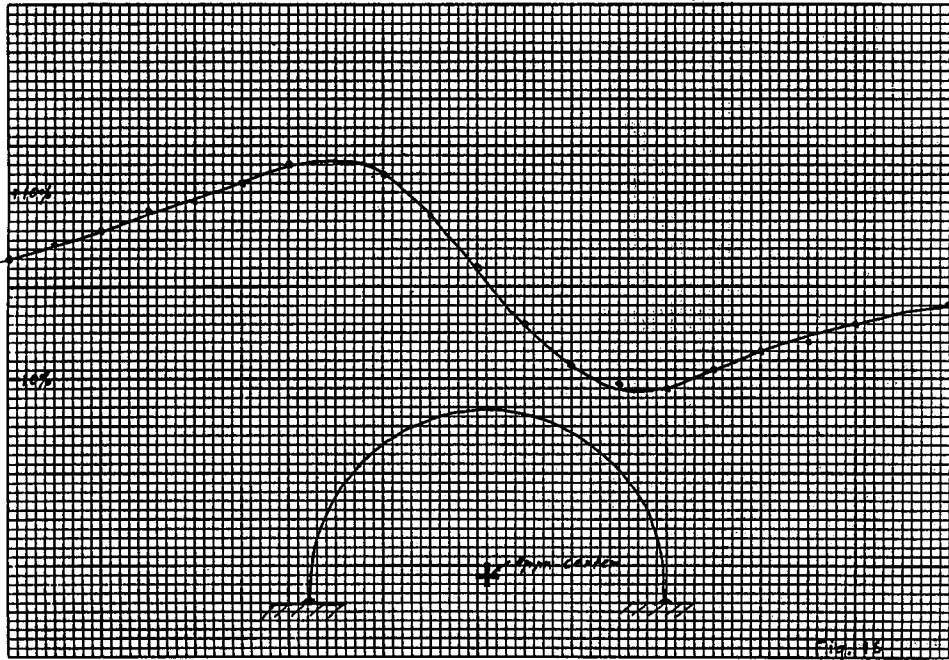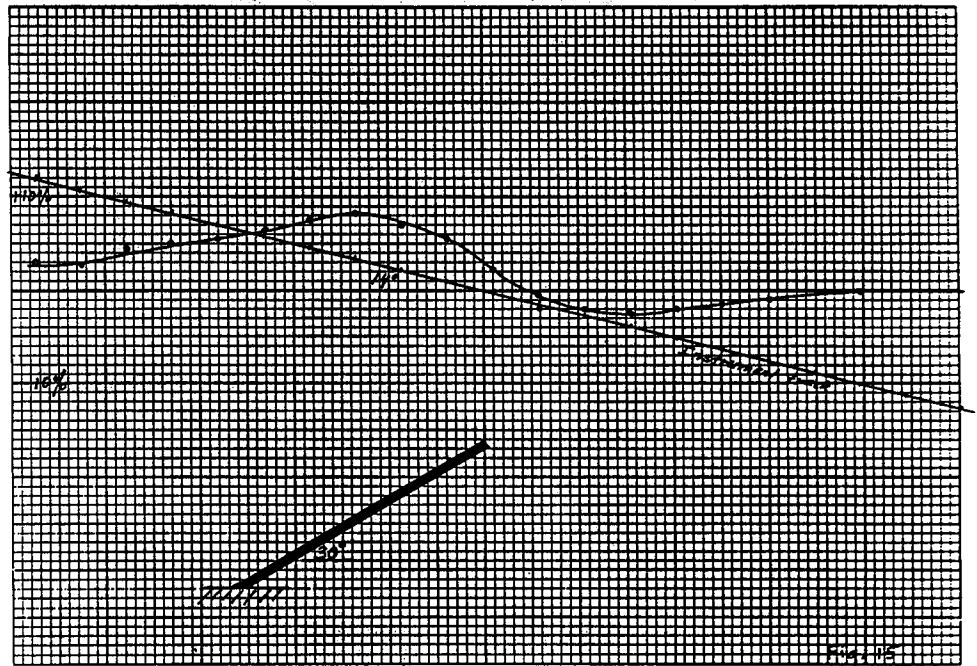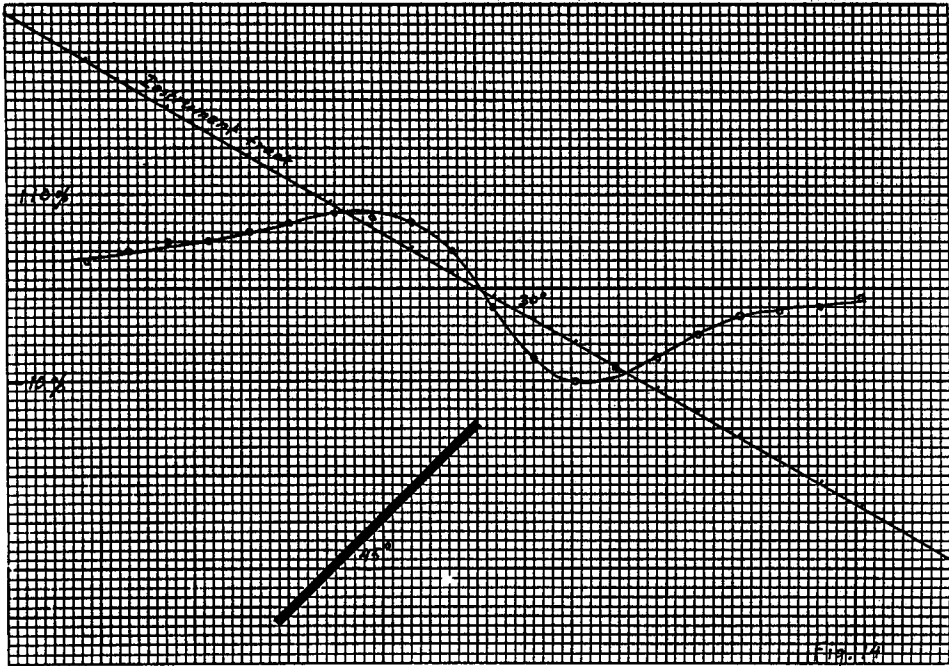The VLF E.M. method is also "passive", in this case employing the radiation from powerful military radio transmitters as the primary signals. Figure 1 shows the approximate location and signal-range of the main transmitters working in the 15 to 25 kHz radio band. Frequencies and power outputs of these and other stations are listed below.

Station	Location	Frequency kHz	Radiated power (kw)
IDO	Rome, Italy	27.2	50
LPZ	Marte Grande, Buenos Aires	23.6	72.1
PKX	Malabar, Java	18.98	162
ROR	Gorki, Russia	17.0	315
UFT	Sainte Assise, Paris, France	20.7	60.8
UMS	Moscow, Russia	17.1	200
NAA	Cutler, Maine, U.S.A.	17.8	1000
NLK/NPG	Jim Creek, Wash, U.S.A.	18.6	300
NPM	Lualualei, Hawaii, U.S.A.	21.4	300
NWC	North West Cape, Australia	22.3	1000
WWVL	Fort Collins, Colo, U.S.A.	20.0	4
GBR	Rugby, England	16.0	500

The radiation from these transmitters contains both electric and magnetic components and travels in three modes: skywave, spacewave and groundwave. At the large distances we are concerned with, we receive mainly the skywave wave-guided by the ionosphere and earth surface. The magnetic component is the one of main interest to us, as beneath the ground surface it carries the bulk of the signal energy, and it offers certain advantages in practical field measurement.

Figure 2 illustrates the behaviour of the magnetic field from a distant, vertical radio antenna. The field is polarized roughly cylindrically about the antenna, the vector assuming an attitude roughly parallel to the average ground surface. (At large distances rectangular components can be assumed.)
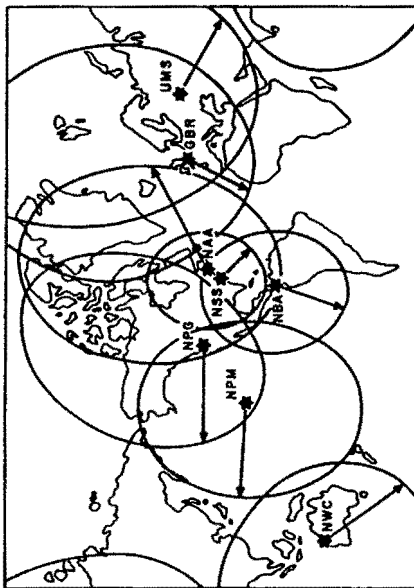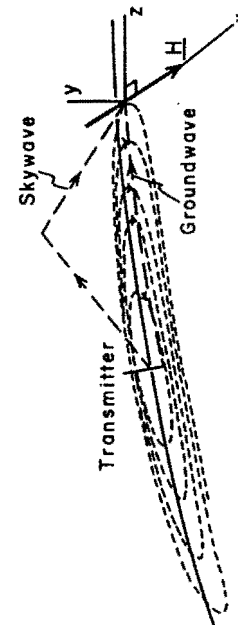
2a

2b

FIGURE 1

FIGURE 2

- 3 -

Below the ground surface the magnetic field is attenuated and consequently distorted both in phase and direction. The behaviour of the field near the ground/air interface has been described by Norton (5): its effect on VLF measurements is under study at the present time.

Attenuation and Phase Shift

For our purposes, (and assuming that $\sigma/\omega\epsilon \gg 1$), we shall take it that the primary magnetic field suffers both attenuation (nepers) and phase shift (radians) roughly equal to

$$\sqrt{\frac{\omega\mu\sigma}{2}} \quad \text{meters}^{-1}$$

where

    ω = angular frequency
    μ = magnetic permeability in henrys/m
    σ = electrical conductivity in mhos/m
    ϵ = dielectric constant in farads/m.

At a frequency of 20 kHz, and at the free-space permeability of 1.26×10^{-6} henrys/m, we obtain:

    Attenuation = .29 nepers/m
    Phase shift = -.29 radians/m

At the "skin depth", primary field amplitude is reduced 1 neper to 1/e of its strength at ground surface, and the field has suffered a negative phase-shift of 1 radian.

In relatively non-conductive rocks ($\sigma = 10^{-3}$ mhos/m) we obtain a skin depth of about 100 meters, and a phase-shift of about 0.01 radians/m.

Attenuation and phase-shift at a range of rock and soil conductivities are shown in Figure 3. Two things are evident from these graphs:

1. Attenuation is a limiting factor in the use of the VLF method in areas of conductive overburden or moderately conductive country rocks (bear in mind that the secondary fields from buried conductors are further attenuated in their passage upward to the measuring instrument).

2. The primary field coupling with buried conductors will be shifted appreciably in phase, even in rocks of relatively low conductivity (and the secondary fields measured at surface will be phase-shifted approximately twice as much).

$$H = H_o e^{-.29\sqrt{\sigma}\,d}$$

FIGURE 3

- 4 -
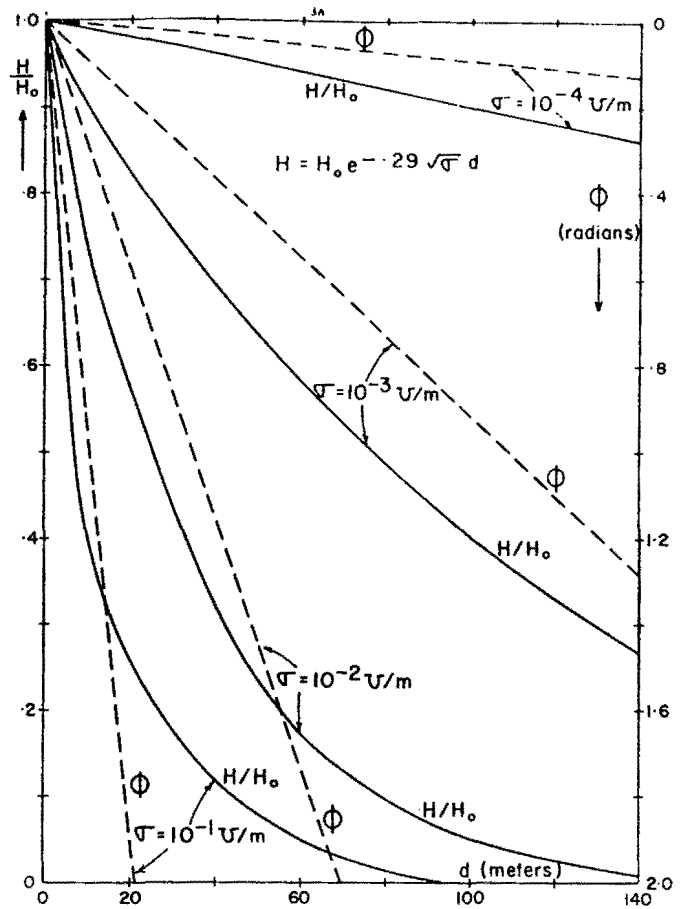
Attenuation is a factor that cannot be overcome and must be kept in mind constantly in applying the VLF E.M. method.

Phase-shift can however be of very real value in distinguishing conductors lying at depth from those confined to the near-surface.

The Polarization Ellipse

Measurements of the secondary field are normally made in the VLF method by comparing signals in the vertical and horizontal directions. Since the primary field is nearly horizontal, we thereby obtain a rough measure of secondary field strength; we can also determine approximate the phase of the secondary field with respect to the primary.

To understand how these measurements are actually made, it is necessary to examine the polarization ellipse.

Assume the primary field H to be horizontal and of zero phase angle:

$$|H| = H\cos\omega t$$

Let the secondary field at the same point in space be represented by:

$$|\Delta H| = \Delta H \cos(\omega t + \phi)$$

where ϕ represents positive or negative phase-shift.

And let ΔH be inclined upward in the plane of H by the angle α.

The components of H and ΔH in the x(horizontal) and y(vertical) directions are:

$$H_x = H\cos\omega t$$
$$H_y = 0$$
$$\Delta H_x = \Delta H \cos(\omega t + \phi)\cos\alpha$$
$$\Delta H_y = \Delta H \cos(\omega t + \phi)\sin\alpha$$

Summing these, we obtain:

$$C_x(t) = H\cos\omega t + \Delta H \cos(\omega t + \phi)\cos\alpha$$
$$= X\cos(\omega t + \phi')$$
$$C_y(t) = H\cos(\omega t + \phi)\sin\alpha$$
$$= Y\cos(\omega t + \phi)$$

4a

$H_x = H\cos\omega t$
$H_y = 0$
$\Delta H_x = \Delta H \cos(\omega t + \phi)\cos\alpha$
$\Delta H_y = \Delta H \cos(\omega t + \phi)\sin\alpha$

FIGURE 4

- 5 -

where $\phi' = \tan^{-1} \dfrac{\Delta H \cos \alpha \sin \phi}{H + \Delta H \cos \alpha \cos \phi}$

By eliminating t, we can derive (6) an expression for the locus of $\underline{C(t)}$ the resultant of the primary and secondary fields:

$$\frac{C_x^2}{X^2} + \frac{C_y^2}{Y^2} - \frac{2C_x C_y}{XY} \cos \delta = \sin 2\delta$$

where $\delta = \phi' - \phi$

This is the equation of an ellipse whose minor axis is inclined to the vertical by the angle θ where:

$$\tan 2\theta = \frac{2XY \cos \delta}{X^2 - Y^2}$$

Evidently the resultant field rotates in space, varying in magnitude as it goes, so as to describe an "ellipse of polarization".

The ratio b/a of minor to major axes (eccentricity) of the ellipse increases as ϕ becomes larger, and can therefore be used to obtain a rough measure of this useful quantity. If ΔH is much smaller than H, the eccentricity becomes:

$$\epsilon = \frac{\Delta H \sin \alpha \sin \phi}{H} \tag{1}$$

while the inclination of the ellipse reduces to

$$\theta = \tan^{-1} \left[\frac{\Delta H}{H} \sin \alpha \cos \phi + \left(\frac{\Delta H}{H} \right)^2 \frac{\sin 2\alpha \sin \phi}{2} \right] \tag{2}$$

In the special case where $\phi = 0$ the ellipse reduces to a straight line, of inclination:

$$\theta = \tan^{-1} \frac{\Delta H}{H} \sin \alpha$$

At the point where $\alpha = 0$ and both primary and secondary fields are horizontal, both the ratio and the inclination are zero.

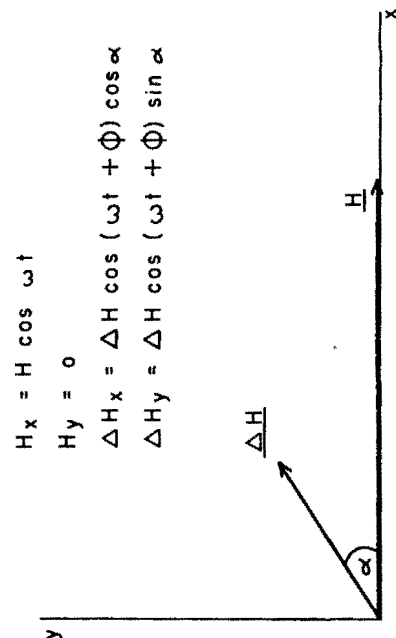It is important to note that the sign of the eccentricity changes as the phase angle goes from positive to negative. The significance of this can be seen from an examination of profiles of ϵ and ϕ in the presence of a cylindrical secondary field about a horizontal line source of current (Figure 6) lying at a depth d below the ground.

Ellipse of Polarization
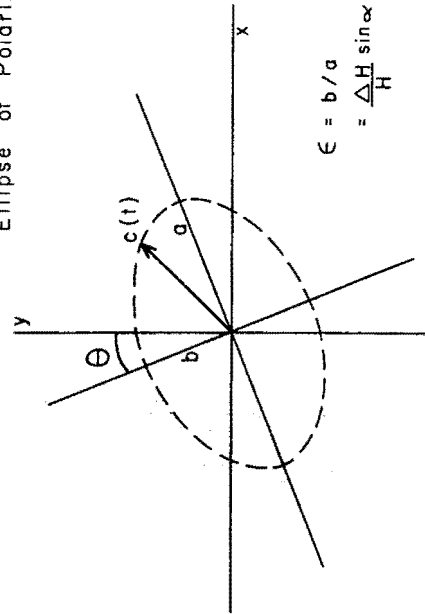
$\epsilon = b/a = \dfrac{\Delta H \sin \alpha \sin \phi}{H}$

$\theta = \tan^{-1} \left[\Delta H/H \cdot \sin \alpha \cos \phi + (\Delta H/H)^2 \dfrac{\sin 2\alpha \sin \phi}{2} \right]$

FIGURE 5

Field over line current source.

$\Delta H/H = (\Delta H/H)_o \cos \alpha$

FIGURE 6

- 6 -

We may write:

$$\alpha = \tan^{-1} - x/_d \tag{3}$$

$$\Delta H/H \propto \frac{1}{\sqrt{x^2 + d^2}}$$

$$\propto \frac{\cos \alpha}{d}$$

which we may also write:

$$\left(\Delta H/_H \right)_p = \left(\Delta H/_H \right)_o \cos \alpha \tag{4}$$

Let us consider two cases, representing (I) a good conductor lying in a weakly conductive ground; (II) a very poor conductor lying in non-conductive ground or on the ground surface.

(I)   In this case ϕ will be negative, as the primary and secondary fields will be delayed in their passage through the ground.

Let $\phi = -45°$ and

let $(\Delta H/H)_o = 0.2$

The profiles in Figure 7 show the form of the ellipse of polarization. Inclination θ reaches its maximum of $\tan^{-1}$ 0.0625 at approximately $x = -d$ and its minimum at $x = +d$, values going from positive to negative in the direction of the primary field $\underline{H}$.

Eccentricity ϵ has its maximum and minimum of $\pm$ 0.0706 at approximately the same points, but values are of the opposite sense.

(II)   In this case ϕ will be weakly positive, as the phase angle of the secondary field from a discrete conductor below the plane of measurement will be positive with respect to the primary field at the same point.

a.   Let $\phi = +10°$ and

let $(\Delta H/H)_o = 0.2$

The profiles in Figure 8 are similar to those in Case (I), only the eccentricity now has the same sense as the inclination. This is consistent with the sense of the expression for eccentricity (equation (1)) as it is affected by the sign of the phase angle ϕ.

Case (I)

Good conductor in weakly conductive ground.

$(\Delta H/H)_o = 0 \cdot 2$

$\phi = -45°$

tan θ

ε

x/d

FIGURE 7

Case (II) a.

Poor conductor in non-conductive ground, or at surface.

$(\Delta H/H)_o = 0 \cdot 2$

$\phi = +10°$

tan θ

ε

x/d

FIGURE 8

- 7 -
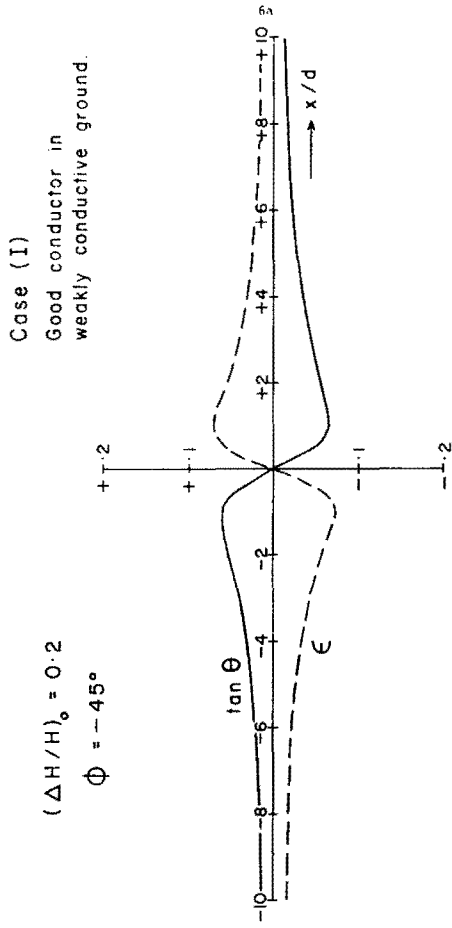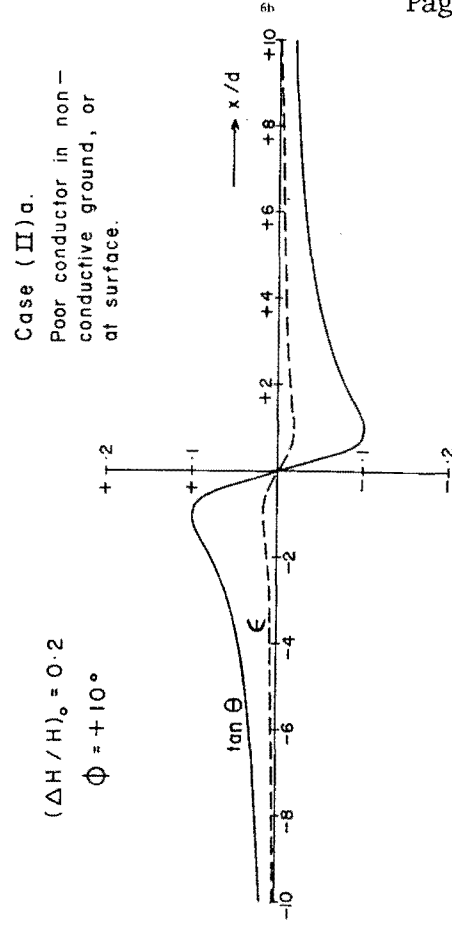
b.   Allow the conductor to assume larger dimensions so that the secondary field becomes a greater fraction of the primary.

Let $\phi = +10°$ and

let $(\Delta H/H)_o = 0.5$

The profiles in Figure 9 resemble those of Figure 8 scaled up by the factor 2.5. In fact, the inclination and eccentricity are both nearly proportional to the ratio of secondary to primary fields (phase angle remaining constant), becoming increasingly so for small secondary fields.

Case (II) b.

Poor conductor of large dimensions in non-conductive ground, or at surface.

$(\Delta H/H)_o = 0 \cdot 5$

$\phi = +10°$

tan θ

ε

x/d

FIGURE 9

- 8 -

Effect of Azimuth

So far we have considered only primary and secondary fields in the same vertical plane. In practice this is seldom the case so we must examine the effect of varying the horizontal angle ψ (azimuth) of the secondary field relative to the primary.

In this case equation (1) remains the same, as the vertical component, $\Delta H \sin \alpha$, is the only one that affects the eccentricity.

Equation (2) assumes the factor $\cos \psi$ in its second term, affecting the inclination only slightly for low secondary field strengths.

$$\theta = \tan^{-1}\left[\frac{\Delta H}{H} \sin \alpha \cos \phi + \left(\frac{\Delta H}{H}\right)^2 \frac{\sin 2\alpha \cos \psi \sin \phi}{2}\right] \qquad (5)$$
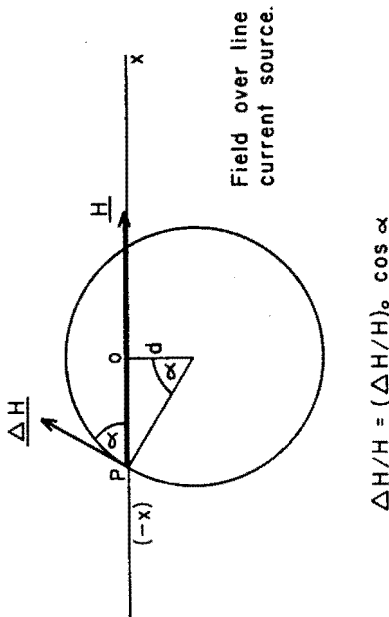
If the profile is measured in the direction of the primary field, equation (3) becomes

$$\alpha = \tan^{-1} - \frac{x \cos \psi}{d} \qquad (6)$$

Equation (4) is unaffected, though it must be remembered that $(\Delta H/H)$ will be reduced roughly in proportion to $\cos\psi$ for sheet- or ribbon-like conductors.

The net effect of varying the azimuth of the secondary field is to stretch out the anomaly either side of its cross-over and to reduce the strength of both the inclination and eccentricity values roughly in proportion to $\cos \psi$. The reduction of the inclination values will be slightly less in the case of negative phase angles than for positive phase angles.
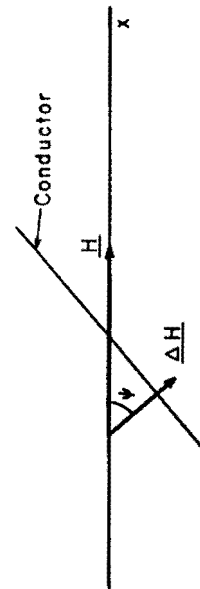
FIGURE 10

- 9 -

METHOD OF OPERATION

General

It is apparent from the above that the VLF polarization ellipse in the vicinity of an electrical conductor is to some extent characteristic of the properties of the conductor. We have also seen that two particular parameters of the ellipse - the inclination and the eccentricity - reflect the relative field strength and phase of the primary and secondary fields. Let us examine this more closely.

For relatively small secondary field strengths equation (2) reduces to

$$\theta = \tan^{-1} \frac{\Delta H}{H} \sin \alpha \cos \phi$$

$$= \tan^{-1} \frac{\Delta H_V}{H} \text{ (real)}$$

indicating that the tangent of the inclination (and hence the inclination itself, for small angles) is nearly proportional to the real component of the secondary field, measured in the vertical direction.

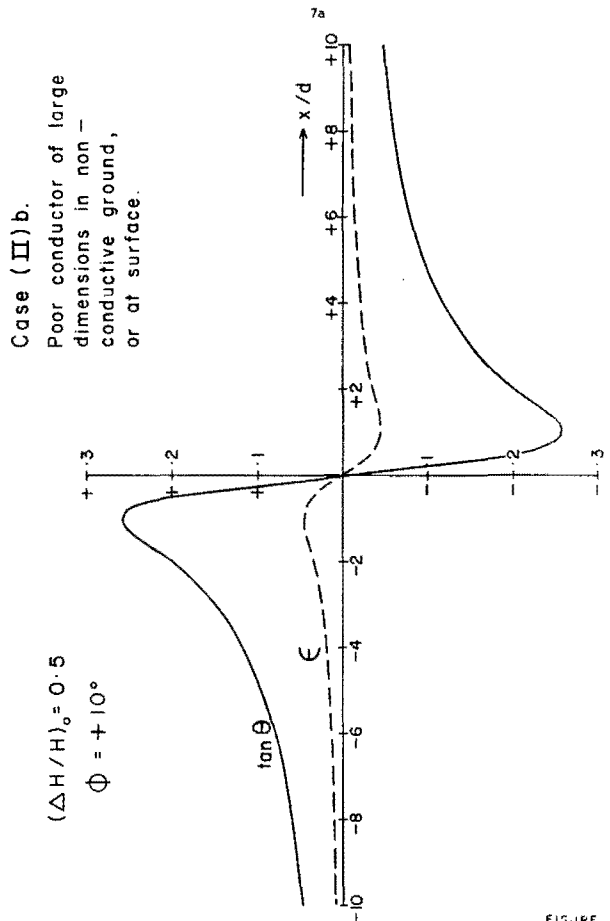The error in this approximately increases for large secondary fields, reaching approximately 10% for $(\Delta H/H)_0 = 0.5$.

The eccentricity ϵ expressed in equation (1), can be written as

$$\epsilon = \frac{\Delta H_V}{H} \text{ (quadrature)}$$

showing a direct proportionality to the quadrature component of the vertical secondary field. The approximation inherent in this expression leads to small errors at large secondary field strengths.

Measurements therefore of inclination and eccentricity are nearly proportional to the real and quadrature components of the vertical secondary field; and they may be used to represent these quantities within acceptable limits.

Principle of E.M.-16

Mr. Vaino Ronka used the above relationships in the design of the first VLF instrument, the Geonics E.M.-16 (4).

The instrument has two receiving coils: the signal coil with a normally vertical axis, and the reference coil with a horizontal axis. Each coil is tuned to the

Direction to station

Primary Field

Survey Line

Primary Field

Primary Field
And Survey Lines

Conductor Ahead

Conductor Behind

- 10 -
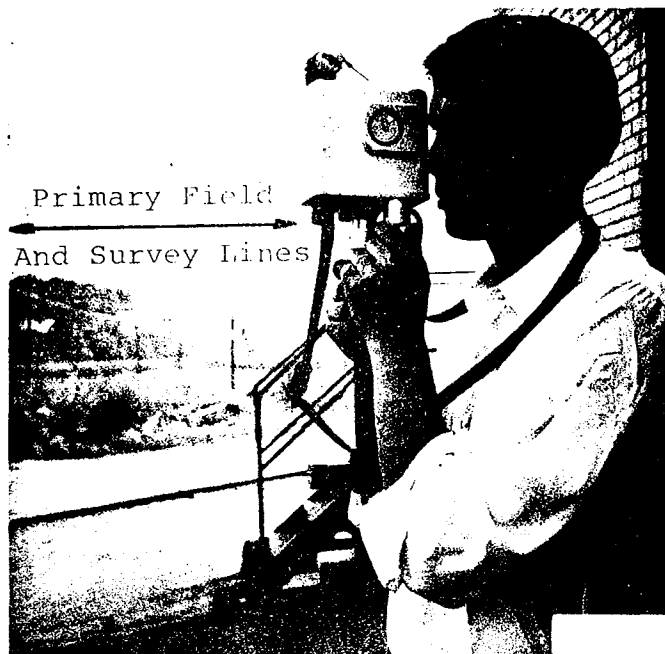
same primary signal by means of plug-in crystal modules, but each has a separate amplifier. To obtain a reading the instrument is operated in the manner shown in Figure 11. In this figure it is assumed that the primary field is parallel to the survey line; the 'station' refers to the transmitter location.

The direction of the primary field is first determined by holding the signal coil horizontal (Figure 11a) and orienting the instrument for minimum coupling. This is detected by a minimum audible signal in the loud-speaker mounted on the console.

The instrument is then held vertically with its reference coil in a direction at right angles to the transmitter location (Figure 11b), at which point it is receiving the full effect of the primary field.

The operator then rotates the instrument (Figures 11c, d) in the vertical plane until a minimum signal is registered. At this point the signal coil is oriented along the minor axis of the ellipse of polarization, and the tilt angle of the instrument is the angle of inclination of the ellipse. The tangent of the tilt angle is therefore an approximation to the ratio of the real component of the vertical secondary field to the horizontal primary field. The E.M.-16 registers both the tilt angle in degrees and the tangent of the angle, expressed in percent.

Holding the instrument steady in the minimum direction the operator then rotates the "quadrature" knob with his left hand (Figures 11c, d), until the best signal minimum is obtained. Through this adjustment a proportion of the voltage in the reference coil (after first shifting its phase 90°) is used to compensate the voltage in the signal coil. The calibration of the knob registers the percentage of the reference signal used in the compensation, thereby providing a direct measurement of the ratio of the signal strengths in the two receiver coils. As we have seen (equation (1)), this quantity is an approximation to the ratio of the quadrature component of the vertical secondary field to the horizontal primary field.

Profiles recorded with the E.M.-16 resemble closely those in Figures 7 - 9, with the ordinates expressed in percent rather than in fractions.

- 11 -

Field Operation and Applications

The E.M.-16 and other VLF ground E.M. instruments share the same advantages in field operations.

1. They are light (2 - 3 lbs.) and exceedingly portable.

2. They need no transmitter, further reducing complexity, cost, and operating personnel (the instrument is normally operated by one man).

3. Readings are extremely rapid, as signals are strong and nulls clear and un-wavering within the recommended operating range of transmitters.

4. Power consumption is negligible (one set of "penlite" batteries generally lasts well over a month).

5. The operation is so simple that unskilled personnel can be trained as operators in a matter of hours.

From a geological point of view the following advantages are pertinent:

1. The method is capable of a large depth of exploration in non-conductive rocks (see Figure 3).

2. The relatively high frequency provides high response factors for bodies of quite small dimensions. Relatively "disconnected" sulphide ores have been found to produce measurable VLF signals.

3. For the same reason, poor conductors such as sheared contacts, breccia zones, narrow faults, alteration zones and porous flow tops normally produce VLF anomalies. The method can therefore be used effectively for geological mapping.

4. The method can be used without difficulty in mountainous terrain, though if the ground is conductive the profile will be distorted in the direction of the ground surface. This can often be recognized and/or removed semi-quantitatively.

There are relatively few disadvantages to the method, and none from an operating standpoint.

1. In conductive ground the depth of exploration is severely limited (see Figure 3).

- 12 -

2. Anomalies tend to be generated by conductivity changes in the overburden, or at the overburden/bedrock interface. These may be difficult to recognize from anomalies due to conductors within the bedrock.

3. Since the frequency is high, the response factor of many geological conductors (including orebodies) is above the range where appreciable quadrature effects are generated. Phase-shifts are more usually associated with the effects of conductive ground on the primary and secondary signals, (see Figure 3). Quadrature measurements cannot often be used to assist in discriminating between geological conductors of higher and lower conductivities.

Because of restrictions 2 and 3, it is often advisable to follow up the VLF survey with one or more profiles by the horizontal loop E.M. or other discriminatory method, before costly drilling is carried out.

Data Reduction and Interpretation

Because VLF anomalies are produced by such a wide range of geological effects, profiles tend to be "cluttered", and the interpreter may need some assistance in distinguishing trends and classifying groups and patterns. This may be done by digitizing the data and performing filtering, trend analysis and cross-correlation.

Fraser (7) has developed a simple technique of filtering and differentiating tilt angle profiles that can be applied effectively in the field or office for rapid geological correlation and interpretation. By averaging pairs of stations and taking differences between pairs separated by a distance that is appropriate to a particular depth of interest, values may be plotted and contoured in plan that transform inflections (including cross-overs) into "highs" and "lows", and smooth or accentuate in accordance with the depth to the anomaly source. An example of the application of this method is shown in the next section.

VLF interpretation has been mainly qualitative to data, though theoretical work is being done currently at several centres. Simple rules-of-thumb are easy to develop, based on the assumption of a plane, horizontal, primary field.

For a small, spherical body, depth to centre is approximately

$$d = \triangle x, \quad \text{where } \triangle x \text{ is the horizontal distance between points of maximum and minimum inclination}$$

and radius is approximately

$$r = 1.3 \, d \, \sqrt[3]{\tan^{-1} \theta \, max.}$$

For a thin cylinder, depth to centre is approximately

$$d = 0.86 \, \triangle x$$

and radius is approximately

$$r = 1.22 \, d \, \sqrt{\tan^{-1} \theta \, max.}$$

- 13 -

From Figures 7 - 9 it can be seen that for a line source, depth is approximately

$$d = \frac{\triangle x}{2}$$

This model approximates the steeply dipping sheet, or half-plane.

FIELD EXAMPLES

Figures 12(1) to 12(8) show examples of VLF E.M. profiles over a variety of bedrock conductors, and have been selected to illustrate some of the important features of the method. All of the drill holes in these examples were drilled to test the VLF anomalies.

Example 12(1)   Denton Township, Ontario

The in-phase (real component) profile shows the asymmetry typical of a relatively flat dip. The peaks occur roughly 75 feet from the inflection point, which is consistent with a conductor depth of about 50 feet. The quadrature profile shows a weak, positive inflection, suggesting that the body is a very poor conductor, and that overburden is relatively non-conductive.

Example 12(2)   Timmins, Ontario

These are fairly typical profiles, showing a positive in-phase cross-over and a negative quadrature anomaly. The conductor here is relatively massive and wide; the overburden is 70 - 80 feet thick and moderately conductive ($5 - 10 \times 10^{-3}$ mhos/m). The shape of the in-phase anomaly is consistent with a broad body, and also suggests a contribution from the overburden itself. The quadrature anomaly is caused almost entirely by the conducting body.

Example 12(3)   Mississippi Lead District

The profiles show a number of anomalies, of which only one has been drilled. Depth in this case is 250 feet, which is consistent with the depth derived from a sphere model using the adjacent peaks on either profile. The conducting body is probably discrete and flat-lying.

The relatively strong quadrature component suggests moderately conductive country rocks, in the range typical of limestones and dolomites.

- 14 -

The body itself is probably a poor conductor, though at VLF frequencies it clearly generates a respectable secondary field.

Example 12(4)   Gooderham, Ontario

The scale of this figure is more compressed than the others, but two or possibly three conductors are clearly indicated. The left-hand anomaly is typical of a good conductor lying close to surface - and drilling confirms this. The right-hand anomaly is suggestive of a very weak conductor, also close to surface. This has not been drilled, but low frequency E.M. and I.P. surveys confirm that it is probably poorly connected. The central conductor looks like an overburden effect.

Example 12(5)   Coppermine River, N.W.T.

This is a very typical anomaly for the area, where extensive VLF surveys have been carried out to map faults and breccia zones. The weak, negative quadrature response indicates that the fault zone is a moderate conductor. This is confirmed by I.P. survey and drilling. Chloritization and hematization in and adjacent to the fault may contribute to the conductivity.

Example 12(6)   Windsor, Nova Scotia

The country rocks here are moderately conductive and it is surprising that more quadrature response is not obtained. Possibly the main anomaly is caused by conductive material lying close to surface. It would be interesting to drill a deep hole to test the strong quadrature anomaly to the right of the known ore-zone.

Example 12(7)   Tudhope and Bryce Townships, Ontario

This example is included mainly to show the quadrature response that can be produced from a good conductor even at shallow depth in relatively non-conductive rocks. The quadrature profile also reflects the dip of the conductor.

- 15 -

Example 12(8)   Coppermine River, N.W.T.

This is an example of VLF in-phase data processed and contoured in accordance with Fraser's (7) program. The ease with which this map can be compared with the geology and other geophysical results, is one of its main advantages. Certain trends, in particular the one inclined to the west of the main north-south anomaly, are emphasized by this presentation of the data.

The quadrature profile, shown superimposed on the in-phase contours, is used to assist in identifying the conductors. In this case, the major faults appear to correlate with the stronger, negative quadrature anomalies.

CONCLUSIONS

The usefulness of the VLF E.M. method in mineral exploration and geological mapping has been established, and there is no doubt that it will enjoy continued popularity.

Measurements of the quadrature component are helpful in resolving anomalies from the various geological sources.

Better methods of data processing and interpretation are required if the VLF E.M. method is to be used to its fullest advantage, particularly in airborne surveys.

Airborne methods appear to have tremendous potential in both prospecting and mapping. Instrumentation for both helicopter and fixed wing use is being field tested and will shortly be in routine operation.

"Active" radio frequency methods for exploration from drill holes have been proven to be effective, and will probably find greater acceptance now that VLF E.M. has established its place in ore prospecting.

15a

DENTON TWP. ONT.

FIGURE 12(1)

15b

TIMMINS, ONT.
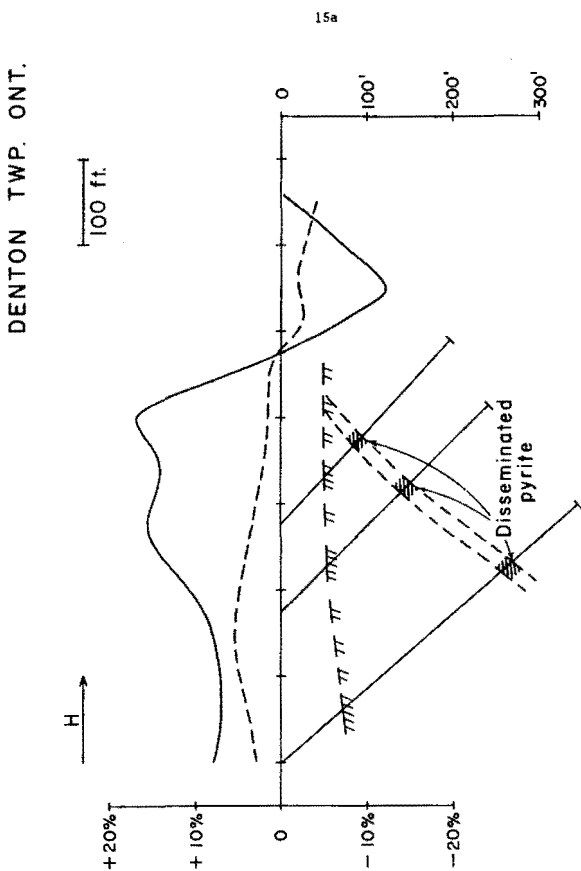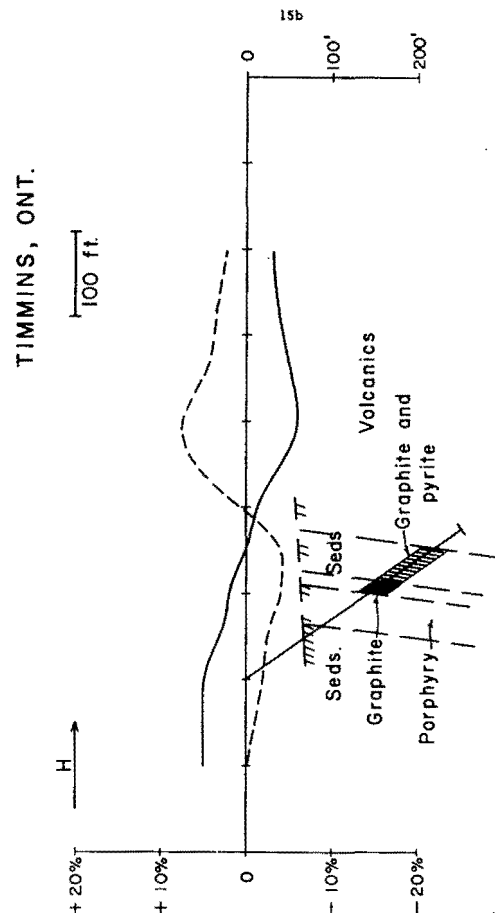
FIGURE 12(2)

COPPERMINE RIVER, N.W.T.

H →

100 ft.

+20%
+10%
0
−10%
−20%

0
100'
200'

Basalt, massive
vuggy
massive
altered
Fault zone
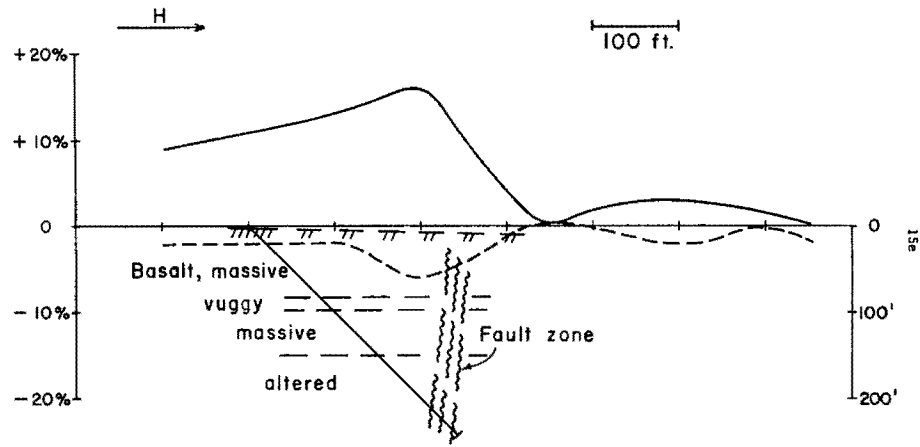
FIGURE 12 (5)

MISSISSIPPI LEAD
DISTRICT

H →

100 ft.

+20%
+10%
0
−10%
−20%

0
100'
200'
300'

Buff dol.
Drab dol.
Marcasite and
sphalerite
(approx. 15% comb.)
Trenton

FIGURE 12 (3)

WINDSOR, N.S.

H →

100 ft.

+20%
+10%
0
−10%
−20%

0
100'
200'
300'

Windsor Fm.
ls., sh., gyp., anh.

Horton Fm.
Sandstone, cgl.

Pyrite, galena,
sphalerite
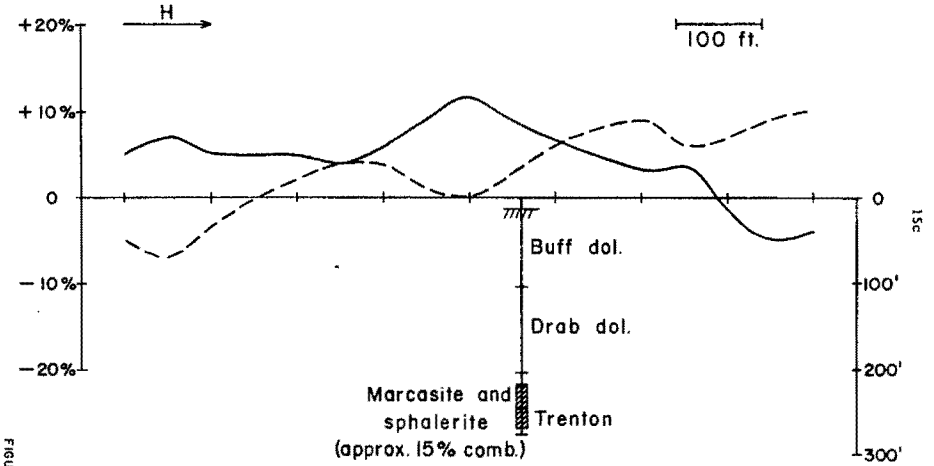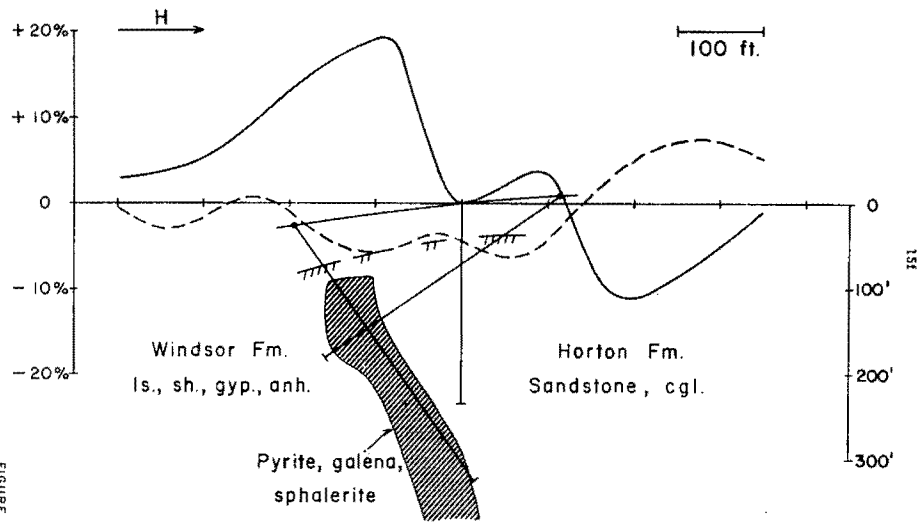
FIGURE 12 (6)

GOODERHAM, ONT.

H →

100 m.

+60%
+40%
+20%
0
−20%
−40%
−60%

0
100m
200m
300m

Massive
sulphides

Diss.
sulphides ?

Granite, gneiss, meta-seds.

FIGURE 12 (4)

TUDHOPE – BRYCE TWPS. ONT.

FIGURE 12 (7)

COPPERMINE RIVER, N.W.T.   FIGURE 12 (8)
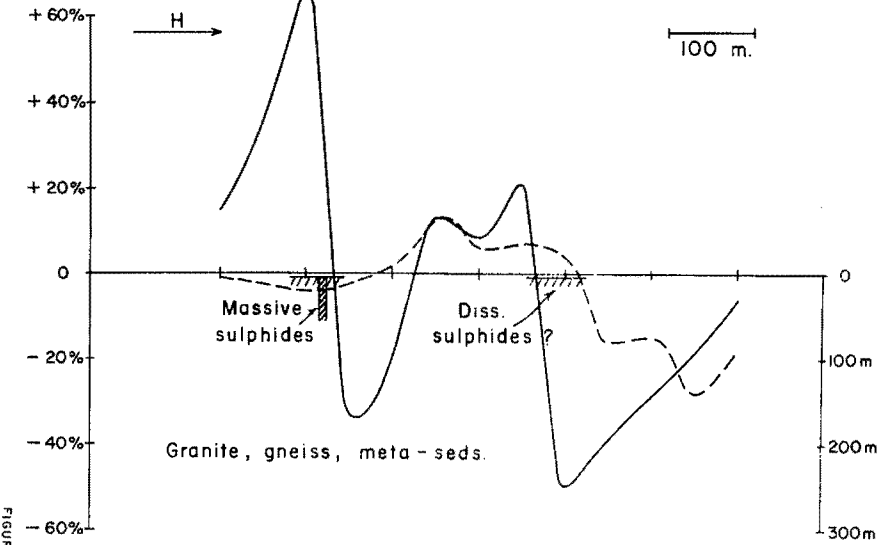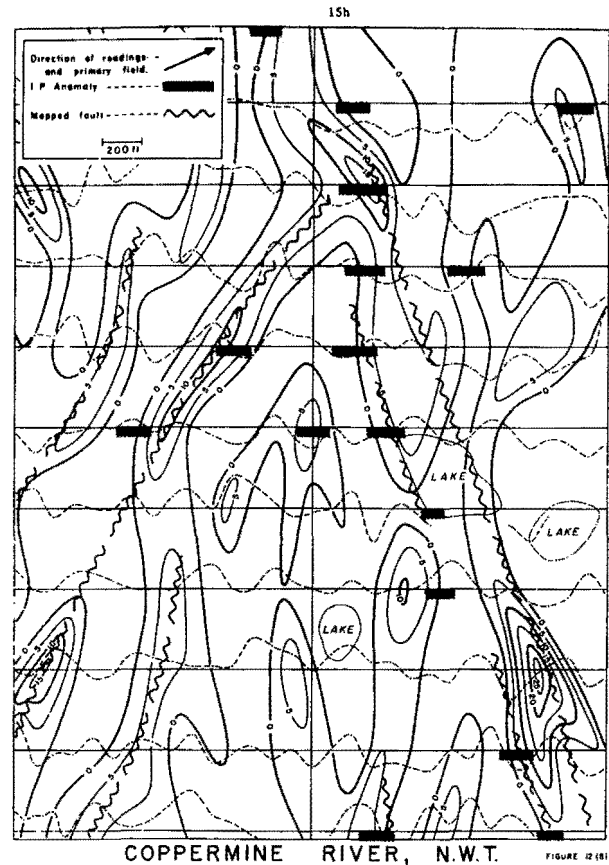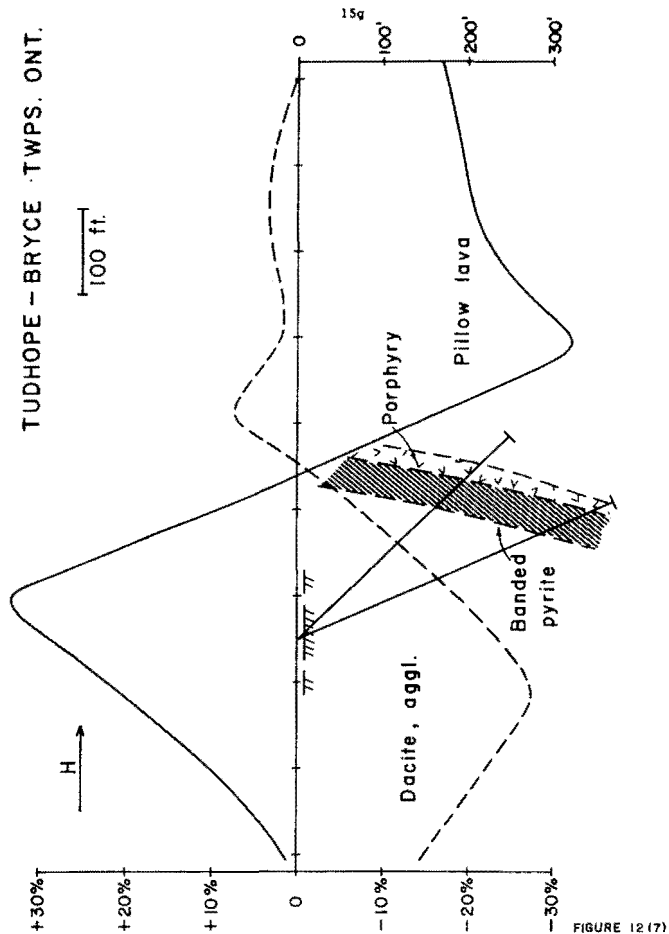
- 16 -

REFERENCES

1.   Heiland, C.A.; "Geophysical Exploration"; Prentice Hall, New
         York, 1946; pp.816-818.

2.   Eve, A.S. and Keyes, D.A.; A.I.M.E. Tech.Pub. No.316.

3.   Popov, A.A. and Frish, V.F.; "Subsurface Exploration with Radio
         Waves"; U.N.O. Interregional Siminar on New Methods
         for Mineral Exploration, Moscow, July 1967.

4.   Geonics Ltd.; "E.M.-16 Operating Manual"; 2 Thorncliffe Park
         Drive, Toronto 17, Ontario.

5.   Norton, K.A.; "The Propagation of Radio Waves over the Surface
         of the Earth and in the Upper Atmosphere"; Proc. I.R.E.,
         Vol.25, No.9, September 1937, p.1203.

6.   Grant, F.S. and West, G.F.; "Interpretation Theory in Applied
         Geophysics"; McGraw-Hill Book Co., New York etc.,
         1965; pp.482-484.

7.   Fraser, D.C.; "Contouring of VLF - E.M. Data"; GEOPHYSICS
         (in process).

GEONICS LIMITED

REPRINT FROM

GEOLOGICAL SURVEY OF CANADA

PAPER 76-25

GEOLOGICAL SURVEY
PAPER 76-25

VLF MAPPING OF GEOLOGICAL STRUCTURE

W.M. TELFORD
W.F. KING
A. BECKER

1977

CONTENTS

Illustrations

VLF MAPPING OF GEOLOGICAL STRUCTURE

Abstract

Field measurements with the EM16 instrument, in several areas definitely confirm the usefulness of the VLF method for mapping shallow geological structure. Results obtained across a portion of the Gloucester fault southeast of Ottawa indicate that this technique is particularly suitable in areas where the geology is simple. The field results generally agree rather well with theoretical model data. The latter, however, indicates that mapping with the EM16 alone produces little quantitative information, although the relative positions of the high and low resistivity beds are generally clear. For this reason, it is desirable to supplement the EM16 data occasionally with surface impedance measurements to obtain apparent resistivities on both sides of the contact. This is especially true where it is suspected that the observed anomaly is caused by an accident in the bedrock topography rather than by the opposition of beds of differing resistivity.

Résumé

Des mesures, sur terrain, avec l'appareil EM16 confirment l'utilité de la méthode TBF comme outil de cartographie des structures géologiques peu profondes. Les résultats obtenus à travers la faille de Gloucester au sud-ouest d'Ottawa indiquent que cette technique s'adapte très bien au problème posé dans des situations géologiquement simples.

Les résultats de terrain concordent très bien avec les calculs théoriques. Cependant ceux-ci démontrent qu'il est difficile d'obtenir des informations quantitatives à partir des mesures EM16 seules. Afin d'obtenir des résistivités apparentes des deux côtés du contact, on doit compléter les mesures EM16 avec des mesures de l'impédance de surface. Ceci est surtout vrai dans des cas où l'on soupçonne que l'anomalie est liée à un accident topographique de la roche en place plutôt que par une opposition des lits de résistivité différente.

VLF MAPPING OF GEOLOGICAL STRUCTURE

W.M. Telford[1], W.F. King[2] and A. Becker[3]

Foreword

This paper is a summary of the work done by W.F. King while working under the direction of Dr. A. Becker as a graduate assistant for the Geological Survey of Canada during the summers of 1969 and 1970. The data described form part of his M.Sc. Thesis dissertation, working under thesis supervisor, Prof. W.M. Telford, Department of Mining Engineering and Applied Geophysics, McGill University. This paper is a product of the application of new geophysical techniques being adapted to the geological mapping mission of the Electrical Methods Section, Resource Geophysics and Geochemistry Division, Geological Survey of Canada.

L.S. Collett,
Head, Terrain Geophysics Program,
Resource Geophysics and Geochemistry Division

INTRODUCTION

It has long been observed that electromagnetic plane waves propagating along the earth's surface are locally distorted by near-surface discontinuitites in electrical resistivity. In such cases the horizontal magnetic field components normally present induce in the ground a non-uniform eddy current distribution which results in an anomalous vertical magnetic field component. In the
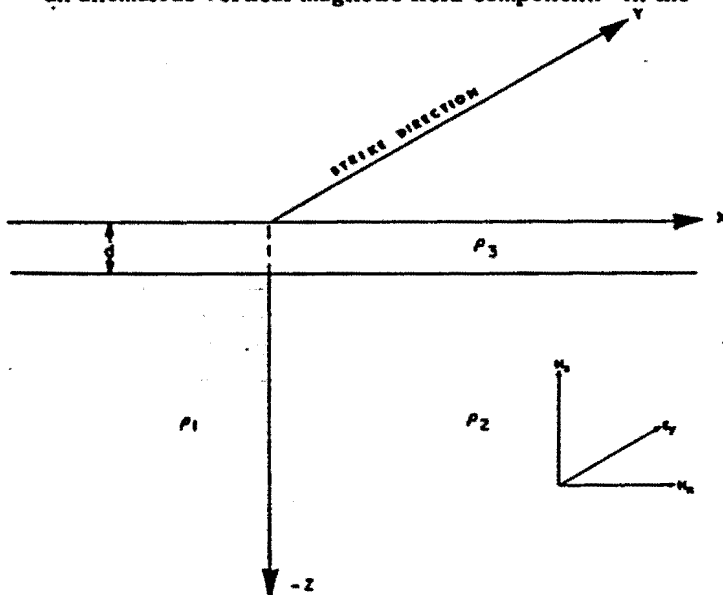
Figure 1. Two-dimensional fault with strike length infinite in y-direction: insert shows E polarization vectors.

[1] Department of Geophysics, McGill University. P.O. Box 6070, Station A, Montreal H3C 3G1, Canada

[2] Chevron Standard Company Ltd., 400 5th Ave. S.W. Calgary, Alberta

[3] Managing Director, IREM-MERI, P.O Box 6079, Station A, Montreal H3C 3A7, Canada

extra low frequency range (ELF) this phenomenon is readily observable near coastlines (Weaver, 1963) while in the audiofrequency range (AFMAG) the effect was first observed by Shaw (oral comm., 1961) in the vicinity of faults and shear zones. More recent y. Collett and Bell (1971) have discussed how the AFMAG method can serve as a useful tool in structural mapping. Finally at very low frequencies (VLF) i.e. in the 10-20 kHz range the effect of geological structure has been observed by Becker (1967), Fraser (1969) and Patterson and Ronka (1971).

These effects were explained theoretically by Weaver (1963) who obtained closed form solutions for plane waves incident on a semi-infinite conducting medium divided by a vertical discontinuity into two regions of different resistivity. Weaver's calculations were later confirmed experimentally by Dosso (1976) on a laboratory scale model. Both authors forecast a sharp increase in vertical magnetic field component near an electrical discontinuity. This quantity exhibits a maximum value at the discontinuity and decreases gradually to zero away from it.

The rate of decrease is a function of the electrical properties of the material on either side of the discontinuity, being greater on the conductive side. More recently this problem was studied by Geyer (1972a, b) who found that the spatial variation of the vertical component was strongly influenced by the dip of the interface.

The purpose of the present study was to examine in some detail the variation exhibited by the field components of a plane electromagnetic wave in the vicinity of a fault. In particular we have elected to study the variation in the vertical magnetic component and in the surface wave impedance across the discontinuity. As will be shown later, in the results section, we were fortunate to be able to perform the measurements in relatively simple geological environments so that a good comparison could be made between our theoretical predictions of electromagnetic field behaviour and the observed variations.
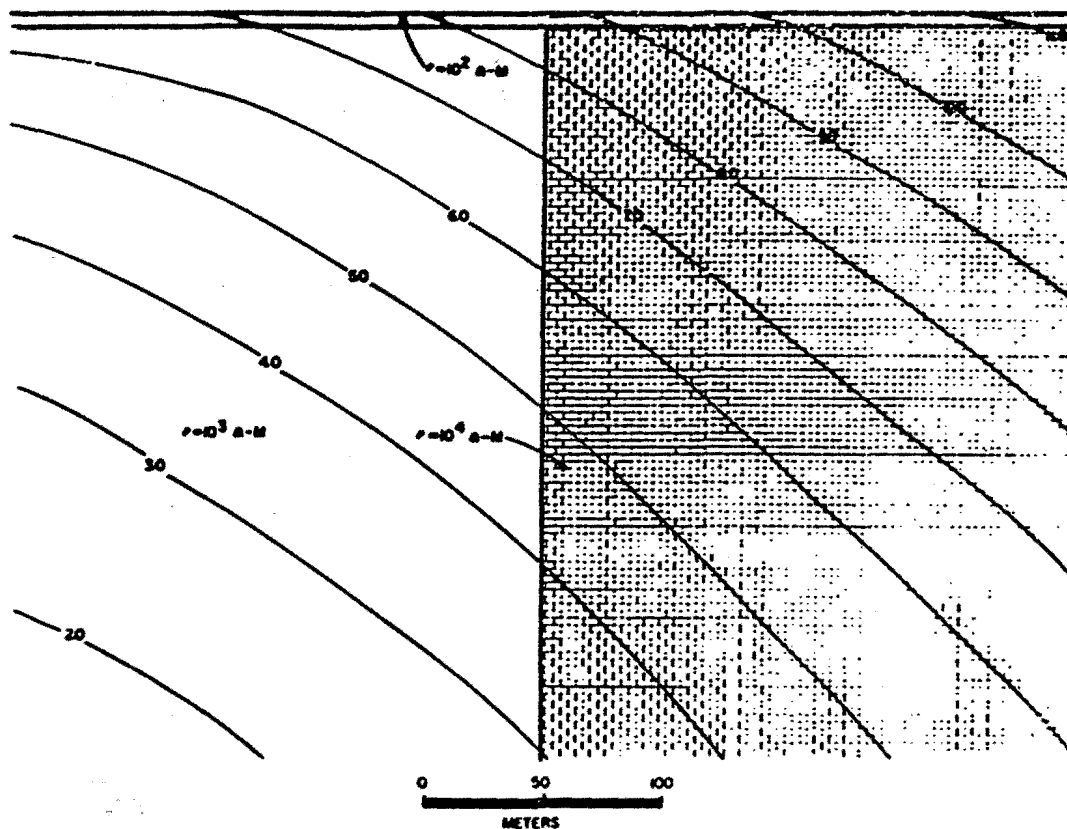
Figure 2.

Subsurface current flow (E_y, relative amplitude distribution) at 10 kHz in the structure of Figure 1.

Figure 3. Theoretical profiles of H_x, H_z and Δ_{z-x} over structure of Figure 2.

THEORY

Vertical magnetic field variations

A number of authors (Jones and Price, 1970), Swift (1971) have discussed the mathematical basis for the distortion of an electromagnetic plane wave over a vertical discontinuity separating two half-spaces of different conductivity, with and without an overburden layer above. For a remote natural EM source the direction of E, the electrical and H, the magnetic horizontal vectors is random with respect to the co-ordinate system shown in Figure 1. These vectors, however, may be resolved into components parallel and normal to the contact. The appropriate Maxwell equations thus become:

$$\frac{\partial E_z}{\partial x} - \frac{\partial E_x}{\partial z} = j\omega\mu_o H_y$$

$$\frac{\partial H_y}{\partial z} = -\sigma E_x \qquad \begin{array}{l}\text{for E normal to strike} \\ \text{(H polarization)}\end{array}$$

$$\frac{\partial H_y}{\partial x} = \sigma E_z$$

and:

$$\frac{\partial E_y}{\partial x} = -j\omega\mu_o H_z$$

$$\frac{\partial E_y}{\partial z} = j\omega\mu_o H_x \qquad \begin{array}{l}\text{for E parallel to strike} \\ \text{(E polarization)}\end{array}$$

$$\frac{\partial H_x}{\partial z} - \frac{\partial H_z}{\partial x} = \sigma E_y$$

Figure 4. Tilt and ellipticity profiles for d/δ = 1/10, 0 for the structure of Figure 2.
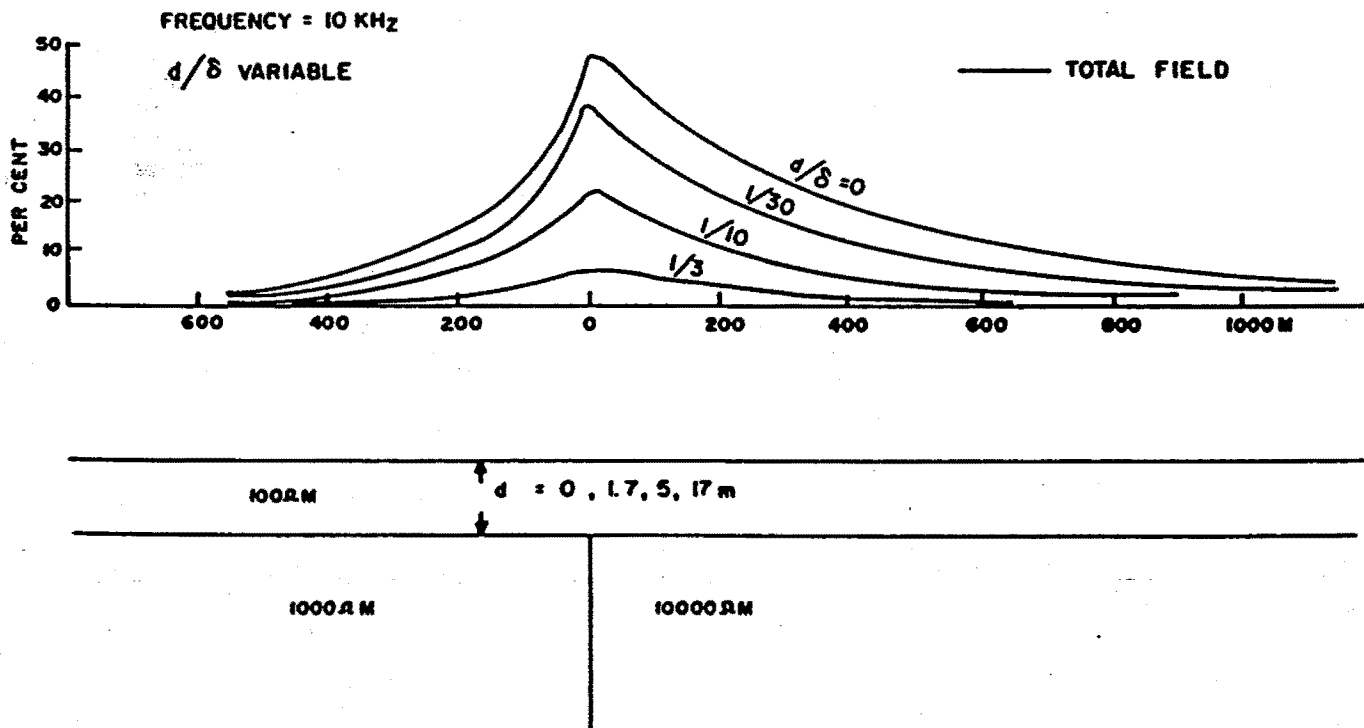
Figure 5. Total field, $|H_z/H_x|$, profiles over the structure of Figure 2 with d/δ = 0, 1/30, 1/10, 1/3.

3

The E polarization is particularly convenient for the VLF method, which measures H_z and H_x. It is customary, where possible, to select a remote station whose H_x vector is roughly parallel to the survey lines, that is, the station location is more or less parallel to strike.

The VLF source field, propagating parallel to the earth surface and refracted vertically downward at the ground interface, thus provides H_x and E_y components approximately in the appropriate direction. The ground current flow may be readily illustrated by calculating with the aid of numerical techniques (Swift, 1967; Madden and Swift, 1969; Ku et al., 1973) the actual subsurface electric field distribution for a given geological situation.
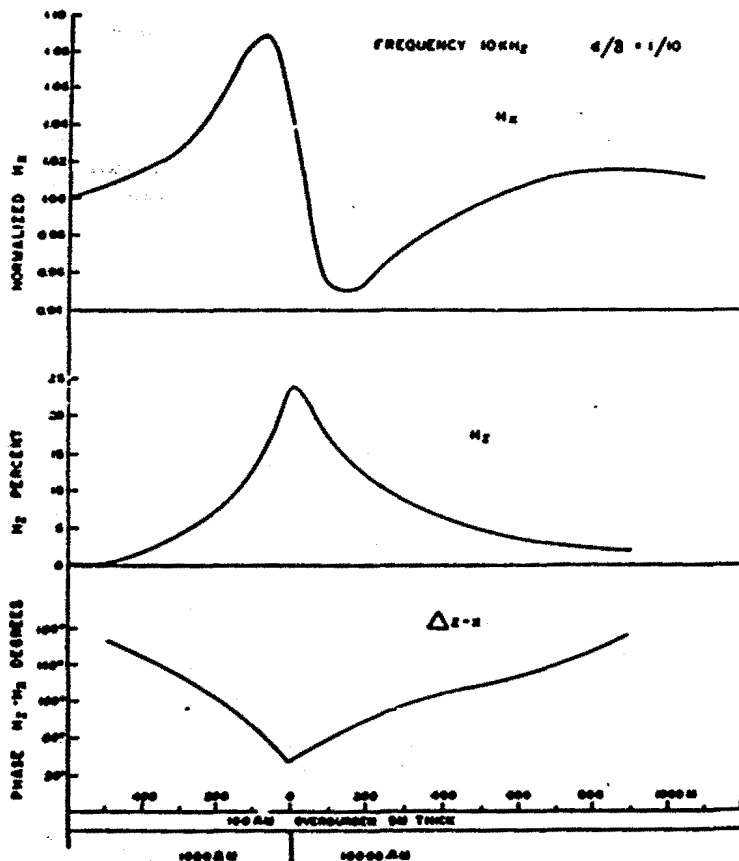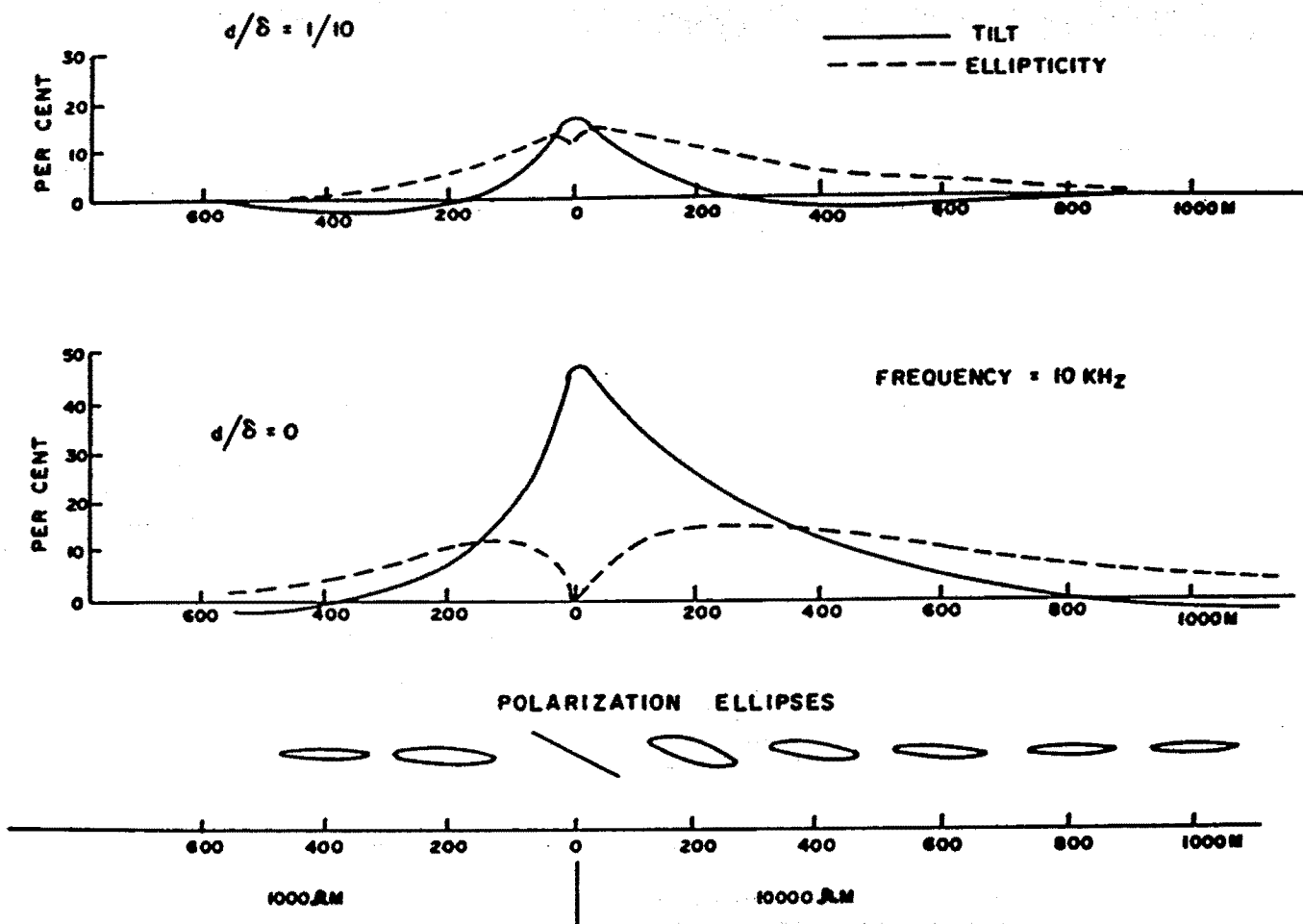
Figure 2 shows the subsurface current flow (actually the E_y field amplitude distribution) at 10 kHz in the structure of Figure 1 with an overburden of 100 Ωm, 5 m thick and the contact separating beds of 1000 and 10 000 Ωm. Since the skin depth ($\delta = 500\sqrt{\rho/f}$) for 100 Ωm and 10 kHz is about 50 m, the EM wave is not greatly attenuated in the overburden. Use is made of the ratio d/δ, where d is overburden thickness, since it involves all the significant overburden parameters.

Theoretical profiles of H_x, H_z and Δ_{z-x} over the same structure, are illustrated in Figure 3. As the fault is approached from the left (conductive side) the horizontal magnetic field increases to a maximum, falls sharply to a minimum as the contact is crossed and then increases slowly to background value as the traverse proceeds to the right. The slope is always steeper on the conductive side of the contact, although increasing overburden thickness and/or conductivity reduces the profile amplitude considerably. For very small values of d/δ the background value of H_x is actually larger on the conductive side than at large distances to the right.

The H_z field shows a peak directly over the contact which decays to zero on the flanks. Again the slope is steeper on the conductive side and the peak amplitude is controlled by d/δ. In the bottom profile, the phase variation, Δ, between H_z and H_x is roughly an inverted image of the vertical magnetic field, with a minimum of 32° above the contact and a more or less linear increase on both sides, the steep slope again appearing over the conductive bed. When d/δ = 0 the phase shift is zero
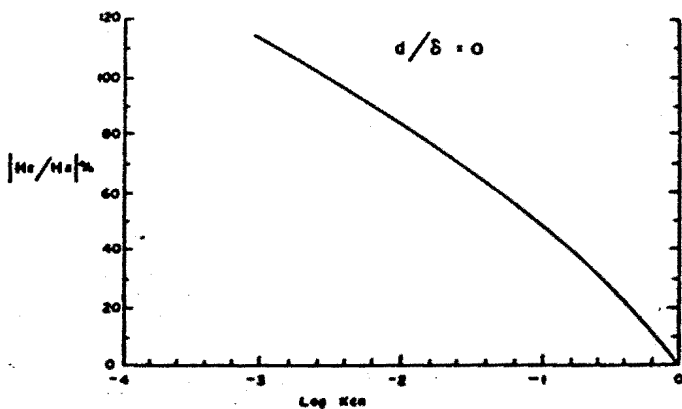
Figure 6. Peak amplitude of total field plotted against log K_{CR} for structure of Figure 2. No overburden.
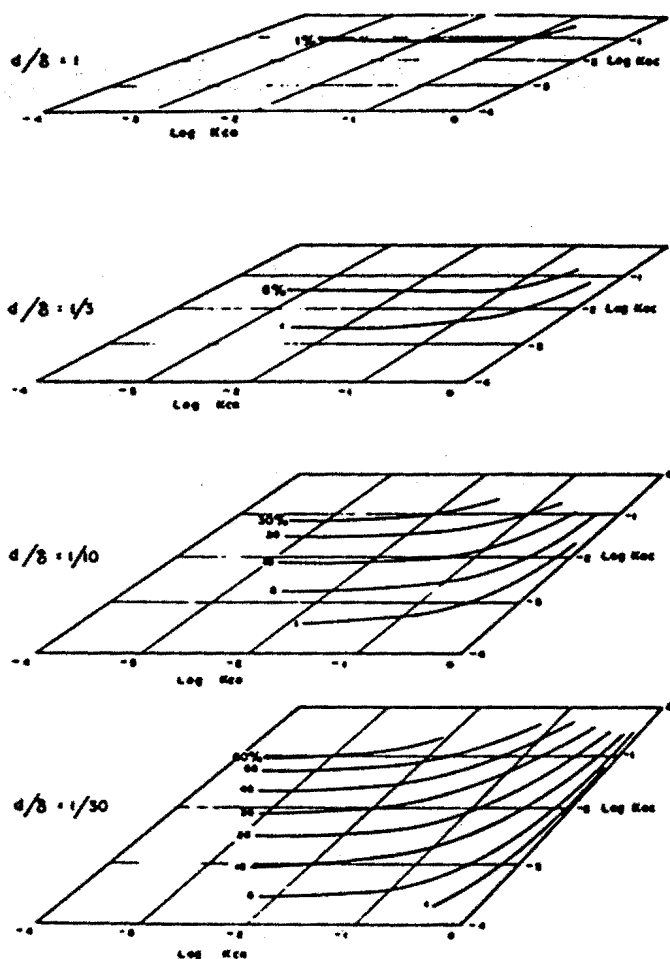
Figure 7. Peak amplitude of total field plotted against log K_{CR} and log K_{OC}, for d/δ = 1, 1/3, 1/10, 1/30 and structure of Figure 2.

at the contact; as this ratio increases, the cusp persists, although its phase increases.

Because H_z and H_x differ in phase in the vicinity of a conductive discontinuity, the resultant EM wave is elliptically polarized (Heiland, 1940; King, 1971; Paterson and Ronka, 1971). The wave tilt θ (inclination of the major axis with respect to the horizontal) and ellipticity r (ratio of minor to major axes) of the ellipse are given by:

$$\tan 2\theta = \frac{2R \cos \Delta}{1 - R^2}$$

$$r^2 = \frac{1 + R^2 - \sqrt{(1+R^2)^2 - 4R^2 \sin^2 \Delta}}{1 + R^2 + \sqrt{(1+R^2) - 4R^2 \sin^2 \Delta}}$$

where $\Delta = \phi_z - \phi_x$ the phase difference between vertical and horizontal field components, and, $R = |H_z/H_x|$ is their amplitude ratio. With a little manipulation and assuming that H_x is considerably larger than H_z, which is generally the case, these relations become:

$$\tan \theta = R \cos \Delta$$

$$r = R \sin \Delta.$$
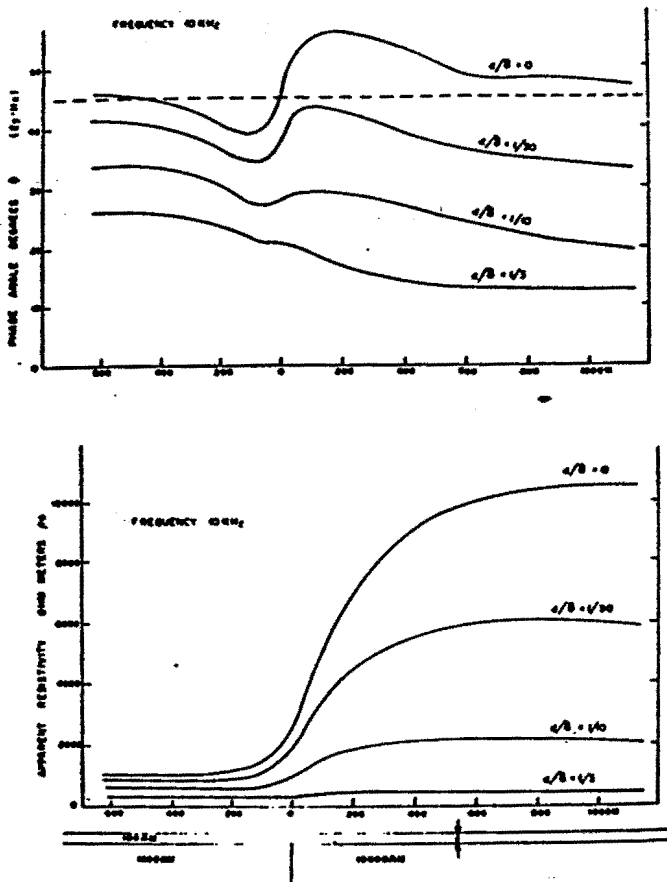
Figure 8. Theoretical profiles of ρ_a and ϕ over structure of Figure 2 for d/δ = 0, 1/30, 1/10, 1/3.

In this case it is useful to note that the total normalized vertical field can be directly calculated from the measurements from:

$$R^2 = \tan^2 \theta + r^2$$

The parameters θ and r are related to "in-phase" and "quadrature" components of the secondary magnetic field (see section on instrumentation). Profiles of tilt and ellipticity, for d/δ = 1/10 and zero (no overburden) are shown in Figure 4. The polarization ellipses at several stations along the traverse are included in the latter profile. Directly above the contact, if the value of Δ is zero, the ellipse degenerates to a straight line whose slope is H_z/H_x.

Clearly the overburden has a pronounced effect on both the tilt and ellipticity profiles. Figure 5 illustrates this point further, where the total vertical secondary field H_z, expressed as a percentage of the primary field, is plotted for increasing values of d/δ.

Two additional parameters may be employed to determine maximum response over the contact. These are K_{CR}, the ratio of resistivities in the conductive and resistive beds and K_{OC}, the ratio of overburden resistivity to the resistivity of the more conductive

bed. When d/δ = 0, the maximum total field response is controlled by K_{CR} only; this is shown in Figure 6, where $|H_z/H_x|$ max is plotted against log K_{CR}. Figure 7 displays total field values for variable K_{OC} as well as K_{CR}, corresponding to d/δ ratios of 1/30, 1/10, 1/3 and 1. When d/δ = 0, the peak response will be 50% for any K_{CR} = 1/10 (10 Ωm vs 100 Ωm, 1000 Ωm vs 10 000 Ωm, etc.); it should be noted, however, that the profile widths will be different. This will also be true for other values of d/δ when K_{CR} and K_{OC} are fixed.

From the foregoing discussion it is clear that, in areas where the overburden resistivity is large compared to rock resistivity or where d ~ 0, it would be possible to use the H_z measurements to determine the structure parameters from the $|H_z/H_x|$ max ratio, from the skewness of the profile, and from the profile width. A conductive overburden, however, affects these quantities greatly and other techniques are required. In general, we may summarize the behaviour of EM field components over a vertical fault as follows:

1. The total field response is an asymmetric peak over the fault and decays more rapidly on the more conductive side.

2. The in-phase component of the secondary vertical magnetic field is also an asymmetric peak above the fault and decays more rapidly on the more conductive side.
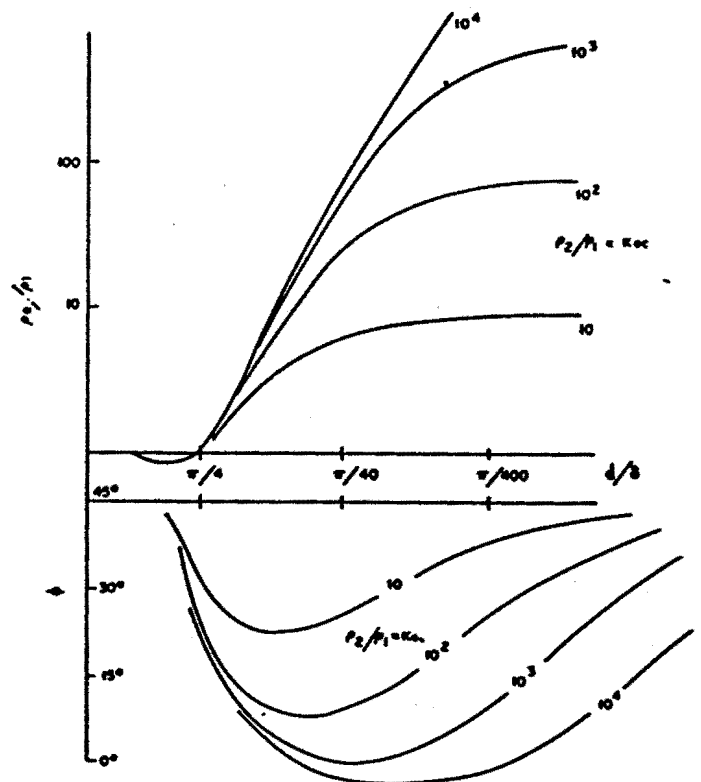
Figure 9. Variations of amplitude $|\rho_a/\rho_1|$ and phase ϕ for two-layer earth with resistive basement (after Cagniard (1953)).

LEGEND

- ▨ Carlsbad Shale
- ▦ Ottawa Limestone
- ▥ Oxford Limestone
- □ March Sandstone
- ⣿ Nepean Sandstone
- x·x·x·x Fault Trace VLF Survey
- ∿∿∿ Fault Trace Geological Survey
- - - - - Aeromagnetic Contours Gammas

GEOLOGY
AEROMAGNETICS
Gloucester Twp., Ontario

Horizontal Scale 0 ___ 1500 feet
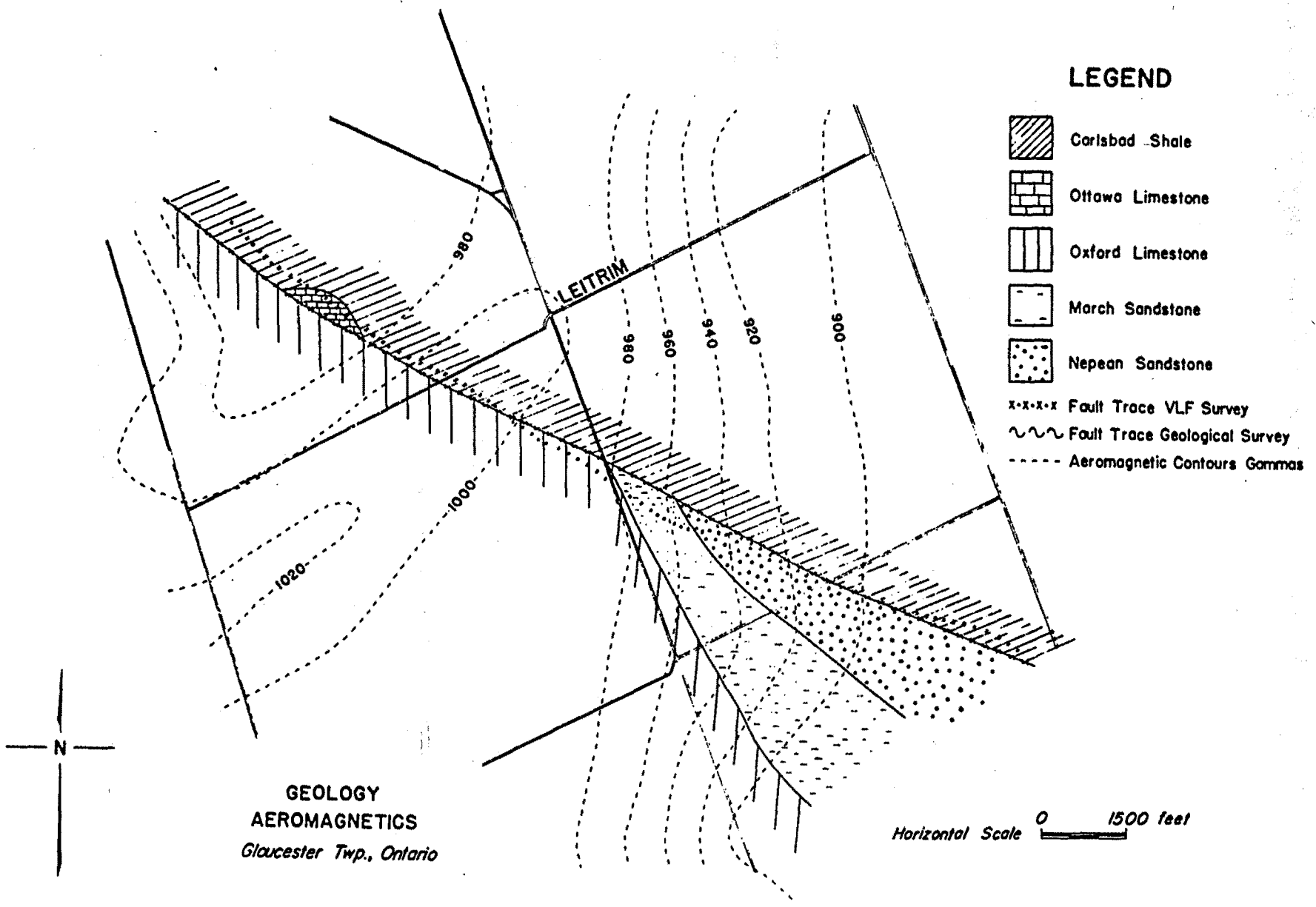
Figure 10. Geology and aeromagnetic contours, Leitrim area.

3. The quadrature component displays a local minimum over the fault, the response being broader than that of the in-phase. The minimum becomes less pronounced with increasing depth of overburden.

4. Both in-phase and quadrature response decrease with increasing depth of overburden. The quadrature response becomes greater than that of the in-phase when the overburden thickness is more than approximately one-half a skin depth.

5. In-phase and quadrature response increase with increasing resistivity contrast across the fault.

6. Anomaly width decreases with increasing frequency, for a given resistivity contrast.

Surface impedance variations

Another method which can be useful for the mapping of lateral discontinuities involves the simultaneous measurement of E_y and H_x as in magnetotellurics (Collett and Becker, 1968). The surface impedance, Z, is the ratio of these two quantities and defines the "apparent resistivity" for the underlying terrain via

$$\rho_a = \frac{1}{\mu\omega} \, |Z|^2 \qquad \text{in MKS units.}$$

Usually, Z is a complex quantity because E_y and H_x are not in phase with each other. Thus Figure 8 shows theoretical profiles for the apparent resistivity and the phase difference between E and H across the original contact of Figures 2 to 6 for the d/δ ratios used previously. It is again apparent that increasing depth of overburden influences the results by decreasing values of both ρ_a and ϕ on each side of the contact, while smoothing the profile slope directly over it.

Although the variation in the apparent resistivity near the contact can only be calculated numerically, the values of this quantity and the accompanying phase difference, remote from the fault, can be computed analytically. Variations of amplitude $|\rho_a|$ and phase ϕ for a two-layer earth — that is, the overburden layer remote from the fault — are shown in Figure 9. These are the standard master curves developed by Cagniard (1953), reproduced only for a conductive upper layer. Although magnetotelluric sounding normally involves measurement of horizontal orthogonal E and H fields over a range of frequencies, it is possible, by assuming a resistive bedrock, to estimate the overburden parameters from this master chart even when $|\rho_a|$ and ϕ have been determined only at a single frequency in the field.

LEGEND

IN PHASE ———
QUADRATURE -----

VLF SURVEY
GEONICS EM-16
Gloucester Twp., Ontario

N → TO CUTLER, MAINE

Horizontal Scale 0 ___ 500 feet

Vertical Scale 0 ___ 60 per cent
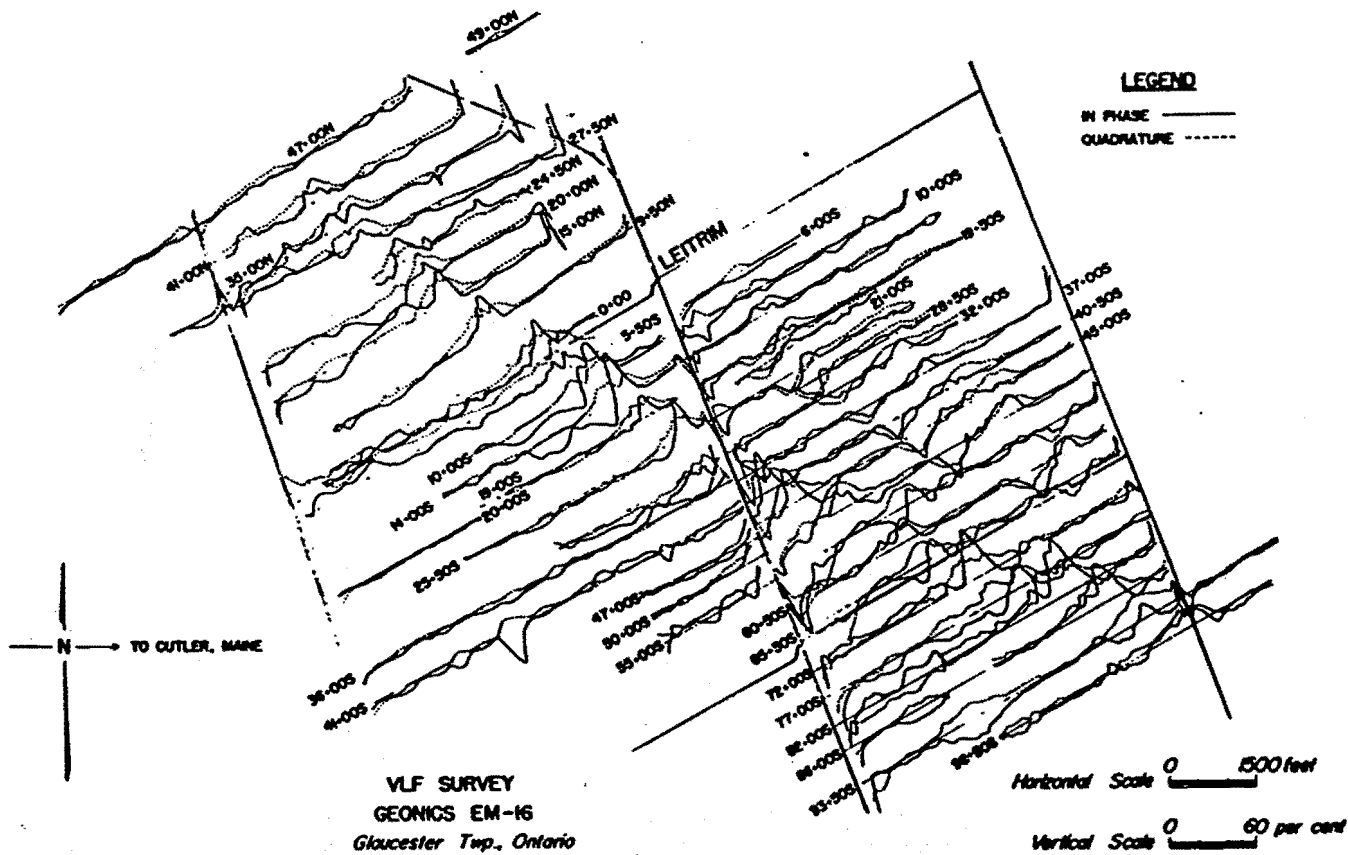
Figure 11. VLF in-phase and quadrature profiles, Leitrim area.

INSTRUMENTATION

Measurement of magnetic field tilt and ellipticity

The Geonics EM16 VLF receiver has been described elsewhere (King, 1971; Paterson and Ronka, 1971; Phillips and Richards, 1975). At least two other instruments — the Scintrex SCOPAS and Crone RADEM — are also designed to measure properties of the polarization ellipse over the same frequency range. With the EM16 a minimum signal is obtained in the receiver by aligning the instrument receiver axes with the major and minor axes of the field polarization ellipse. At this tilt angle, the voltages induced in the two receiver coils are exactly in quadrature with each other and may be directly compared by adding a 90° phase shift to one of them. This comparison is made with the use of the "quadrature" dial which then allows a direct reading of the ellipticity. As indicated previously the tilt angle reading, in percent, is associated with the "in-phase" component of the secondary vertical field and the ellipticity is associated with the "quadrature" component of the same quantity.

In order to avoid ambiguity in profile plotting and interpretation, some sign convention must be maintained during field surveys. From the equations for E-polarization involving H_z and H_x in the previous section, we find that:

$$\frac{H_z}{H_x} = -\frac{\partial E_y/\partial x}{\partial E_y/\partial z}$$

Thus the value of tan θ may be positive or negative, depending on the sign of $\partial E_y/\partial x$; since E_y is larger on the resistive side of the fault, the x-gradient will be positive if the traverse proceeds from the conductive side and vice versa. For consistency the following azimuth orientation was maintained during field work.

For traverses approximately east-west (north-south), the operator faces east (north) as nearly as possible, depending on the transmitter azimuth, to make measurements, while dip angles to the east (north) are reckoned positive. With this convention, both in-phase and quadrature values are positive when the resistive bed lies to the west (south) for an east-west (north-south) traverse, while a negative response indicates the resistive bed is east (north).
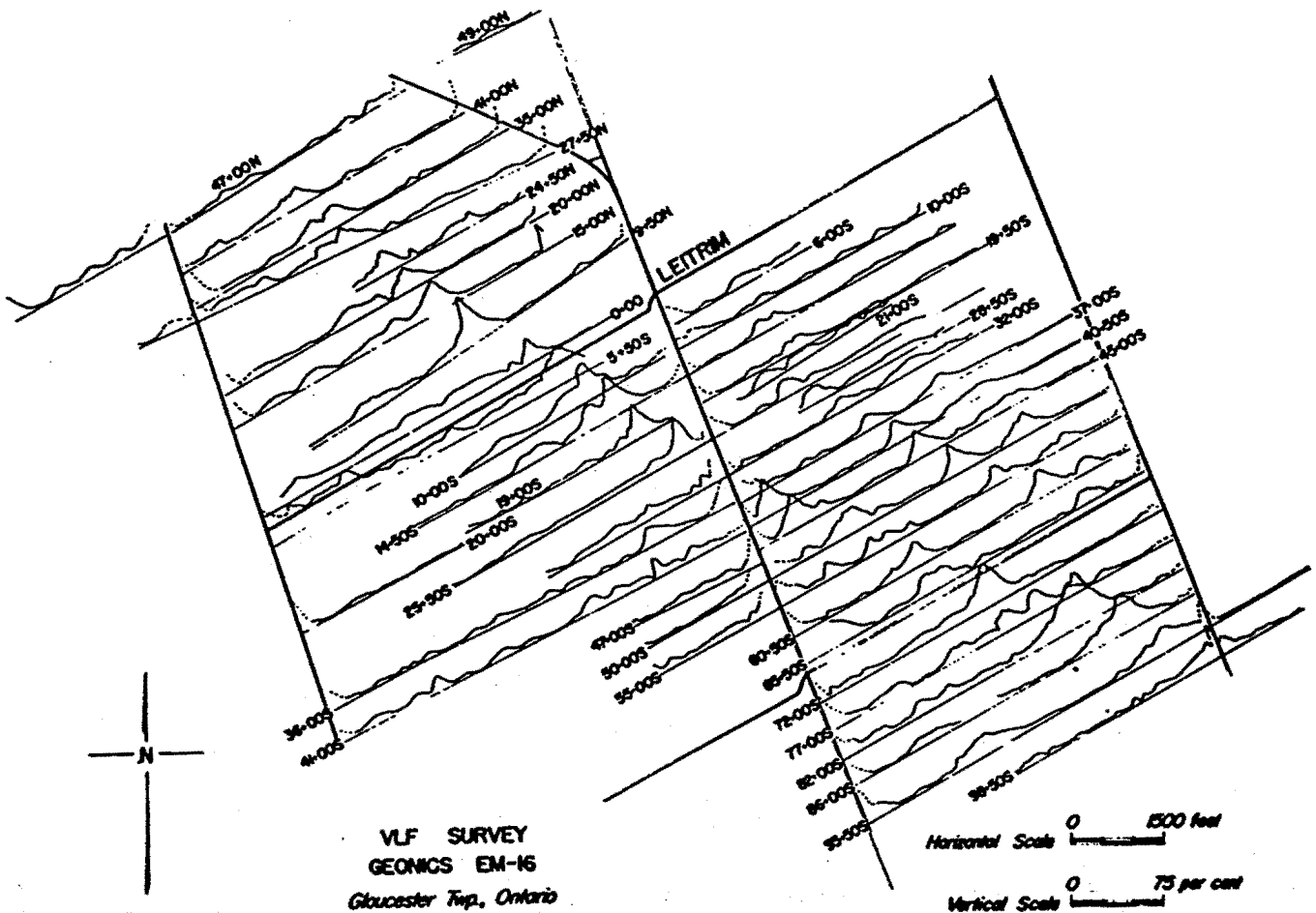
Figure 12. VLF total field profiles, Leitrim area.

8

Measurement of complex wave impedance

The Westinghouse Georesearch Model C-602 VLF Wave Impedance Meter was used for measuring ρ_a and ϕ. A Geonics EM16R unit, unavailable at the time, is equally suitable for this purpose. Both employ the magnetotelluric method, with a horizontal axis coil to detect the H_x magnetic field component and a 10 m dipole, consisting of two electrodes driven into the ground, for the E_y orthogonal electric field. Both are null instruments. With the Westinghouse meter the ρ_a and ϕ values are read off graphs supplied with the instrument. Its frequency range is 10-60 kHz. The EM16R is a modified form of the EM16, whose frequency range is about 15-25 kHz; resistivity and phase readings are obtained from dial readings at null signal.

FIELD WORK

Gloucester Fault

The principal test area for field work was in the vicinity of Leitrim, near Ottawa, where the Gloucester fault strikes roughly southeast for some 30 miles. The map in Figure 10 includes some geology and aeromagnetic contours. Beds of Carlsbad shale form the north side of the contact, adjoining Oxford limestones in the northwest half, while March and Nepean sandstones occupy the southeast portion (Wilson, 1946).

Aeromagnetic contours indicate very little susceptibility contrast between these formations. The fault trace determined by geological mapping is a smooth line; that outlined by the VLF Survey differs only in detail in some areas. This is a nearly vertical dip-slip fault downthrown to the northeast and displaced upwards on the southwest.
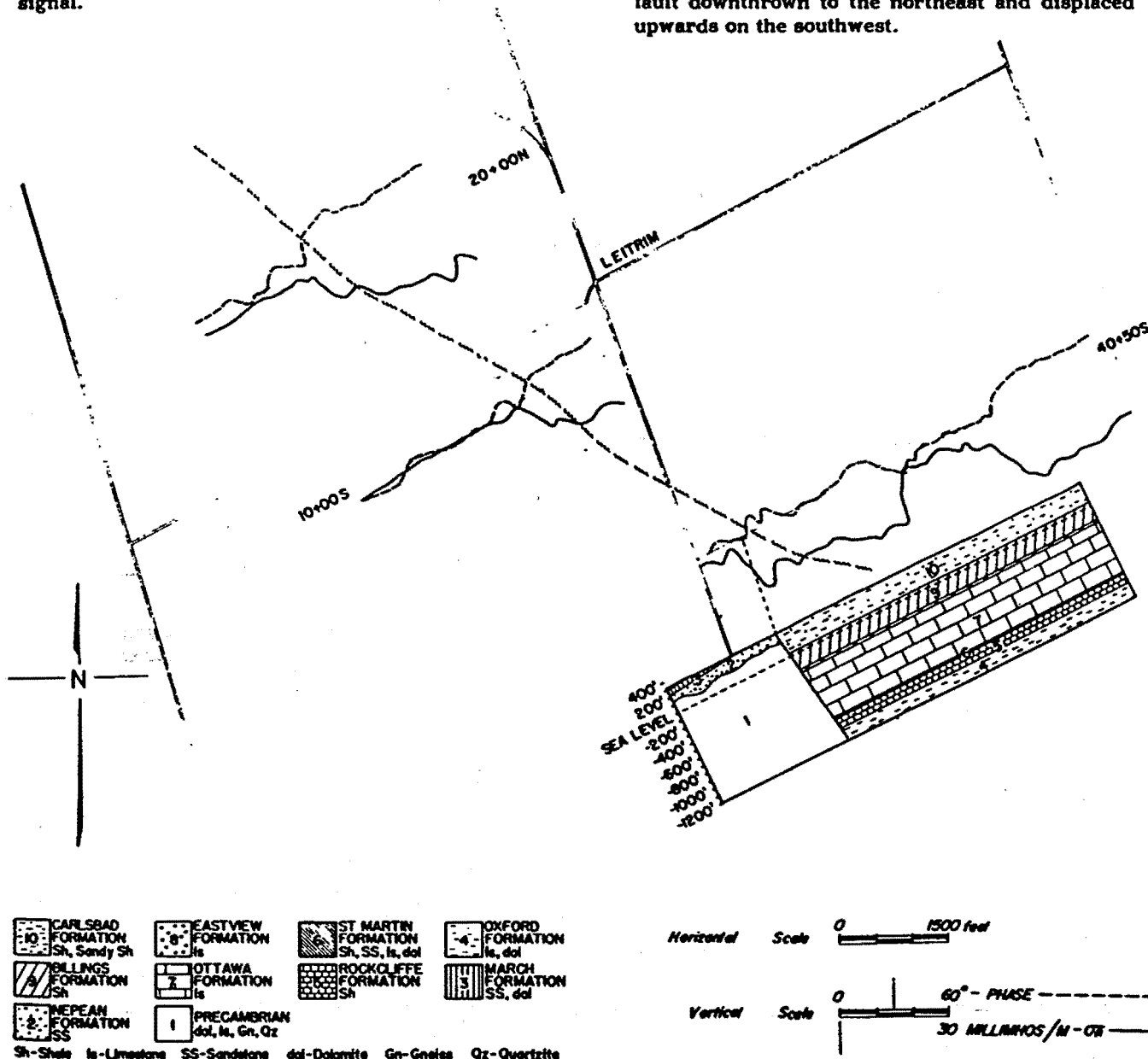
Figure 13. Apparent conductivity (σ_a) and phase (ϕ) profiles on lines 20+00N, 10+00S, and 40+50S, Leitrim area.

A brief description of the various formations and their resistivity is tabulated below (Andrieux written comm., 1971):

Formation	Geology	Resistivity
Carlsbad	Shale, limestone-dolomite	85 Ωm
March	SS-dolomite layers	—
Nepean	SS-siliceous cemented	1500 – 3000
Ottawa	Limestone, shale-SS layers	2000 – 3000
Oxford	Thick dolomite with some ls	5000
Rockcliffe-St. Martin	Shale + SS levels; ls + sh + dolomite	low?

VLF profiles showing in-phase and quadrature response over this area are displayed in Figure 11 and those for the total field (R) in Figure 12. Line spacing was about 500 feet on average and the traverses, approximately normal to the fault, were generally one mile long. As indicated, the lines strike east-northeast; the Cutler Maine transmitter, NAA (17.8 kHz) which is about 400 miles due east of the area, was used for the entire survey. Although a VLF transmitter located approximately north or south of Ottawa would have been more suitable. the Cutler station provided the best signal for this area. Readings were taken facing north. Station spacing varied from 50 feet near the fault to 200 feet remote from it.
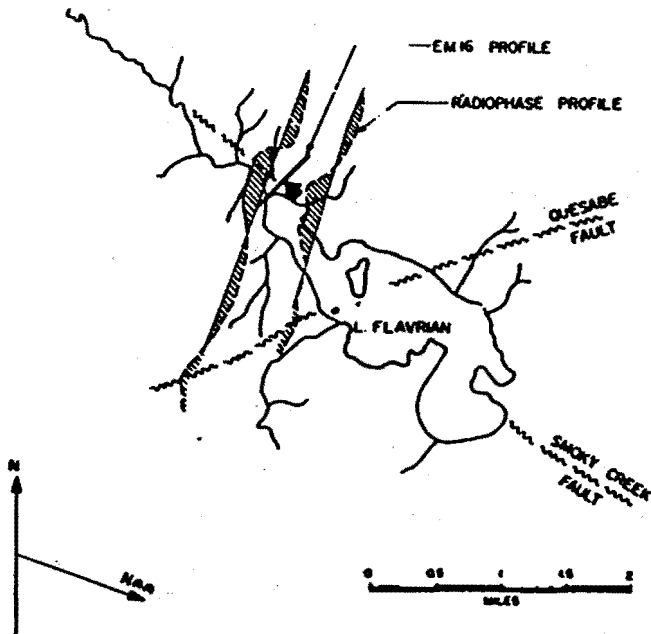
Figure 14. Airborne VLF and traverse line, Smoky Creek fault area, Lake Abitibi-Noranda area.
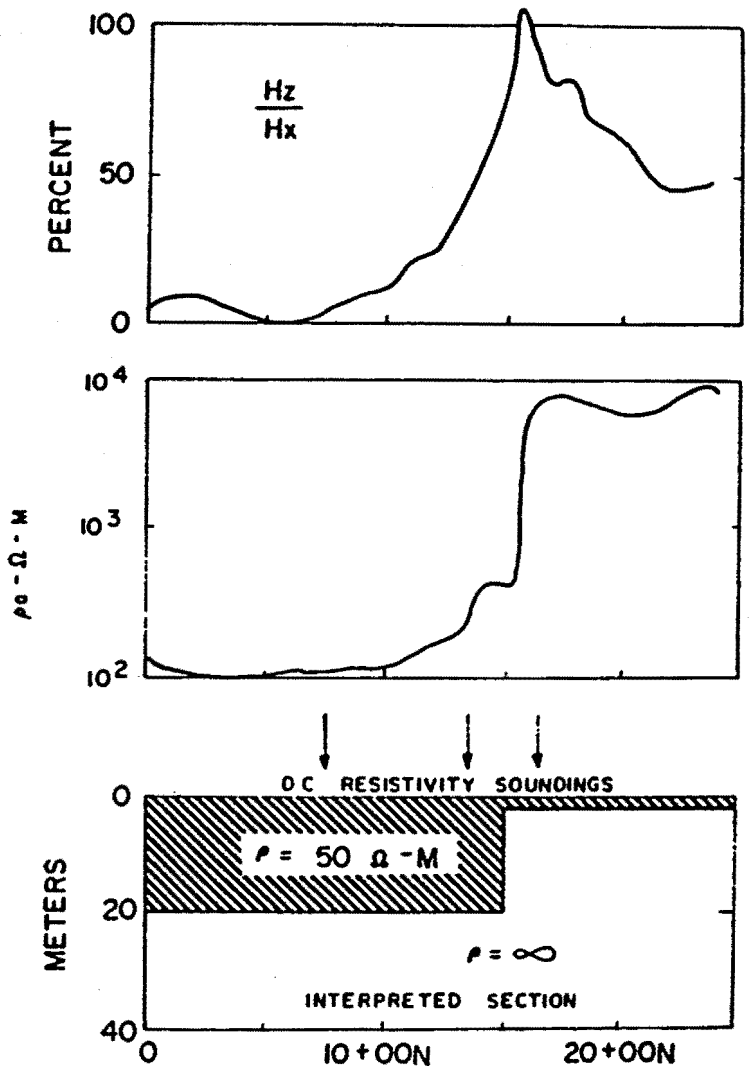
Figure 15. VLF total field, and ρ_a profiles line A3, Smoky Creek fault.

The data displayed in Figure 11 provide excellent examples of the vertical contact between beds of contrasting resistivity. Nearly all the profiles show a pronounced anomaly where the Gloucester fault is expected to occur, consisting of asymmetric in-phase and quadrature peaks with the steeper slope to the northeast, corresponding to the more conductive bed. The quadrature anomalies, which are generally broader, flatter and of smaller amplitude than the in-phase, also have a characteristic local minimum or cusp (e. g. Lines 24+50N, 0+00, 14+00S, 19+00S, 25+50S, 41+00S, 47+00S, 50+00S, 72+00S, 83+00S) coinciding more or less with the in-phase maximum on many profiles.

There is another distinct anomaly about 2000 feet east of the Gloucester fault between lines 21+00S and 65+50S. Both in-phase and quadrature peaks are negative, the latter displaced slightly to the west of the in-phase on several lines, notably 60+50S. The steeper slope is on the southwest. Slight quadrature cusps are evident on lines 40+50S, 45+00S and 50+00S. These data define a second contact with the resistive bed to the northeast.

A third anomaly still farther east appears between lines 32+00S and 60+50S. Here the peaks are positive and the asymmetry indicates the resistive bed is on the southwest side of the contact. The quadrature response is larger than the in-phase on several lines. This feature, which is about 1300 feet east of the second contact on line 32+00S, appears to merge with it to the southeast. On line 60+50S the separation has decreased to about 800 feet, producing a crossover type of response due to the proximity of the positive and negative peaks.

The total field profiles of Figure 12, although they contain less information than Figure 11, probably give a clearer picture of the three contacts discussed above, since the anomalies are all positive and there is less clutter.

Wave impedance profiles carried out on lines 20+00N, 10+00S and 40+50S are shown in Figure 13. Here we have plotted the apparent conductivity (reciprocal of apparent resistivity) and ϕ the phase difference from 45°. On line 20+00N there is one pronounced break for both parameters, approximately at 36+00W. The generally low apparent conductivity 4 - 2 millimhos/m west of this station rises sharply and remains greater than 20 millimhos per metre for the eastern portion of the traverse. The phase angle between E_y and H_x increases abruptly at the same point and there is a difference of 15° - 20° between the average values either side of it. These results agree qualitatively with the theoretical profiles of Figure 8, that is, the more conductive bed on the east produces a larger phase angle than on the resistive side, unless the structure outcrops. In this case the fact that the phase angle on the conductive side exceeds 45° seems to indicate the presence of a resistive overburden on that side.

The profile from 10+00S exhibits the same properties as the one from 20+00N, the contact being at 15+00W. Although the phase break is not as pronounced here, the difference between the average values of east and west sections is about 15°. Comparing all four profiles with Figures 11 and 12, it is clear that the fault is located within 50 feet in all cases.

Three contacts are indicated in the σ_a and ϕ profiles for line 40+50S, near stations 6+00E, 29+00E and 44+50E. These results correlate well with EM16 profiles in Figures 11 and 12, where peaks appear at 5+50E, 29+00E and 44+00E, corresponding respectively to the Gloucester and the two additional faults discussed previously. All the previous remarks concerning lines 20N and 10S apply here as well.

It is to be noted that the geological section derived by Wilson (1946), which is also shown in Figure 13, agrees with the position of the fault as indicated by the VLF measurements. It does not, however, suggest the presence of the other two features farther to the east.

Summing up, the correlation between field results and theory is excellent. In particular, there does not appear to be any anomalous conductivity associated with the faults themselves, such as exhibited by graphite and water-filled shear zones. In Figure 12 the trace of the Gloucester fault as mapped by the VLF

survey wanders somewhat from its location determined geologically by Wilson (1946). The variation, however, is generally within 500 feet.

The wave impedance measurements located all the contacts within 50 feet of their positions found in the tilt angle survey, which is roughly the error in the pace and compass traverses employed. The apparent conductivities of the Carlsbad and Oxford formations obtained by these measurements, about 15 and 3 millimhos/m respectively, do not represent true formation resistivities, because of the presence of overburden. The fact that the phase variations, in the vicinity of Gloucester fault, do not agree with the theoretical profiles in detail is probably due to irregularities in the overburden and/or multilayer beds on both sides of the contact.

Detection of the two faults east of the Gloucester fault indicate a resistive zone in the Carlsbad Shale (see Fig. 13, line 40+50S between 29+00 and 44+00E) which cannot be due to a change in the bedrock terrain, since both overburden and shale resistivities are comparatively low. The resistive block may be Ottawa limestone, locally uplifted from below the Carlsbad; outcrops of this formation are found northwest of Leitrim.

Smoky Creek Fault

Further field tests were carried out over the Smoky Creek fault in the vicinity of Lake Flavrian, several miles northwest of Noranda, Quebec. The fault strikes southeast for about 20 miles in the area. The geological map for the area indicates granodiorite on both sides, that is, there is no contrast in lithology across the contact. This feature was indicated by an early airborne AFMAG survey (Sutherland, 1967) and more recently by an airborne VLF Barringer RADIOPHASE survey (Becker and McNeil, 1969). The field situation is shown in Figure 14 which indicates the position of one VLF profile (line A3) with respect to the fault and the airborne anomalies.

EM16 total field profiles, together with the corresponding apparent resistivity profile are shown in Figure 15 for line A3. Here, the Smoky Creek fault is located at station 15+50N, marked by extremely high (100%) total field peak and a very abrupt increase in resistivity from 100 Ωm to 60J0 Ωm. The steep slope of the EM16 profiles is also consistent with the more conductive zone on the south side.

DC resistivity shallow depth soundings were carried out in an attempt to clarify the EM16 results. These indicate that the thickness of the overburden is at least 57 feet at 7+50N, 43 feet at 13+50N, but 6 feet or less at 16+50N. This abrupt change in depth of a conductive (< 100 Ωm) layer – essentially a steep contact between overburden and resistive bedrock – is the source of the anomaly. Possibly the fault itself, supposedly located at 15+50N, is responsible for the bedrock step, although there is no evidence to support this. Thus the VLF and ρ_a profiles, although characteristic of a contact between two beds of different resistivity, appear to be the reflection of a sudden change in the depth of overburden.

CONCLUSION

The field results described in this report agree very well with the theory of VLF response over a vertical contact between beds of contrasting resistivity, covered by a uniform layer of overburden. Thus the method is a useful qualitative supplement to field geology in mapping such structures. Subsequent work in the Ottawa Valley and St. Lawrence Lowlands (Williams, 1976) has confirmed this.

In areas where there are abrupt changes in depth of overburden, however, the VLF data may be misleading, as described in the survey of the Smoky Creek fault. Similar sudden lateral changes in overburden resistivity, although no examples are given here, would doubtless have the same effect. At present shallow seismic and resistivity sounding are the only geophysical methods available to clarify such situations: both are slow and relatively expensive. Obviously a simple and rapid technique for mapping bedrock terrain and estimating overburden resistivity is very desirable, not only in connection with the type of survey described here, but in many other applications as well.

REFERENCES

Becker, A.
1967: Radio-wave mapping of ground conductivity anomalies; in Report of Activities, Part A; Geol. Surv. Can., Paper 67-1A, p. 130-131.

Becker, A. and McNeil, J.D.
1969: Explanatory notes, Noranda Radiophase Survey; Published by Quebec Department of Natural Resources.

Cagniard, L.
1953: Basic theory of the magneto-telluric method of geophysical prospecting; Geophysics, v. 18, p. 605-635.

Collett, L.S. and Becker, A.
1968: "Radiohm Method for Earth Resistivity Mapping"; Canadian Patent No. 795,919.

Collett, L.S. and Bell, C.K.
1971: AFMAG use in geological interpretation; Can. Min. Metall. Bull., v. 64, p. 39-47.

Dosso, H.W.
1966: Analogue model measurements for electromagnetic variations near a coastline; Can. J. Earth Sci., v. 3, p. 917-936.

Fraser, D.C.
1969: Contouring of VLF-EM data; Geophysics, v. 34, no. 6, p. 958-967.

Geyer, R.G.
1972a: Transient electromagnetic response near a fault zone; Geophys. Prospect., v. 20, p. 829-846.

1972b: The effect of dipping contact on the behaviour of the electromagnetic field; Geophysics, v. 37, p. 337-350.

Heiland, C.A.
1940: Geophysical Prospecting, chap. 10, Prentice-Hall, New York.

Jones, F.W. and Price, A.T.
1970: Perturbations of alternating geomagnetic fields by conductivity anomalies; Geophysc. J. R. Astron. Soc., v. 20, p. 317-334.

King, W.F.
1971: Studies of geologic structures with the VLF method; unpubl. M.Sc. thesis, McGill Univ., Montreal.

Ku, C.C., Hsieh, M.S., and Lim, S.H.
1973: The topographic effect in electromagnetic fields; Can. J. Earth Sci., v. 10, p. 645-656.

Madden, T.R. and Swift, C.M., Jr.
1969: Magneto-telluric studies of the electrical conductivity structure of the Crust and Upper Mantle; in The Earth's Crust and Upper Mantle; Geophysc. Monograph. 13, (ed. P.J. Hart), p. 469-479; Am. Geophys. U., Washington, D.C.

Paterson, N.R. and Ronka, V.
1971: Five years of surveying with the VLF EM Method; Geoexploration, v. 9, p. 7-26.

Phillips, W.J. and Richards, W.E.
1975: A study of the effectiveness of the VLF Method for the location of narrow-mineralized fault zones; Geoexploration, v. 13, p. 215-226.

Sutherland, D.B.
1967: AFMAG for EM mapping; in Mining and Groundwater Geophys.; (ed. L.W. Morley), Geol. Surv. Can., Econ. Geol. Rep. 26, p. 228-237.

Swift, C.M., Jr.
1967: A Magneto-telluric investigation of an electrical conductivity anomaly in the Southwestern United States; unpubl. Ph.D. thesis, M.I.T., Cambridge, Mass.

1971: Theoretical magneto-telluric and Turam Response from 2-dimensional inhomogeneities. Geophysics, v. 36, p. 38-52.

Weaver, J. T.
  1963: The electromagnetic field within a discontinuous
        conductor with reference to geomagnetic
        micropulsations near a coastline; Can. J. Phys.
        v. 41, p. 484-495.

Williams, D. A.
  1976: A study of the fault systems in the St. Lawrence
        Lowlands and Ottawa Valley areas; Ph. D. thesis,
        McGill Univ., Montreal. (in prep.)

Wilson, A. E.
  1946: Geology of the Ottawa-St. Lawrence Lowlands,
        Ontario and Quebec; Geol. Surv. Can.,
        Mem. 241.

CONTOURING OF VLF-EM DATA

By

D.C. Fraser

CONTOURING OF VLF-EM DATA†

D. C. FRASER*

Prospecting for conductive deposits with ground VLF-EM instruments has received considerable impetus with the recent development of lightweight receivers. The large geologic noise component, which results from the relatively high-transmitted frequency, has caused some critics to avoid use of the technique. Those who routinely perform surveys with a VLF-EM unit find that, in some areas, a 5-degree peak-to-peak anomaly can be significant, whereas anomalies having amplitudes in excess of 100 degrees may occur as well. Consequently, there is a dynamic range problem when presenting the results as profiles plotted on a field map.

A data manipulation procedure is described which transforms noisy noncontourable data into less noisy contourable data, thereby eliminating the dynamic range problem and reducing the noise problem. The manipulation is the result of the application of a difference operator to transform zero-crossings into peaks, and a low-pass smoothing operator to reduce noise. Experience has shown that field personnel can routinely perform the calculations which simply involve additions and subtractions.

INTRODUCTION

VLF-EM data can be exceedingly difficult to interpret because a large geologic noise component can result from the relatively high-transmitted frequency of about 20,000 Hz. Routine surveys can yield useless data unless special care is taken both in survey procedure and in data presentation.

The purpose of this paper is to describe the survey procedure and the method of data presentation in use by the Keevil Mining Group and to illustrate the advantages of this approach.

VLF-EM GROUND SURVEY PROCEDURE AND DATA TREATMENT

The primary field

VLF-EM transmitter stations are located at several points around the globe. They broadcast at frequencies close to 20,000 Hz, which is low compared to the normal broadcast band. The purpose of these stations is to allow governmental communication with submarines, and the low frequency allows some penetration of the conductive ocean water. Skin depth is approximately $3.6\sqrt{P}$ meters, where P is the resistivity of a homogeneous halfspace in ohm-m, on the assumption that the frequency is 20,000 Hz and that the halfspace is magnetically nonpolarizable. Consequently, depth of exploration is severely restricted for overburden resistivities less than 200 ohm-m.

Since the area to be prospected normally is of considerable distance from the transmitter stations, the primary field is uniform in the area, allowing rather simple mathematics to be used in anomaly prediction and analysis.

Survey procedure and data treatment

The survey procedure first consists of selecting a transmitter station which provides a field approximately parallel to the traverse direction, i.e., approximately perpendicular to the expected strike of a conductor. The following points relate to the method of data treatment.

1. Readings should be taken every 50 ft, as will be shown below.
2. Transmitter stations should not be changed

for a given block of ground, to avoid distortion in the contour presentation. Hence, fill-in lines should be run with the same transmitter station as other lines in the block. The field direction of this station should be shown on the data map.

3. List the dip angle[1] data in tabular form, as follows:

    a) list in the direction of north (top of paper) to south, or from west to east;

    b) designate south or east dips as negative; and

    c) perform calculations as shown in Table 1.

Thus, the filtered output or contourable quantity simply consists of the sum of the observations at two consecutive data stations subtracted from the sum at the next two consecutive data stations. The theoretical basis for this procedure will be described below.

4. The right-hand column (filtered data) is

[1] This paper assumes that data is recorded as for the Crone Radem which defines a north-dipping field as a south "dip" on the instrument. This convention was chosen because a south reading is interpreted as arising from a conductor to the south.

suitable for contouring. Normally, negative values are not contoured since, being caused by dip angle flanks, they do not aid interpretation but only confuse the picture. The positive values generally are contoured at 10-unit intervals, and the zero contour is shown only when it brackets an anomaly. In quiet areas, 5-unit contours may be meaningful.

Example

Figure 1 presents dip-angle data, according to the Crone convention, in the vicinity of the Temagami mine of Copperfields Mining Corporation Limited in Ontario. This figure illustrates that several conductors are present yielding large dip angles. A complex pattern has resulted which requires some thought to interpret properly.

Figure 2 presents the filtered data in contoured form where only the 0, 20, and 40 contours are shown for simplicity. The conductor pattern is immediately apparent, even to exploration personnel untrained in VLF-EM interpretation. The three anomalies correlate with a zone of nearly massive pyrite and two brecciated fault zones. Depth to bedrock is 15 ft.

In practice, all the data of Figures 1 and 2 are

Table 1. Example of calculations

Location	Measured dips	Apply sign and form the moving sum of pairs of entries		Take first differences of alternate entries	
3+00S	6S	−6			
3+50S	7S	−7	(−6)+(−7) = −13		
4+00S	8S	−8	(−7)+(−8) = −15	(−23)−(−13) = −10	
4+50S	15S	−15	−23	(−39)−(−15) = −24	
			−39	+ 7	
5+00S	24S	−24	−16	+57	
5+50S	8N	+ 8	+18	+38	
6+00S	10N	+10	+22	+ 8	
6+50S	12N	+12	+26	+ 6	
7+00S	14N	+14	+28	(+34)−(+26) = + 8	
7+50S	14N	+14	+34		
8+00S	20N	+20	(14)+(20) =		

960 Fraser

DEGREES 0 20 40
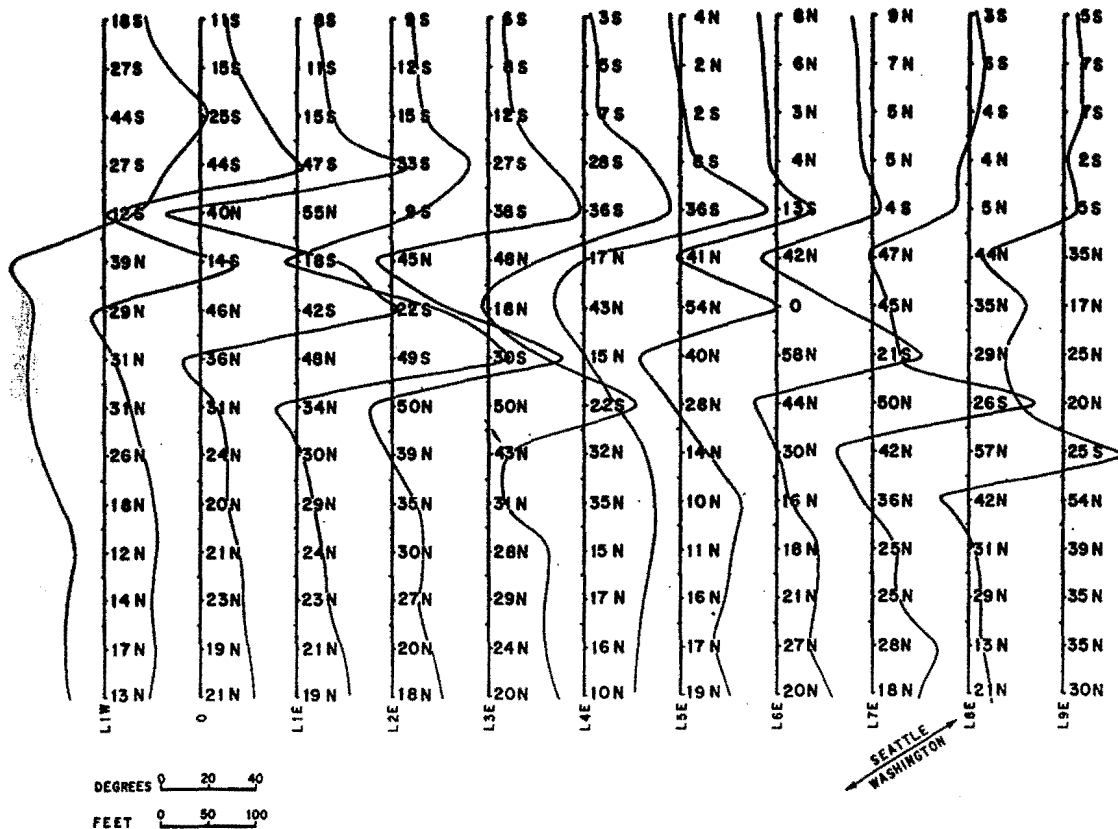
FEET 0 50 100

SEATTLE WASHINGTON

Fig. 1. Dip-angle data in the vicinity of the Temagami mine. The arrow defines the VLF-EM primary field direction from the transmitter at Seattle, Washington.

placed on a single map. The above example illustrates that this very simple one-dimensional filtering scheme yields a practical and effective approach to VLF-EM data handling.

The filter improves the resolution of anomalies, thereby making them easier to recognize. An inflection on the dip profile from a conductor subordinate to a larger one yields a positive peak, thereby emphasizing the presence of such a conductor. Figure 3 illustrates this effect where nine lines were run over an SP (self-potential) anomaly in the Temagami area. The dip-angle anomaly is very poorly resolved due to the regional south dips produced by an areally large conductor to the south of the map area. The contoured VLF-EM data yields a clearly defined anomaly which was located over the negative center of the SP.

THE FILTER AND ITS EFFECT ON ANOMALIES

The filter operator

The filter operator was designed to meet the following criteria:

1. It must phase shift the dip-angle data by 90 degrees so that crossovers and inflections will be transformed into peaks to yield contourable quantities.

2. It must completely remove dc and attenuate long spatial wavelengths to increase resolution of local anomalies.

3. It must not exaggerate the station-to-station random noise.

4. It must be simple to apply so that field personnel can make the calculations without difficulty.

The first two criteria are met by using a simple difference operator, i.e.

$$M_2 - M_1,$$

where M_1 and M_2 are any two consecutive data points.

The third criterion is met by applying a smoothing or low-pass operator to the differences, i.e.
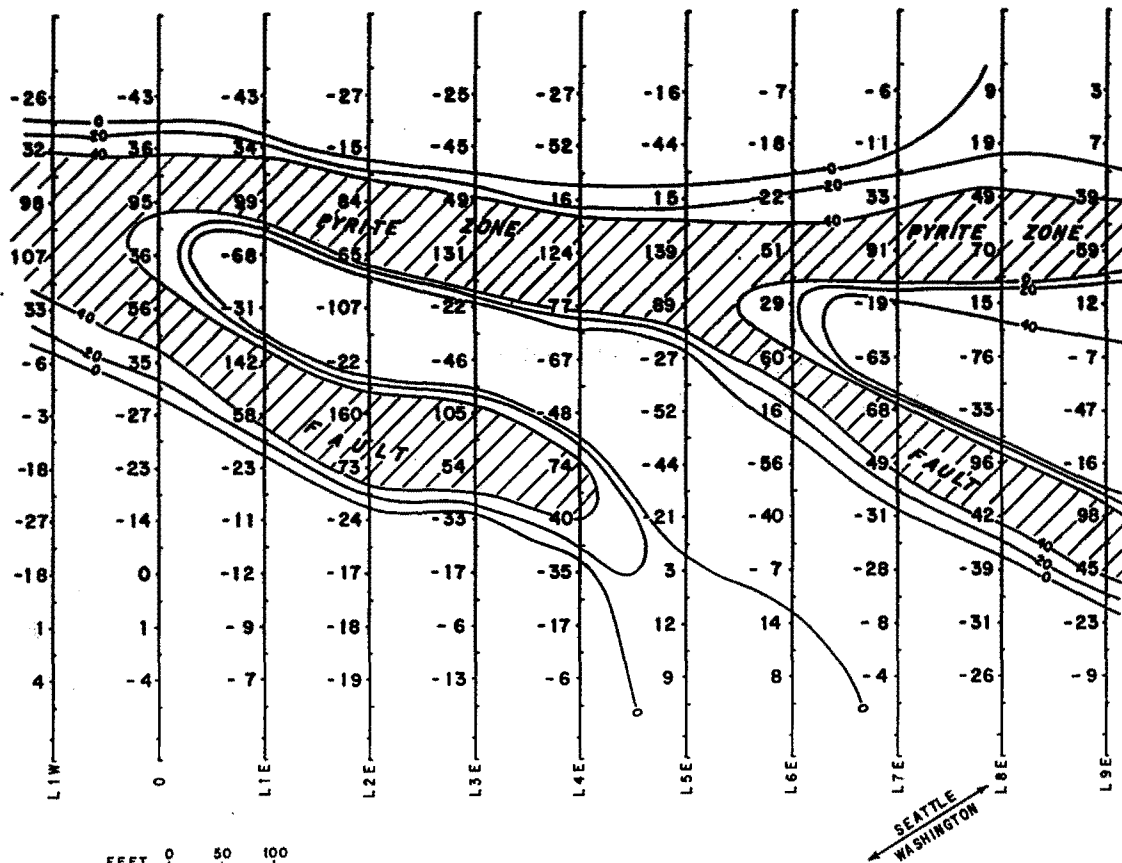
FIG. 2. Filtered data computed from the map of Figure 1.

$\frac{1}{4}(M_2 - M_1) + \frac{1}{2}(M_3 - M_2) + \frac{1}{4}(M_4 - M_3)$,

where M_1, M_2, M_3, and M_4 are any four consecutive data points. The filtered output then is

$\frac{1}{4}(M_2 - M_1) + \frac{1}{2}(M_3 - M_2) + \frac{1}{4}(M_4 - M_3)$

$= \frac{1}{4}[M_3 + M_4 - M_1 - M_2]$.

The final criterion is enhanced by eliminating the constant, so that the plotted function becomes

$f_{2,3} = (M_3 + M_4) - (M_1 + M_2)$,

which is plotted midway between the M_2 and M_3 dip-angle stations.

This filter has its frequency (wavenumber) response displayed in Figure 4, for a station spacing of 50 ft. Its characteristics are as follows:

1. All frequencies are shifted by 90 degrees.
2. Noise having a wavelength equal to the station spacing and dc bias are completely removed.

3. Maximum amplitude occurs for wavelengths of 250 ft, or five times the station spacing.

The frequency (wavenumber) response of the filter is shown for a station spacing of 50 ft, because this is the most suitable spacing for defining sulfide bodies within a few hundred feet of surface. This will be demonstrated below.

The dike model

A conducting dike in a VLF-EM field will produce a secondary induction field from eddy currents maintained in it by the primary field. These eddy currents will tend to flow in such a manner as to form line sources concentrated near the outer edges of the dike since the field is uniform (Figure 5a). This dike may be replaced by a loop of wire of dimensions traced out by the main current concentration in the dike. The secondary field geometry of the loop and dike then will be practically identical, as has been shown by Fraser (1966), Parry (1966), and Parry et al (1965). This
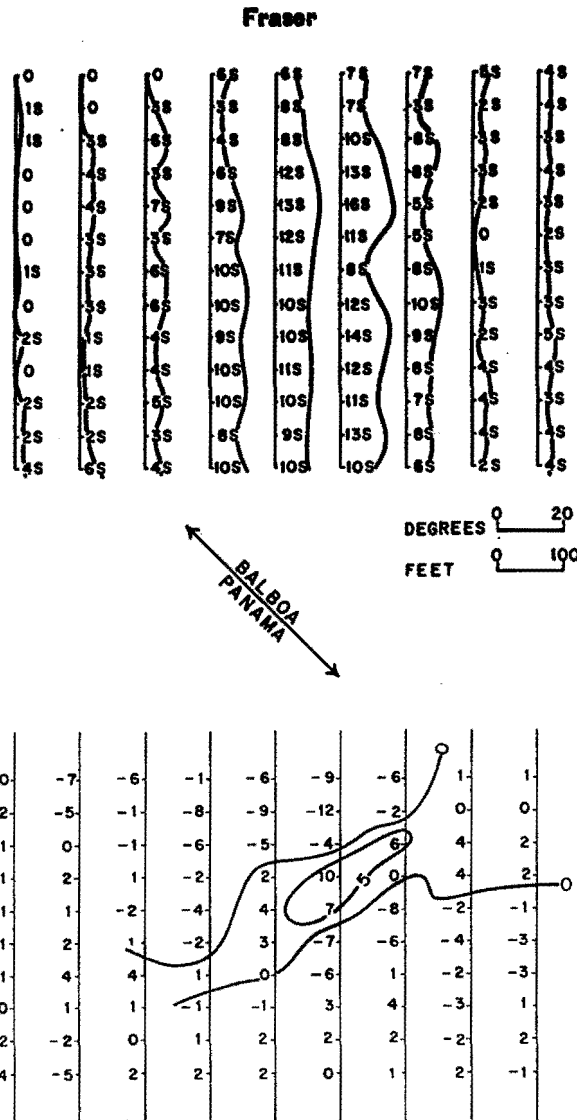
Fraser

FIG. 3. Dip-angle (upper map) and filtered data (lower map) over a small grid in the Temagami area. The arrow defines the VLF-EM primary field direction from the transmitter at Balboa, Panama.

allows a mathematical model of a dike to be constructed because the field from a line source is known.

For brevity, only a dike which is large in depth extent and in length will be considered herein. Only the top line source of Figure 5a will contribute to the measured dip angles because the other current line sources are very far away.

The horizontal Hs_x and vertical Hs_z secondary fields are (Figure 5b)

$$Hs_x = kH_0 \frac{z}{x^2 + z^2}$$

$$Hs_z = kH_0 \frac{x}{x^2 + z^2},$$

where k is a positive constant having the dimension of length and is related to the conductivity and dimensions of the dike, and where H_0 is the primary VLF-EM strength at the dike. The measured dip angle is

$$\alpha = \tan^{-1}\left[\frac{H_{sz}}{Hs_x + H_0}\right]$$

$$= \tan^{-1}\left[\frac{kx}{kz + x^2 + z^2}\right].$$

Model dip profiles can be computed for various depths z only by assuming a value for k.

As a means of testing the effect of the filter operator, a single k value was chosen to yield a

FILTER CHARACTERISTICS

(a) Amplitude is identically zero for zero frequency
(b) All frequencies ore phase shifted 90 degrees.

REJECT

PASS   BAND   REJECT

AMPLITUDE

GAIN

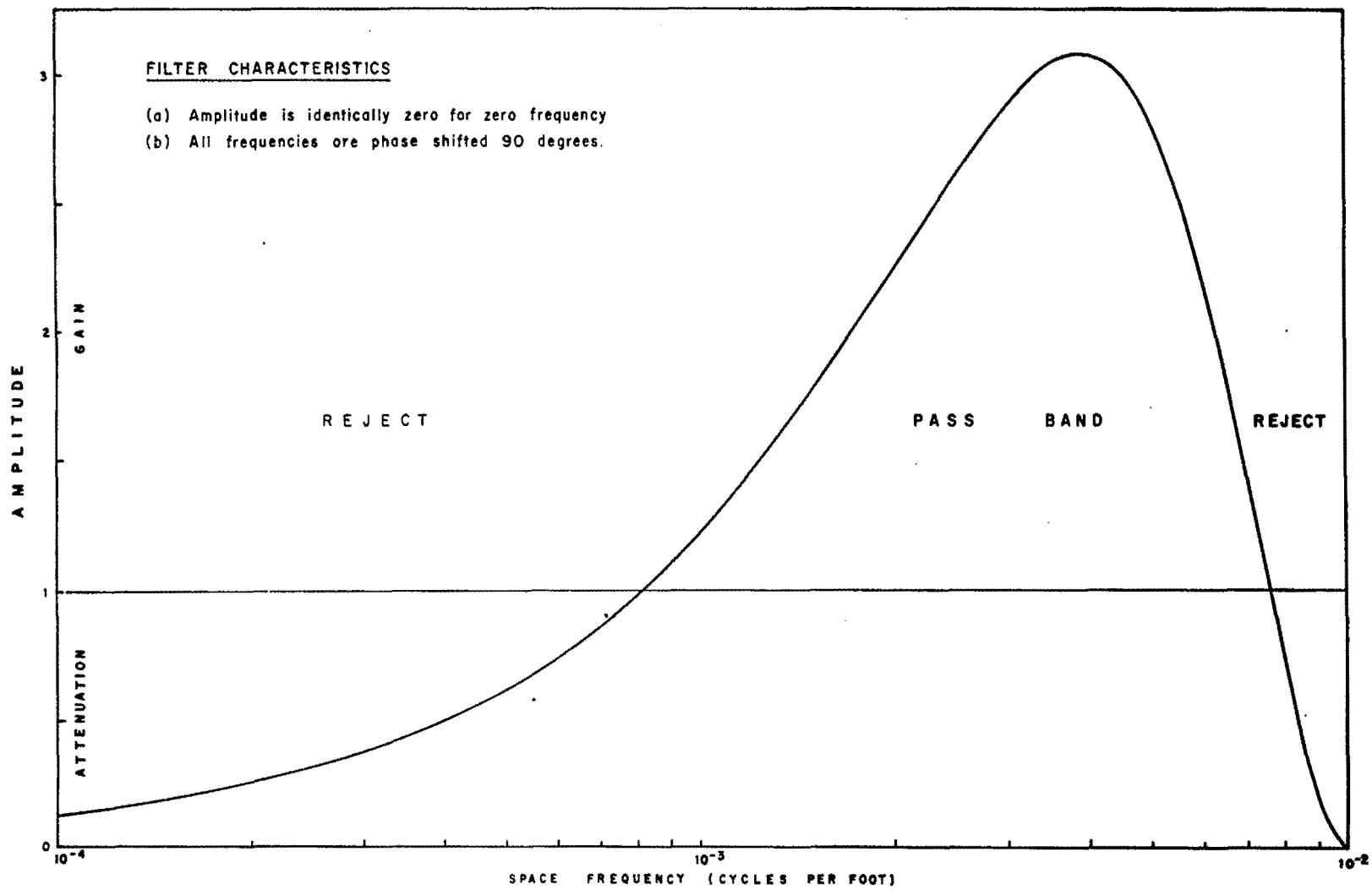ATTENUATION

SPACE   FREQUENCY   (CYCLES PER FOOT)

FIG. 4. Frequency response of filter operator for station spacing of 50 ft.
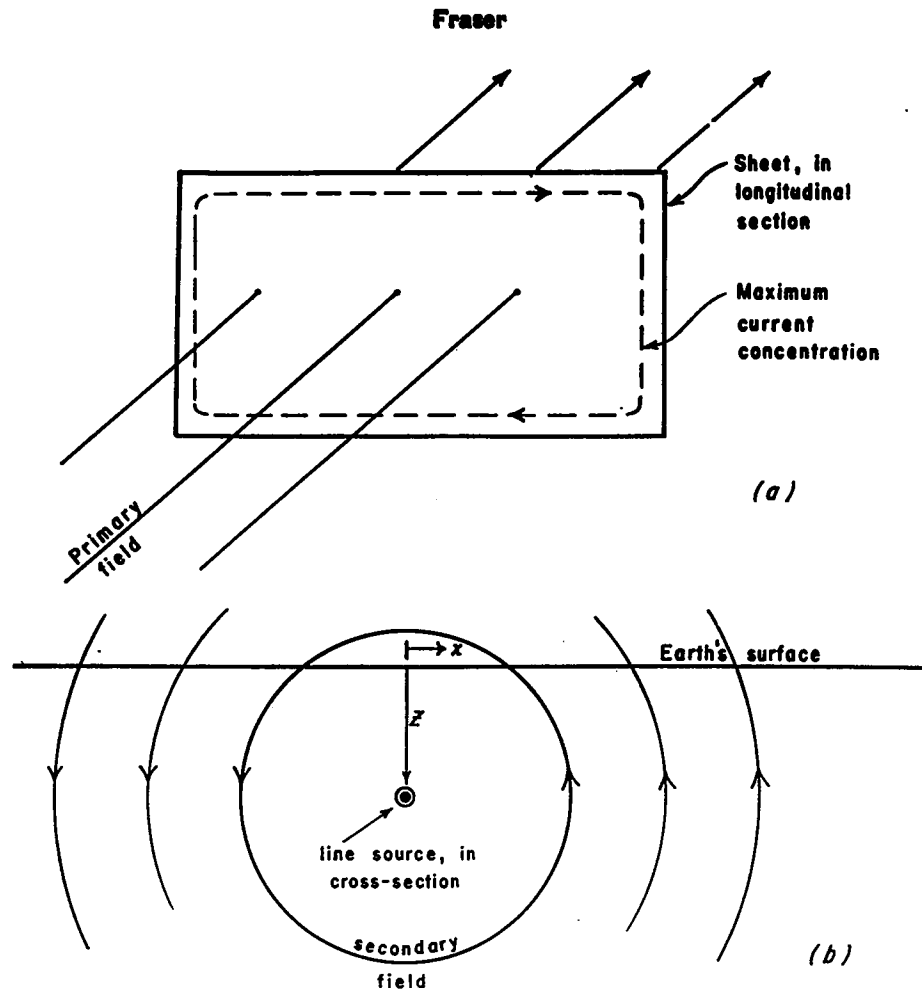
Fraser

Fig. 5. (a) A sheet in a uniform primary field will have maximum current concentrated near its edges. (b) A line source, corresponding to the upper current concentration in (a), yields a secondary magnetic field of cylindrical shape.

maximum dip angle of 35 degrees when depth z to top of dike (or line source) was 100 ft. Figure 6 illustrates the dip angle and filtered profiles for this case for a station spacing of 50 ft and for several depth values.

The following are the main characteristics of these dike and filtered anomalies:

1. Peak-to-peak angles vary from 93 degrees for $z = 50$ ft to 25 degrees for $z = 500$ ft. Filtered peaks vary from 118 degrees for $z = 50$ ft to 8 degrees for $z = 500$ ft. Thus, the filter amplifies near-surface anomalies and attenuates deep-source anomalies. There is neither amplification nor attenuation when z is 100 ft.

2. On the basis of anomaly resolution and usual noise levels, dip angle data can detect dike-like conductors in a resistive medium to a

depth of 500 ft, while filtered data can detect such bodies to a depth of 300 ft. Conductors in the upper 200 ft generally will be more easily recognized on the filtered data.

VLF-EM data commonly is measured at 100-ft intervals in Canada. A change in the sample interval from the 50 ft recommended herein to 100 ft causes the passband curve of Figure 4 to shift to the left, such that the peak is at 2×10^{-3} cpf rather than 4×10^{-3} cpf. Similarly, the anomaly curves of Figure 6 remain correct in shape provided all distance dimensions are doubled. Consequently, detection of conductors to a depth of 500 ft, when utilizing the filter operator, might appear facilitated by use of a 100-ft station interval rather than a 50-ft interval. However, anomalies from near-surface conductors will have poorly defined waveforms for a 100-ft
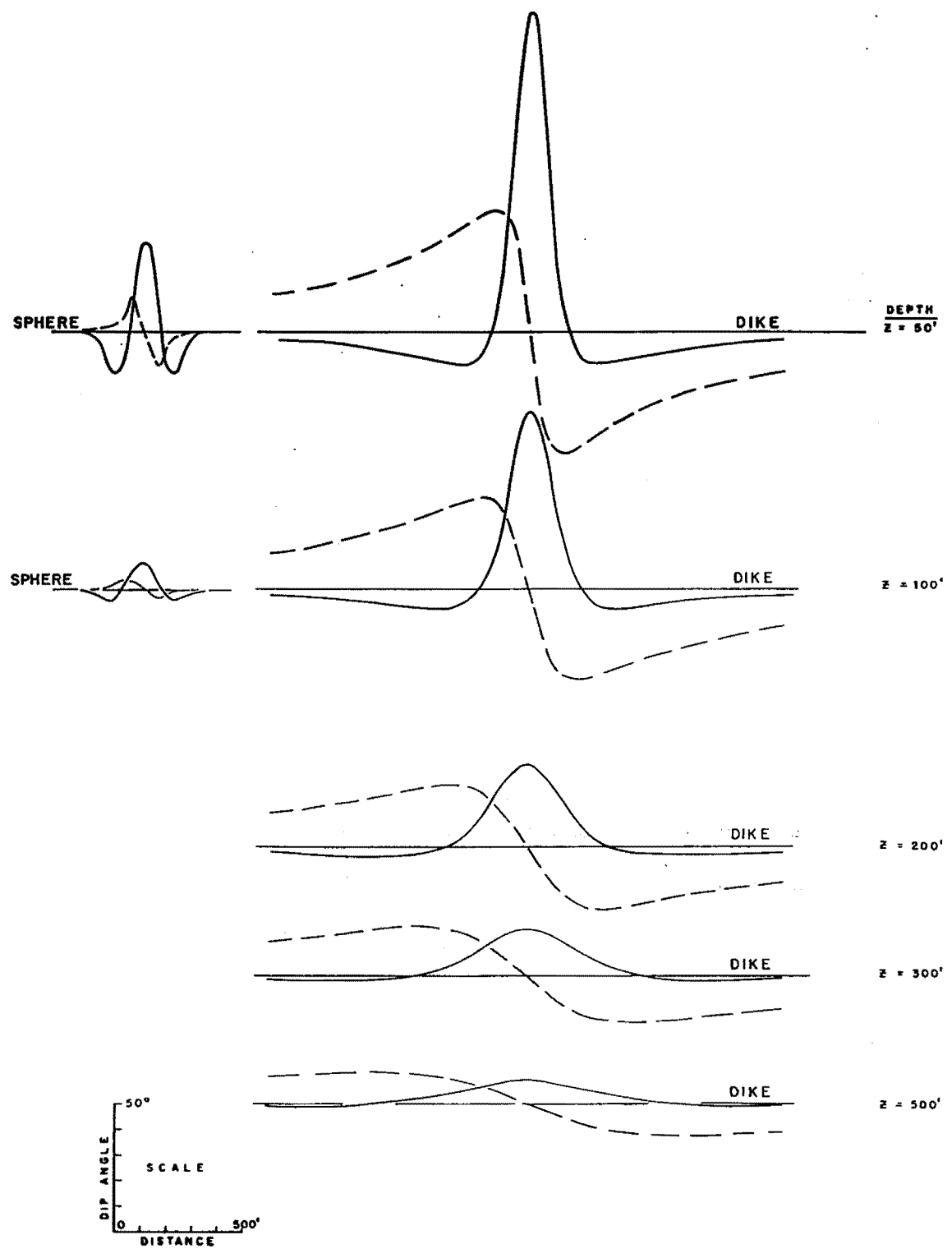
Fɪɢ. 6. Dip-angle (dashed) and filtered (solid) curves for model dike and sphere for several depths of burial, where z is depth to top of dike and to center of sphere.

data station interval, and will alias as deeper conductors. This "geologic noise" will somewhat confuse the contoured output. Generally, a comparison of the 50-ft data station dip angle profiles with the contoured filtered output suffices to indicate approximate depth to source and to allow recognition of sources deeper than 300 ft.

As an aside, some geophysicists have claimed that a reasonable dike model depth estimate can be obtained directly as half the distance between dip angle peaks, because the vertical field Hs_z peaks at $x = \pm z$. However, this formula is not applicable to dip-angle data, as can be seen by the dike curves of Figure 6. For this example, the formula provides erroneous depth estimates of 150, 200, 325, 425, and 625 for true depths of 50, 100, 200, 300, and 500 ft.

The sphere model

A conducting sphere in a VLF-EM field will produce an anomaly according to equations in Ward (1967). For a traverse directly over a sphere having its center at depth z, and run in the direction of the primary field H_0, the anomaly is,

$$Hs_x = kH_0 \frac{(2x^2 - z^2)}{(x^2 + z^2)^{5/2}}$$

$$Hs_z = kH_0 \frac{3xz}{(x^2 + z^2)^{5/2}},$$

where k is a positive constant which saturates at $R^3/2$, where R is the sphere radius, and where quadrature is ignored. The measured dip angle as a function of station location x is (where x is zero directly over the sphere center),

$$\alpha = \tan^{-1}\left(\frac{Hs_z}{Hs_x + H_0}\right)$$

$$= \tan^{-1}\left[\frac{3kxz}{k(2x^2 - z^2) + (x^2 + z^2)^{5/2}}\right].$$

Model dip profiles can be computed for various depths z only by assuming a value for k. The sphere curves of Figure 6 assume a saturated k-value for a sphere radius of 50 ft. Obviously, a sphere having its center at a depth of greater than twice its radius generally will not be detectable. However, the filter operator aids in the recognition of a spherical conductor because it amplifies the anomaly, for the small sphere sizes

usually encountered in nature, assuming data spacing is 50 ft.

TOPOGRAPHIC EFFECT

Whittles (1969) recently described a topographic effect which may arise when surveying with VLF-EM in mountainous regions. The spatial wavelengths which result from the phenomenon he describes are greatly attenuated by the filter and generally do not appear on the contoured maps. Whittles advocates the use of first derivatives to remove the topographic effect. The filter operator described herein uses the first difference (i.e., the discrete first derivative) as one of its components.

ADDITIONAL APPLICATIONS

The simplicity of the calculations allows practical application of the filter to any form of ground geophysical data which yields zero-crossings over tragets, such as vertical loop EM and Afmag. However, it is difficult to justify the use of the filter on vertical loop EM data because neither dynamic range of anomalies nor geologic noise is large. In Afmag, utilization of the filter is not recommended because of the varying direction of the primary field.

Airborne VLF-EM systems, which measure parameters yielding zero-crossings over targets, are being marketed. If the data were collected on magnetic tape, a computer could be used to apply the filter, thereby allowing contouring of the data. However, in this situation more sophisticated filter operators should be employed.

If the filter is to be applied to data other than ground VLF-EM, the sample interval should be selected to ensure that the passband of the filter is correct relative to the frequency components of the anomalies sought.

CONCLUSIONS

A consideration of geologic noise and conductor shapes illustrates that VLF-EM data should be collected at 50-ft intervals, and that the described filter operator should be employed. The filtered data, when contoured, provides a data presentation which simplifies interpretation. The filter also amplifies anomalies from near-surface, highly conducting ore pods which is an important feature in several mining districts such as at Tribag and Temagami, both in Ontario, and in Louvicourt Township of Quebec.

REFERENCES

Fraser, D. C., 1966, Rotary field electromagnetic prospecting: Ph.D. thesis, Univesity of California at Berkeley.

Parry, J. R., 1966, A theoretical and experimental investigation of finite dikes in a uniform electromagnetic field: M.Sc. thesis, University of California at Berkeley.

———— Fraser, D. C., and Ward, S. H., 1965. Investigation of finite dikes in a uniform electromagnetic field: Presented at the 35th Annual International SEG Meeting, Dallas, Texas.

Ward, S. H., 1967, Electromagnetic theory for geophysical applications, in Mining Geophysics, Vol. II: Tulsa, SEG, p. 80.

Whittles, A. B., 1969, Prospecting with radio frequency EM-16 in mountainous regions: Western Miner, February 1969, p. 51–56.